Chapter 3. Higher Dimensionality Effects

The descriptions of the basic quantum-mechanical effects, given in the previous chapter, may be extended to higher dimensions in an obvious way. This is why this chapter is focused on the phenomena (*such as the AB effect and the Landau levels*) *that cannot take place in one dimension due to topological reasons, and also on the key 3D problems* (*such as the Born approximation in the scattering theory, and the axially and spherically symmetric systems*) *that are important for numerous applications.*

3.1. Quantum interference and the AB effect

In the past two chapters, we have already discussed some effects of the de Broglie wave interference. For example, standing waves inside a potential well, or even on the top of a potential barrier, may be considered as a result of interference of incident and reflected waves. However, there are some remarkable new effects made possible by the spatial separation of such waves, and such separation requires a higher (either 2D or 3D) dimensionality. A good example of wave separation is provided by the Young-type experiment (Fig. 1) in which particles, emitted by the same source, are passed through two small holes (or narrow slits) in an otherwise opaque partition.

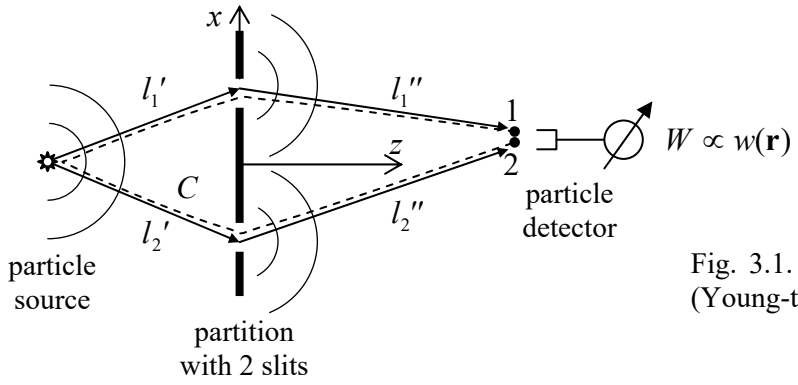

Fig. 3.1. The scheme of the "two-slit" (Young-type) interference experiment.

According to Eq. (1.22), if particle interactions are negligible (which is always true if the emission rate is sufficiently low), the average rate of particle counting by the detector is proportional to the probability density $w(\mathbf{r}, t) = \Psi(\mathbf{r}, t)\,\Psi^*(\mathbf{r}, t)$ to find a single particle at the detector's location $\mathbf{r}$, where $\Psi(\mathbf{r}, t)$ is the solution of the single-particle Schrödinger equation (1.25) for the system. Let us calculate this rate for the case when the incident particles may be represented by virtually monochromatic waves of energy E (e.g., very long wave packets), so their wavefunction may be taken in the form given by Eqs. (1.57) and (1.62): $\Psi(\mathbf{r}, t) = \psi(\mathbf{r})\exp\{-iEt/\hbar\}$. In this case, in the free-space parts of the system, where $U(\mathbf{r}) = 0$, $\psi(\mathbf{r})$ satisfies the stationary Schrödinger equation (1.78a):

$$-\frac{\hbar^2}{2m}\nabla^2\psi = E\psi\,. \tag{3.1a}$$

With the standard definition $k \equiv (2mE)^{1/2}/\hbar$, it may be rewritten as the 3D Helmholtz equation:

3D Helmholtz equation

$$\boxed{\nabla^2\psi + k^2\psi = 0\,.} \tag{3.1b}$$

The opaque parts of the partition may be well described as classically forbidden regions, so if their size scale a is much larger than the wavefunction penetration depth δ described by Eq. (2.59), we may use on their surface S the same boundary conditions as for the well's walls of infinite height:

$$\psi\big|_S = 0 . \tag{3.2}$$

Eqs. (1) and (2) describe the standard boundary problem of the theory of propagation of scalar waves of any nature. For an arbitrary geometry, this problem does not have a simple analytical solution. However, for a conceptual discussion of wave interference, we may use certain natural assumptions that will allow us to find its particular, approximate solution.

First, let us discuss the wave emission, into free space, by a small-size, isotropic source located at the origin of our reference frame. Naturally, the emitted wave should be spherically symmetric: $\psi(\mathbf{r}) = \psi(r)$. The well-known expression for the Laplace operator in spherical coordinates[1] shows that in this case, Eq. (1) is reduced to the following ordinary differential equation:

$$\frac{1}{r^2}\frac{d}{dr}\left(r^2\frac{d\psi}{dr}\right) + k^2\psi = 0 . \tag{3.3}$$

Let us introduce a new function, $f(r) \equiv r\psi(r)$. Plugging the reciprocal relation $\psi = f/r$ into Eq. (3), we see that for the function f, it gives the standard 1D wave equation:

$$\frac{d^2 f}{dr^2} + k^2 f = 0 . \tag{3.4}$$

As was discussed in Sec. 2.2, for a fixed k, the general solution of Eq. (4) may be represented in the form of two traveling waves:

$$f = f_+ e^{ikr} + f_- e^{-ikr} \tag{3.5}$$

so the full solution of Eq. (3) is

$$\psi(\mathbf{r}) = \frac{f_+}{r}e^{ikr} + \frac{f_-}{r}e^{-ikr}, \quad \text{i.e. } \Psi(\mathbf{r},t) = \frac{f_+}{r}e^{i(kr-\omega t)} + \frac{f_-}{r}e^{-i(kr+\omega t)}, \quad \text{with } \omega \equiv \frac{E}{\hbar} = \frac{\hbar k^2}{2m}. \tag{3.6}$$

If the source is located at point $\mathbf{r}' \neq 0$, the obvious generalization of Eq. (6) is

$$\Psi(\mathbf{r},t) = \frac{f_+}{R}e^{i(kR-\omega t)} + \frac{f_-}{R}e^{-i(kR+\omega t)}, \quad \text{with } R \equiv |\mathbf{R}|, \text{ where } \mathbf{R} \equiv \mathbf{r} - \mathbf{r}'. \tag{3.7}$$

The first term of this solution describes a spherically symmetric wave propagating from the source outward, while the second one represents a wave converging onto the source point $\mathbf{r}'$ from large distances. Though the latter solution is possible in some very special circumstances (say, when the outgoing wave is reflected back from a perfectly spherical shell), for our current problem, only the outgoing waves are relevant, so we may keep only the first term (proportional to f_+) in Eq. (7). Note that the factor R is the denominator (that was absent in the 1D geometry) has a simple physical sense: it provides the independence of the full probability current $I = 4\pi R^2 j(R)$, with $j(R) \propto k\Psi\Psi^* \propto 1/R^2$, of the distance R between the observation point and the source.

[1] See, e.g., MA Eq. (10.9) with $\partial/\partial\theta = \partial/\partial\varphi = 0$.

Now let us assume that the partition's geometry is not too complicated – for example, it is either planar as shown in Fig. 1, or nearly-planar, and consider the region of the particle detector location far behind the partition (at $z >> 1/k$), and at a relatively small angle to the normal: $|x| << z$. Then it should be physically clear that the spherical waves (7) emitted by each point inside the slit cannot be perturbed too much by the opaque parts of the partition, and their only role is the restriction of the set of such emitting points to the area of the slits. Hence, an approximate solution of the boundary problem is given by the following *Huygens principle*: the wave behind the partition looks as if it was the sum of the contributions (7) from two point sources located in the slits, with each source's strength f_+ proportional to the amplitude of the wave arriving at this pseudo-source from the real source – see Fig. 1. This principle finds its confirmation in the strict wave theory, which shows that with our assumptions, the solution of the boundary problem (1)-(2) may be represented as the following *Kirchhoff integral*:[2]

Kirchhoff integral

$$\psi(\mathbf{r}) = c\int_{\text{slits}} \frac{\psi(\mathbf{r}')}{R} e^{ikR} d^2r', \qquad \text{with } c = \frac{k}{2\pi i}. \tag{3.8}$$

If the source is also far from the partition, its wave's front is almost parallel to the slit plane, and if the slits are not too broad, we can take $\psi(\mathbf{r}')$ constant ($\psi_{1,2}$) at each slit, so Eq. (8) is reduced to

$$\psi(\mathbf{r}) = a''_1 \exp\{ikl''_1\} + a''_2 \exp\{ikl''_2\}, \qquad \text{with } a''_{1,2} = \frac{cA_{1,2}}{l''_{1,2}}\psi_{1,2}, \tag{3.9}$$

where $A_{1,2}$ are the slit areas, and $l''_{1,2}$ are the distances from the slits to the detector. The wavefunctions on the slits may be calculated approximately[3] by applying the same Eq. (7) to the region *before* the slits: $\psi_{1,2} \approx (f_+/l'_{1,2})\exp\{ikl'_{1,2}\}$, where $l'_{1,2}$ are the distances from the source to the slits – see Fig. 1. As a result, Eq. (9) may be rewritten as

Wave-function superposition

$$\psi(\mathbf{r}) = a_1 \exp\{ikl_1\} + a_2 \exp\{ikl_2\}, \qquad \text{with } l_{1,2} \equiv l'_{1,2} + l''_{1,2}; \quad a_{1,2} \equiv \frac{c f_+ A_{1,2}}{l'_{1,2} l''_{1,2}}. \tag{3.10}$$

(As Fig. 1 shows, each of $l_{1,2}$ is the full length of the classical path of the particle from the source, through the corresponding slit, and further to the observation point $\mathbf{r}$.)

According to Eq. (10), the resulting rate of particle counting at point $\mathbf{r}$ is proportional to

Quantum interference

$$w(\mathbf{r}) = \psi(\mathbf{r})\psi^*(\mathbf{r}) = |a_1|^2 + |a_2|^2 + 2|a_1 a_2|\cos\varphi_{12}, \tag{3.11}$$

where

$$\varphi_{12} \equiv k(l_2 - l_1) \tag{3.12}$$

is the difference between the total wave phase accumulations along each of the two alternative paths. The last expression may be evidently generalized as

[2] For the proof and a detailed discussion of Eq. (8), see, e.g., EM Sec. 8.5.

[3] A possible (and reasonable) concern about the application of Eq. (7) to the field in the slits is that it ignores the effect of opaque parts of the partition. However, as we know from Chapter 2, the main role of the classically forbidden region is reflecting the incident wave toward its source (i.e. to the left in Fig. 1). As a result, the contribution of this reflection to the field inside the slits is insignificant if $A_{1,2} >> \lambda^2$, and even in the opposite case provides just some rescaling of the amplitudes $a_{1,2}$, which is not important for our conceptual discussion.

$$\varphi_{12} = \oint_C \mathbf{k} \cdot d\mathbf{r}, \tag{3.13}$$

Quantum interference: phase difference

with integration along the virtually closed contour C (see the dashed line in Fig. 1), i.e. from point 1, in the positive (i.e. counterclockwise) direction all the way to point 2. (From our discussion of the 1D WKB approximation in Sec. 2.4, we may expect such generalization to be valid even if k changes, sufficiently slowly, along the paths.)

Our result (11)-(12) shows that the particle counting rate oscillates as a function of the difference $(l_2 - l_1)$, which in turn changes with the detector's position, giving the famous interference pattern, with its amplitude proportional to the product $|a_1 a_2|$, and hence vanishing if any of the slits is closed. For the wave theory, this is a well-known result,[4] but for particle physics, it was (and still is :-) rather shocking. Indeed, our analysis is valid for a very low particle emission rate, so there is no other way to interpret the pattern other than resulting from a particle's interference *with itself* – or rather the interference of its de Broglie waves passing through each of two slits.[5] As was already noted in Sec. 1.1(v), nowadays such interference is reliably observed not only for electrons but also for much heavier particles: atoms and molecules including very complex organic ones.

Let us now discuss a very interesting effect of magnetic field on quantum interference. To simplify our discussion, let us consider a slightly different version of the two-slit experiment, in which each of the two alternative paths is constricted to a narrow channel using lateral confinement – see Fig. 2. (In this arrangement, moving the particle detector without changing the channels' geometry and hence local values of k may be more problematic experimentally, so let us think about its position $\mathbf{r}$ as fixed.) In this case, because of the effect of the walls providing the path confinement, we cannot use Eqs. (10) for the amplitudes $a_{1,2}$. However, from the discussions in Sec. 1.6 and Sec. 2.2, it should be clear that the first of the expressions (10) remains valid, though maybe with a value of k specific for each channel.

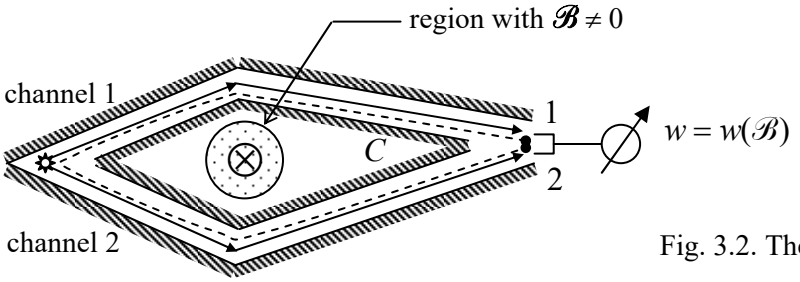

Fig. 3.2. The AB effect.

In this geometry, we can apply some local magnetic field $\mathscr{B}$, say normal to the plane of particle motion, whose lines would pierce but not touch the contour C drawn along the particle propagation channels – see the dashed line in Fig. 2. In classical electrodynamics,[6] the external magnetic field's effect on a particle with electric charge q is described by the *Lorentz force*

[4] See, e.g., a detailed discussion in EM Sec. 8.4.

[5] Here I have to mention the fascinating experiments (first performed in 1987 by C. Hong *et al.* with photons, and recently, in 2015, by R. Lopes *et al*., with non-relativistic particles – helium atoms) on the interference of de Broglie waves of *independent* but *identical* particles, in the same internal quantum state and virtually the same values of E and k. These experiments raise the important issue of particle *indistinguishability*, which will be discussed in Sec. 8.1.

[6] See, e.g., EM Sec. 5.1. Note that Eq. (14), as well as all other formulas of this course, are in the SI units.

$$\mathbf{F}_{\mathscr{B}} = q\mathbf{v}\times\mathscr{B}\,, \tag{3.14}$$

where $\mathscr{B}$ is the field value at the point of its particle's location, so for the experiment shown in Fig. 2, $\mathbf{F}_{\mathscr{B}} = 0$, and the field would not affect the particle motion at all. In quantum mechanics, this is not so, and the field does affect the probability density w, even if $\mathscr{B} = 0$ at all points where the wavefunction $\psi(\mathbf{r})$ is not equal to zero.

In order to describe this surprising effect, let us first develop a general framework for an account of electromagnetic field effects on a charged quantum particle, which will also give us some by-product results important for forthcoming discussions. To do that, we need to calculate the Hamiltonian of such a particle in electric and magnetic fields. For an electrostatic field, this is easy. Indeed, from classical electrodynamics[7] we know that this field may be represented as a gradient of its electrostatic potential ϕ,

$$\mathscr{E} = -\nabla\phi(\mathbf{r}), \tag{3.15}$$

so the force exerted by the field on a particle with electric charge q,

$$\mathbf{F}_{\mathscr{E}} = q\mathscr{E}, \tag{3.16}$$

may be described by adding the field-induced potential energy,

$$U(\mathbf{r}) = q\phi(\mathbf{r}), \tag{3.17}$$

to other possible components of the full potential energy. As was already discussed in Sec. 1.4, such potential energy may be included in the particle's Hamiltonian operator just by adding it to the kinetic energy operator – see Eq. (1.41).

However, the magnetic field's effect is peculiar: since its Lorentz force (14) is perpendicular to the classical particle's velocity, it cannot do any work on it:

$$d\mathscr{W}_{\mathscr{B}} \equiv \mathbf{F}_{\mathscr{B}}\cdot d\mathbf{r} = \mathbf{F}_{\mathscr{B}}\cdot\mathbf{v}dt = q(\mathbf{v}\times\mathscr{B})\cdot\mathbf{v}\,dt = 0, \tag{3.18}$$

and hence the field cannot be represented by any potential energy, so it may not be immediately clear how to account for it in the Hamiltonian. The crucial help comes from the analytical-mechanics approach to classical electrodynamics:[8] in the non-relativistic limit, the Hamiltonian function of a particle in an electromagnetic field looks like that in the electric field only:

$$H = \frac{mv^2}{2} + U = \frac{p^2}{2m} + q\phi\,; \tag{3.19}$$

however, the momentum $\mathbf{p} \equiv m\mathbf{v}$ that participates in this expression is now the difference

$$\mathbf{p} = \mathbf{P} - q\mathbf{A}\,. \tag{3.20}$$

Here $\mathbf{A}$ is the vector potential of the field, defined by the well-known relations:[9]

$$\mathscr{E} = -\nabla\phi - \frac{\partial\mathbf{A}}{\partial t}, \qquad \mathscr{B} = \nabla\times\mathbf{A}\,, \tag{3.21}$$

[7] Note that here (until Chapter 9) we are describing the *particle* quantum-mechanically but the *fields*, classically.
[8] See, e.g., EM Sec. 9.7, in particular, Eq. (9.196).
[9] See, e.g., EM Sec. 6.1, in particular Eqs. (6.7).

while **P** is the *canonical momentum*, whose Cartesian components may be calculated (in classics) from the Lagrangian function L by using the standard formula of analytical mechanics,

$$P_j \equiv \frac{\partial L}{\partial v_j}. \tag{3.22}$$

To emphasize the difference between the two momenta, $\mathbf{p} = m\mathbf{v}$ is frequently called the *kinematic momentum* (or "m**v**-momentum"). The distinction between **p** and $\mathbf{P} = \mathbf{p} + q\mathbf{A}$ becomes more clear if we notice that the vector potential is not *gauge-invariant*: according to the second of Eqs. (21), at the so-called *gauge transformation*

$$\mathbf{A} \to \mathbf{A} + \nabla\chi, \tag{3.23}$$

with an arbitrary single-valued scalar *gauge function* $\chi = \chi(\mathbf{r}, t)$, the magnetic field does not change. Moreover, according to the first of Eqs. (21), if we make the simultaneous replacement

$$\phi \to \phi - \frac{\partial \chi}{\partial t}, \tag{3.24}$$

the gauge transformation does not affect the electric field either. With that, the gauge function's choice does not affect the classical particle's equation of motion, and hence the velocity **v** and momentum **p**. Hence, the kinematic momentum is gauge-invariant, while **P** is not, because according to Eqs. (20) and (23), the introduction of χ changes it by $q\nabla\chi$.

Now the standard way of transfer to the wave mechanics is to use Eq. (1.26) for the operator of the canonical rather than the kinematic momentum:[10]

$$\boxed{\hat{\mathbf{P}} = -i\hbar\nabla}. \tag{3.25}$$

Canonical momentum: operator

Hence the Hamiltonian operator corresponding to the classical Hamiltonian function (19) is

$$\boxed{\hat{H} = \frac{1}{2m}\left(-i\hbar\nabla - q\mathbf{A}\right)^2 + q\phi \equiv -\frac{\hbar^2}{2m}\left(\nabla - i\frac{q}{\hbar}\mathbf{A}\right)^2 + q\phi}, \tag{3.26}$$

so the stationary Schrödinger equation (1.60) of a particle moving in an electromagnetic field (but otherwise free) is

Charged particle in EM field

$$\boxed{-\frac{\hbar^2}{2m}\left(\nabla - i\frac{q}{\hbar}\mathbf{A}\right)^2\psi + q\phi\psi = E\psi}, \tag{3.27}$$

We may now repeat all the calculations of Sec. 1.4 for the case $\mathbf{A} \neq 0$, and get the following generalized expression for the probability current density:

$$\mathbf{j} = \frac{\hbar}{2im}\left[\psi^*\left(\nabla - i\frac{q}{\hbar}\mathbf{A}\right)\psi - \text{c.c}\right] \equiv \frac{1}{2m}\left(\psi^*\hat{\mathbf{p}}\,\psi - \text{c.c.}\right) \equiv \frac{\hbar}{m}|\psi|^2\left(\nabla\varphi - \frac{q}{\hbar}\mathbf{A}\right). \tag{3.28}$$

We see that the current density is gauge-invariant (as required for any observable) only if at the transformation (23), the wavefunction's phase φ changes as

[10] The validity of this choice is clear from the fact that if the *kinetic* momentum was described by this differential operator, the Hamiltonian operator corresponding to the classical Hamiltonian function (19), and the corresponding Schrödinger equation would not describe the magnetic field effects at all.

$$\varphi \to \varphi + \frac{q}{\hbar}\chi \,. \tag{3.29}$$

This may be a point of conceptual concern: since quantum interference is described by the spatial dependence of the phase φ, can the observed interference pattern depend on the gauge function's choice? (That would not make any sense, because we may change the gauge in our mind.) Fortunately, this is not true, because according to Eq. (29), the spatial phase *difference* between two interfering paths, participating in Eq. (12), is gauge-transformed as

$$\varphi_{12} \to \varphi_{12} + \frac{q}{\hbar}(\chi_2 - \chi_1). \tag{3.30}$$

But χ has to be a single-valued function of coordinates; hence in the limit when the points 1 and 2 coincide, $\chi_1 = \chi_2$, so φ_{12} is gauge-invariant, and so is the interference pattern.

However, the difference φ_{12} *may be* affected by the magnetic field, even if it is localized outside the channels in which the particle propagates. Indeed, in this case, the field cannot affect the particle distribution across the channels, so, for an externally-fixed total flow of particles in each of them, we can take

$$\mathbf{j}(\mathbf{r})\Big|_{\mathscr{B}\neq 0} = \mathbf{j}(\mathbf{r})\Big|_{\mathscr{B}=0}\,, \tag{3.31}$$

and the last form of Eq. (28) yields

$$\nabla\varphi(\mathbf{r})\Big|_{\mathscr{B}\neq 0} = \nabla\varphi(\mathbf{r})\Big|_{\mathscr{B}=0} + \frac{q}{\hbar}\mathbf{A}\,. \tag{3.32}$$

Integrating this equation along the contour C (Fig. 2), for the phase difference between points 1 and 2 we get

$$\varphi_{12}\Big|_{\mathscr{B}\neq 0} = \varphi_{12}\Big|_{\mathscr{B}=0} + \frac{q}{\hbar}\oint_C \mathbf{A}\cdot d\mathbf{r}\,, \tag{3.33}$$

where the integral should be taken along the same contour C as before (in Fig. 2, from point 1, counterclockwise along the dashed line to point 2). But from classical electrodynamics, we know[11] that as points 1 and 2 tend to each other, i.e. the contour C becomes closed, the last integral is just the magnetic flux $\Phi \equiv \int \mathscr{B}_n d^2r$ through any smooth surface limited by this contour, so Eq. (33) may be rewritten as

AB effect

$$\boxed{\varphi_{12}\Big|_{\mathscr{B}\neq 0} = \varphi_{12}\Big|_{\mathscr{B}=0} + \frac{q}{\hbar}\Phi\,.} \tag{3.34a}$$

In terms of the interference pattern, this means a shift of interference fringes, proportional to the magnetic flux.

This phenomenon is usually called the "Aharonov-Bohm" (or just the *AB*) *effect*.[12] For particles with a single elementary charge, $q = \pm e$, this result is frequently represented as

[11] See, e.g., EM Sec. 5.3.

[12] I prefer the latter, less personable name because the effect had been actually predicted by Werner Ehrenberg and Raymond Siday in 1949, i.e. well before it was rediscovered (also theoretically) by Y Aharonov and D. Bohm in 1959. To be fair to Aharonov and Bohm, it was their work that triggered a wave of interest in the phenomenon, leading to its first experimental observation by Robert G. Chambers in 1960 and several other groups soon after that. Later, the experiments were improved using ferromagnetic cores and/or superconducting shielding to provide a better separation between the electrons and the applied field – as in the work whose result is shown in Fig. 3.

$$\varphi_{12}\Big|_{\mathcal{B}\neq 0} = \varphi_{12}\Big|_{\mathcal{B}=0} \pm 2\pi\frac{\Phi}{\Phi_0'}, \tag{3.34b}$$

where the fundamental constant $\Phi_0' \equiv 2\pi\hbar/e \approx 4.14\times10^{-15}$ Wb has the meaning of the magnetic flux necessary to change φ_{12} by 2π, i.e. to shift the interference pattern (11) by one period, and is called the *normal magnetic flux quantum* – "normal" because of the reasons we will soon discuss.

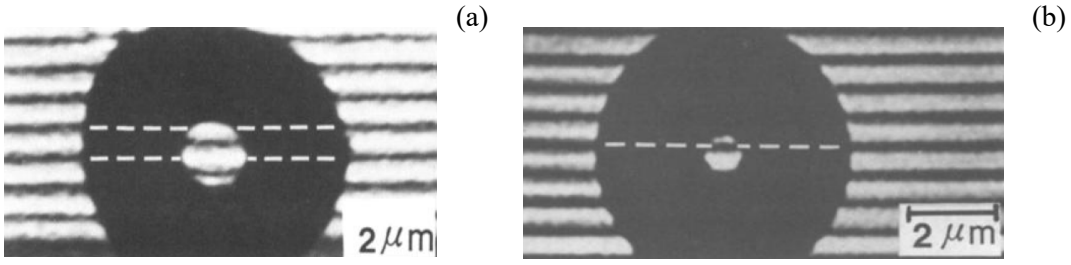

Fig. 3.3. Typical results of a two-paths interference experiment by A. Tonomura *et al*., *Phys. Rev. Lett*. **56**, 792 (1986), showing the AB effect for electrons shielded from the applied magnetic field. In this particular experimental geometry, the AB effect produces a relative shift of the interference patterns inside and outside the dark ring. (a) $\Phi = \Phi_0'/2$, (b) $\Phi = \Phi_0'$. © 1986 APS.

The AB effect may be "almost explained" classically, in terms of Faraday's electromagnetic induction. Indeed, a change $\Delta\Phi$ of magnetic flux in time induces a vortex-like electric field $\Delta\mathscr{E}$ around it. That field is *not* restricted to the magnetic field's location, i.e. may reach the particle's trajectories. The field's magnitude (or rather of its integral along the contour C) may be readily calculated by integration of the first of Eqs. (21):

$$\Delta V \equiv \oint_C \Delta\mathscr{E}\cdot d\mathbf{r} = -\frac{d\Phi}{dt}. \tag{3.35}$$

I hope that in this expression the reader readily recognizes the integral ("undergraduate") form of Faraday's induction law.[13] To calculate the effect of this electric field on the particles, let us assume that the variable separation described by Eq. (1.57) may be applied to the endpoints 1 and 2 of the particle's alternative trajectories as two independent systems,[14] and that the magnetic flux' change by a certain amount $\Delta\Phi$ does not change the spatial factors $\psi_{1,2}$, provided that the phases $\varphi_{1,2}$ are included into the time-dependent factors $a_{1,2}$. Then we may repeat the arguments that were used in Sec. 1.6 at the discussion of the Josephson effect, and since the change (35) leads to the change of the potential energy difference $\Delta U = q\Delta V$ between the two points, we may rewrite Eq. (1.72) as

$$\frac{d\varphi_{12}}{dt} = -\frac{\Delta U}{\hbar} = -\frac{q}{\hbar}\Delta V = \frac{q}{\hbar}\frac{d\Phi}{dt}. \tag{3.36}$$

Integrating this relation over the time of the magnetic field's change, we get

[13] See, e.g., EM Sec. 6.1.

[14] This assumption may seem a little bit of a stretch, but the resulting relation (37) may be indeed proven for a rather realistic model, though that would take more time/space than I can afford.

$$\Delta\varphi_{12} = \frac{q}{\hbar}\Delta\Phi\,, \tag{3.37}$$

– superficially, the same result as given by Eq. (34).

However, this interpretation of the AB effect is limited. Indeed, it requires the particle to be in the system (on the way from the source to the detector) during the flux change, i.e. when the induced electric field $\mathscr{E}$ may affect its dynamics. On the contrary, Eq. (34) predicts that the interference pattern would shift even if the field change has been made when there was no particle in the system, and hence the field $\mathscr{E}$ could not be felt by it. Experiment confirms the latter conclusion. Hence, there is *something* in the space where a particle propagates (i.e., outside of the magnetic field region), that transfers the information about even the static magnetic field to the particle. The standard interpretation of this surprising fact is as follows: the vector potential **A** is not just a convenient mathematical tool, but a physical reality (just as its scalar counterpart ϕ is), despite the large freedom of choice we have in prescribing specific spatial and temporal dependences of these potentials without affecting any observable – see Eqs. (23)-(24).

To conclude this section, let me briefly discuss the very interesting form taken by the AB effect in superconductivity. To be applied to this case, our results require two changes. The first one is simple: since superconductivity may be interpreted as a result of the Bose-Einstein condensate of Cooper pairs with electric charge $q = -2e$, Φ_0' has to be replaced by the so-called *superconducting flux quantum*[15]

Super-conducting flux quantum

$$\boxed{\Phi_0 \equiv \frac{\pi\hbar}{e} \approx 2.07\times10^{-15}\ \text{Wb} = 2.07\times10^{-7}\ \text{Gs}\cdot\text{cm}^2.} \tag{3.38}$$

Second, since the pairs are Bose particles and are all condensed in the same (ground) quantum state described by the same wavefunction, the total electric current density, proportional to the probability current density j, may be extremely large – in practical superconducting materials, up to ~10^{12} A/m^2. In these conditions, one cannot neglect the contribution of that current into the magnetic field and hence into its flux Φ, which (according to the Lenz rule of the Faraday induction law) tries to compensate for changes in external flux. To see possible results of this contribution, let us consider a closed superconducting loop (Fig. 4). Due to the Meissner effect (which is just another version of the flux self-compensation), the current and magnetic field penetrate into a superconductor by only a small distance (called the *London penetration depth*) $\delta_L \sim 10^{-7}$ m.[16] If the loop is made of a superconducting "wire" that is considerably thicker than δ_L, we may draw a contour deep inside the wire, at which the current density is negligible. According to the last form of Eq. (28), everywhere at the contour,

$$\nabla\varphi - \frac{q}{\hbar}\mathbf{A} = 0\,. \tag{3.39}$$

Integrating this equation along the contour as before (in Fig. 4, from some point 1, all the way around the ring to the virtually coinciding point 2), we need to have the phase difference φ_{12} equal to $2\pi n$, because the wavefunction $\psi \propto \exp\{i\varphi\}$ at the initial and final points 1 and 2 should be "essentially" the same, i.e. produce the same observables. As a result, we get

[15] One more bad, though common term: a wire may (super)conduct, but a quantum hardly can!
[16] For more detail, see EM Sec. 6.4.

$$\Phi \equiv \oint_C \mathbf{A}\cdot d\mathbf{r} = \frac{\hbar}{q} 2\pi n \equiv n\Phi_0 . \tag{3.40}$$

Flux quantization

This is the famous *flux quantization effect*,[17] which justifies the term "magnetic flux quantum" for the constant Φ_0 given by Eq. (38).

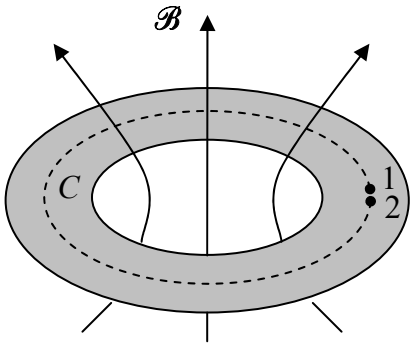

Fig. 3.4. The magnetic flux quantization in a superconducting loop (schematically).

Here I have to mention the very interesting effects of "flux semi-quantization" that arise when superconductor loops are closed with Josephson junctions, forming the so-called *Superconducting QUantum Interference Devices* ("SQUIDs"). Such devices may be used, in particular, for supersensitive magnetometry and ultrafast low-power computing,[18] and are currently explored as a possible basis for quantum computation and cryptography – see Sec. 8.5 below.

3.2. Landau levels and quantum Hall effect

In the last section, we have used the Schrödinger equation (27) for an analysis of static magnetic field effects in "almost-1D", circular geometries shown in Figs. 1, 2, and 4. However, this equation describes very interesting effects in fully higher dimensions as well, especially in the 2D case. Let us consider a quantum particle free to move within the [*x, y*] plane only (say, due to its strong confinement in the perpendicular direction *z* – see the discussion at the beginning of Sec. 2.1). In this case, Eq. (27) reduces to a similar equation but with the Laplace operator acting only in the directions *x* and *y*:

$$-\frac{\hbar^2}{2m}\left(\mathbf{n}_x\frac{\partial}{\partial x}+\mathbf{n}_y\frac{\partial}{\partial y}-i\frac{q}{\hbar}\mathbf{A}\right)^2\psi = E\psi . \tag{3.41}$$

Let us find its solutions for the simplest case when the applied static magnetic field is uniform and normal to the motion plane:

$$\mathscr{B} = \mathscr{B}\mathbf{n}_z . \tag{3.42}$$

According to the second of Eqs. (21), this relation imposes the following restriction on the choice of the vector potential:

$$\frac{\partial A_y}{\partial x}-\frac{\partial A_x}{\partial y} = \mathscr{B} , \tag{3.43}$$

[17] It was predicted in 1949 by Fritz London and experimentally discovered (independently and virtually simultaneously) in 1961 by two experimental groups: B. Deaver and W. Fairbank, and R. Doll and M. Näbauer.
[18] A brief review of these applications, and recommendations for further reading may be found in EM Sec. 6.5.

but the gauge transformations still give us a lot of freedom in its choice. The natural axially symmetric form, $\mathbf{A} = \mathbf{n}_\varphi \rho \mathscr{B}/2$, where $\rho = (x^2 + y^2)^{1/2}$ is the distance from some z-axis, leads to cumbersome math. In 1930, L. Landau realized that the energy spectrum of Eq. (41) may be obtained by making a much simpler, though very counter-intuitive gauge choice:

$$A_x = 0, \quad A_y = \mathscr{B}(x - x_0), \tag{3.44}$$

(with arbitrary x_0), which evidently satisfies Eq. (43), though ignores the physical symmetry of the x and y directions for the field (42).

Now, expanding the eigenfunction into the Fourier integral in the y-direction:

$$\psi(x,y) = \int X_k(x) \exp\{ik(y - y_0)\} dk, \tag{3.45}$$

we see that for each component of this expansion, Eq. (41) yields a specific equation

$$-\frac{\hbar^2}{2m}\left\{\mathbf{n}_x \frac{d}{dx} + i\mathbf{n}_y\left[k - \frac{q}{\hbar}\mathscr{B}(x - x_0)\right]\right\}^2 X_k = EX_k. \tag{3.46}$$

Since the two vectors inside the curly brackets are mutually perpendicular, its square has no cross-terms, so Eq. (46) reduces to

$$-\frac{\hbar^2}{2m}\frac{d^2}{dx^2}X_k + \frac{q^2}{2m}\mathscr{B}^2(x - x_0')^2 X_k = EX_k, \qquad \text{where } x_0' \equiv x_0 + \frac{\hbar k}{q\mathscr{B}}. \tag{3.47}$$

But this 1D Schrödinger equation is identical to Eq. (2.261) for a 1D harmonic oscillator,[19] with the center at point x_0', and the frequency ω_0 equal to

$$\omega_c = \frac{|q\mathscr{B}|}{m}. \tag{3.48}$$

In the last expression, it is easy to recognize the *cyclotron frequency* of the classical particle's rotation in the magnetic field. (It may be readily obtained using the 2nd Newton law for a circular orbit of radius r,

$$m\frac{v^2}{r} = F_{\mathscr{B}} \equiv qv\mathscr{B}, \tag{3.49}$$

and noting that the resulting ratio $v/r = |q\mathscr{B}|/m$ is just the radius-independent angular velocity ω_c of the particle's rotation.) Hence, the energy spectrum for each Fourier component of the expansion (45) is the same:

Landau levels

$$E_n = \hbar\omega_c\left(n + \frac{1}{2}\right), \tag{3.50}$$

independent of x_0, y_0, and k.

[19] This result may become a bit less puzzling if we recall that at the classical circular cyclotron motion of a particle, each of its Cartesian coordinates, including x, performs sinusoidal oscillations with frequency (48), just as a 1D harmonic oscillator with this frequency.

Hence, this is a good example of a highly *degenerate* system: for each eigenvalue E_n, there are many similarly-structured eigenfunctions that differ by the positions $\{x_0, y_0\}$ of their centers and the rate k of their phase change along the y-axis. They may be used to assemble a large variety of linear combinations, including 2D wave packets whose centers move along classical circular orbits. Note, however, that the radius of such rotation cannot be smaller than the so-called *Landau radius*,

$$r_L \equiv \left(\frac{\hbar}{m\omega_c}\right)^{1/2} \equiv \left(\frac{\hbar}{|q\mathscr{B}|}\right)^{1/2}, \quad (3.51)$$

Landau radius

which characterizes the minimum size of the wave packet, and follows from Eq. (2.276) after the replacement $\omega_0 \to \omega_c$. This radius is remarkably independent of the particle mass, and may be interpreted in the following way: the scale $\mathscr{B}A_{min}$ of the applied magnetic field's flux through the effective area $A_{min} = 2\pi r_L^2$ of the smallest wave packet is just one normal flux quantum $\Phi_0' \equiv 2\pi\hbar/|q|$.

A detailed analysis of such wave packets (for which we would not have time in this course) proves, in particular, the virtually evident fact: the applied magnetic field does not change the *average* density dN_2/dE of different 2D states on the energy scale, given by Eq. (1.92), but just "assembles" the states them on the Landau levels (see Fig. 5a), so the number of different orbital states on each Landau level (per unit area) is

$$n_L \equiv \frac{N_2}{A} = \frac{1}{A}\frac{dN_2}{dE}\Big|_{\mathscr{B}=0}\Delta E \equiv \frac{1}{A}\frac{dN_2}{d^2k}\Big|_{\mathscr{B}=0}\frac{d^2k}{dk}\frac{1}{dE/dk}\Delta E = \frac{1}{A}\frac{A}{(2\pi)^2}2\pi k\frac{1}{\hbar^2 k/m}\hbar\omega_c \equiv \frac{|q\mathscr{B}|}{2\pi\hbar}. \quad (3.52)$$

This expression may again be interpreted in terms of magnetic flux quanta: $n_L\Phi_0' = \mathscr{B}$, i.e. there is one particular state on each Landau level per each normal flux quantum.

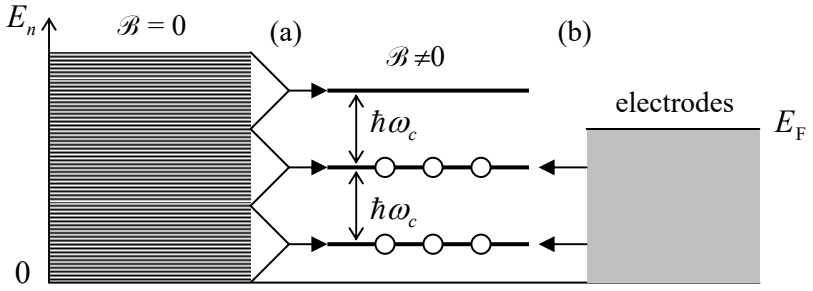

Fig. 3.5. (a) The "assembly" of 2D states on Landau levels, and (b) filling the levels with electrons at the quantum Hall effect.

The most famous application of the Landau levels picture is the explanation of the *quantum Hall effect*[20]. It is usually observed in the "Hall bar" geometry sketched in Fig. 6, where electric current I is passed through a rectangular conducting sample placed into magnetic field $\mathscr{B}$ perpendicular to the sample's plane. The classical analysis of the effect may be based on the notion of the Lorentz force (14). As the magnetic field is turned on, this force starts to deviate the effective charge carriers (electrons or holes) from their straight motion between the electrodes, bending them toward the insulated sides of the

[20] It was first observed in 1980 by a group led by Klaus von Klitzing, while the classical version (54) of the effect was first observed by Edwin Hall a century earlier – in 1879.

bar (in Fig. 6, parallel to the x-axis). Here the carriers accumulate, generating a gradually increasing electric field $\mathscr{E}$ until its force (16) exactly balances the Lorentz force (14):

$$q\mathscr{E}_y = qv_x\mathscr{B}, \tag{3.53}$$

where v_x is the drift velocity of the carriers along the bar (Fig. 6), providing the sustained balance condition $\mathscr{E}_y/v_x = \mathscr{B}$ at each point of the sample.

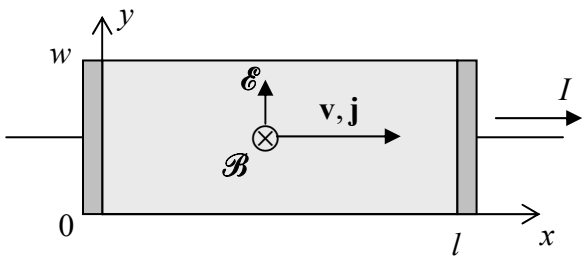

Fig. 3.6. The Hall bar geometry. Darker rectangles show external (3D) electrodes.

With n_2 carriers per unit area, in a sample of width w, this balance condition yields the following classical expression for the so-called *Hall resistance* R_H, remarkably independent of w and l:

Classical Hall effect

$$R_H \equiv \frac{V_y}{I_x} = \frac{\mathscr{E}_y w}{qn_2 v_x w} = \frac{\mathscr{B}}{qn_2}. \tag{3.54}$$

This formula is broadly used in practice for the measurement of the 2D density n_2 of the charge carriers and of the carrier type: electrons with $q = -e < 0$, or holes with the effective charge $q = +e > 0$.

However, in experiments with high-quality (low-defect) 2D samples, at sub-kelvin temperatures[21] and high magnetic fields, the linear growth of R_H with $\mathscr{B}$, described by Eq. (54), is interrupted by virtually horizontal plateaus (Fig. 7).

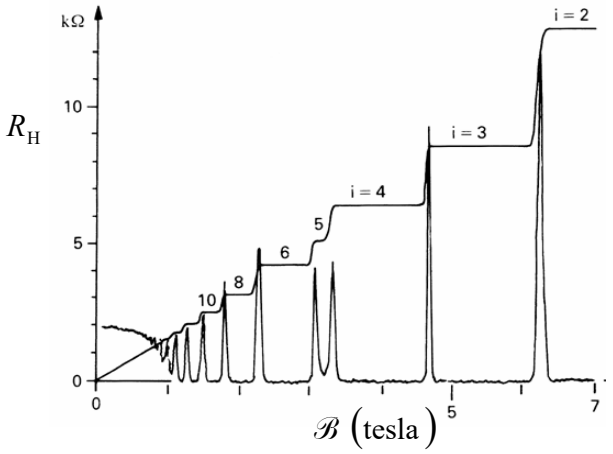

Fig. 3.7. A typical record of the integer quantum Hall effect. The lower trace (with sharp peaks) shows the diagonal element, V_x/I_x, of the resistance tensor. (Adapted from https://www.nobelprize.org/nobel_prizes/physics/laureates/1998/press.html).

[21] In some systems, such as the *graphene* (virtually perfect 2D sheets of carbon atoms – see Sec. 4 below), the effect may be more stable to thermal fluctuations, due to their topological properties, so it may be observed even at room temperature – see, e.g., K. Novoselov *et al., Science* **315,** 1379 (2007). Note also that in some spontaneously-magnetized ferromagnetic layers, the quantum Hall effect may be observed in the absence of an *external* magnetic field – see, e.g., M. Götz *et al.*, *Appl. Phys. Lett.* **112**, 072102 (2018) and references therein.

Most remarkably, the experimental values of R_H on these plateaus are reproduced with extremely high accuracy (up to ~10^{-9}) from sample to sample.[22] They are described by the following formula:

$$R_H = \frac{1}{i} R_K, \qquad \text{where } R_K \equiv \frac{2\pi\hbar}{e^2}, \tag{3.55}$$

Quantum Hall effect

with the following value:

$$R_K \approx 25.812\,807\,459\,304\,\text{k}\Omega, \tag{3.56}$$

and i is (only until the end of this section, following tradition!) the plateau number, i.e. a real integer.

This effect may be explained using the Landau-level picture. The 2D sample is typically in weak contact with 3D electrodes whose conductivity electrons, at low temperatures, fill all states with energies below a certain Fermi energy E_F – see Fig. 5b. According to Eqs. (48) and (50), as $\mathscr{B}$ is increased, the spacing $\hbar\omega_c$ between the Landau levels increases proportionately, so fewer and fewer of these levels are below E_F (and hence in equilibrium, all their states are filled), and within certain ranges of field variations, the number i of the filled levels is constant. (In the schematic Fig. 5b, $i = 2$.) So, plugging $n_2 = in_L$ and $q = -e$ into Eq. (54), and using Eq. (52) for n_L, we get

$$R_H = \frac{1}{i}\frac{\mathscr{B}}{qn_L} = \frac{1}{i}\frac{2\pi\hbar}{e^2}, \tag{3.57}$$

i.e. exactly the experimental result (55).

This admittedly oversimplified explanation of the quantum Hall effect does not take into account at least two important factors:

(i) the nonuniformity of the background potential $U(x, y)$ in realistic Hall bar samples, and the role of the quasi-1D *edge channels* this nonuniformity produces;[23] and

(ii) the Coulomb interaction of the electrons, in high-quality samples leading to the formation of R_H plateaus with not only integer but also fractional values of i (1/3, 2/5, 3/7, etc.).[24]

Unfortunately, a thorough discussion of these very interesting features is well beyond the framework of this course.[25,26]

---

[22] Due to this high accuracy (which is a rare exception in solid-state physics!), the *von Klitzing constant* R_K was used in metrology for the "legal" ohm's definition. Since 2018, the values of $\hbar$ and e, and hence of R_K, are considered exactly known and fixed – see *Appendix UCA*: *Selected Units and Constants.*

[23] Such quasi-1D regions, with the width of the order of r_L, form along the lines where the Landau levels cross the Fermi surface and are actually responsible for all the electron transfer at the quantum Hall effect (giving the pioneering example of what is nowadays called the *topological insulators*). The particle motion along these channels is effectively one-dimensional; because of this, it is unaffected by modest unintentional nonuniformities of the potential $U(x, y)$. This fact is responsible for the extraordinary accuracy of Eq. (55).

[24] This *fractional quantum Hall effect* was discovered in 1982 by D. Tsui, H. Stormer, and A. Gossard. In contrast, the effect described by Eq. (55) with integer i (Fig. 7) is now called the *integer quantum Hall effect*.

[25] For a comprehensive discussion of these effects, I can recommend either the monograph by D. Yoshioka, *The Quantum Hall Effect*, Springer, 1998, or the review by D. Yennie, *Rev. Mod. Phys.* **59,** 781 (1987). (See also the later publications cited above.)

[26] Note also that the quantum Hall effect is sometimes discussed in terms of the so-called *Berry phase*, one of the *geometric phases* – the notion apparently pioneered by S. Pancharatnam in 1956. However, in the "usual" quantum Hall effect the Berry phase equals zero, and I believe that this concept should be saved for the discussion of more topologically involved systems. Unfortunately, I will have no time/space for a discussion of such systems

3.3. Scattering and diffraction

The second class of quantum effects that become richer in multi-dimensional spaces, is typically referred to as either *diffraction* or *scattering* – depending on the context. In classical physics, these two terms are used to describe very different effects. The term "diffraction" is used for the interference of the *waves* re-emitted by elementary components of extended objects, under the effect of a single incident *wave*.[27] On the other hand, the term "scattering" is used in classical mechanics to describe the result of the interaction of a beam of *particles*[28] incident upon an object called the *scatterer* – see Fig. 8.

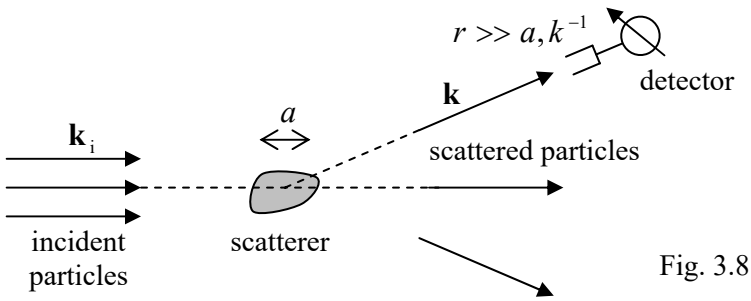

Fig. 3.8. Scattering (schematically).

Most commonly, the detector of the scattered particles is located at a large distance $r >> a$ from the scatterer. In this case, the main observable independent of r is the *flux* (the number per unit time) of particles scattered in a certain direction, i.e. their flux per unit solid angle Ω. Since it is proportional to the incident flux of particles per unit area, the efficiency of scattering in a particular direction may be characterized by the ratio of these two fluxes. This ratio is called the *differential cross-section* of the scatterer:

Differential cross-section

$$\frac{d\sigma}{d\Omega} \equiv \frac{\text{flux of scatterd particles per unit solid angle}}{\text{flux of incident particles per unit area}}. \tag{3.58}$$

Such terminology and notation stem from the fact that the integral of $d\sigma/d\Omega$ over all scattering angles,

Total cross-section

$$\sigma \equiv \oint \frac{d\sigma}{d\Omega} d\Omega = \frac{\text{total flux of scattered particles}}{\text{incident flux per per unit area}}, \tag{3.59}$$

evidently having the dimensionality of area, has a simple interpretation as the *total cross-section* of scattering. For the simplest case when a solid object scatters all classical particles hitting its surface but does not affect the particles flying by it, σ is just the geometric area of the scatterer, as observed from the direction of the incident particles. In classical mechanics, we first calculate the particle's scattering angle as a function of its *impact parameter b* and then average the result over all values of b, considered random. [29]

---

in this course, and have to refer the interested reader to special literature – see, e.g., either the key original papers collected by A. Shapere and F. Wilczek, *Geometric Phases in Physics*, *World Scientific*, 1992, or the monograph by A. Bohm *et al*., *The Geometric Phase in Quantum Systems*, Springer, 2003.

[27] The notion of interference is very close to diffraction, but the former term is typically reserved for the wave re-emission by just a few components, such as two slits in the Young experiment – see Figs. 1 and 2. A detailed discussion of diffraction and interference of electromagnetic waves may be found in EM Secs. 8.3-8.8.

[28] In the classical wave theory, the term "scattering" is typically reserved for wave interaction with disordered sets of small objects – see, e.g., EM Sec. 8.3.

[29] See, e.g., CM Sec. 3.5.

In quantum mechanics, due to the particle/wave duality, a relatively broad, parallel beam of incident particles of the same energy E may be fairly represented with a plane de Broglie wave (1.88):

$$\psi_{\rm i} = \left|\psi_{\rm i}\right| \exp\{i\mathbf{k}_{\rm i}\cdot\mathbf{r}\}, \tag{3.60}$$

with the free-space wave number $k_{\rm i} = k = (2mE)^{1/2}/\hbar$. As a result, the particle scattering becomes a synonym of the de Broglie wave diffraction, and (somewhat counter-intuitively) the description of the effect becomes simpler, excluding the notion of the impact parameter. Indeed, the wave (60) corresponds to a constant probability current density (1.49):

$$\mathbf{j}_{\rm i} = \left|\psi_{\rm i}\right|^2 \frac{\hbar}{m}\mathbf{k}_{\rm i}, \tag{3.61}$$

which is exactly the flux of incident particles per unit area that is used in the denominator of Eq. (58), while the numerator of that fraction may be simply expressed via the probability current density $\mathbf{j}_{\rm s}$ of the scattered de Broglie waves:

$$\frac{d\sigma}{d\Omega} = \frac{j_{\rm s} r^2}{j_{\rm i}}, \qquad \text{at } r >> a. \tag{3.62}$$

Hence the task of finding $d\sigma/d\Omega$ is reduced to the calculation of $j_{\rm s}$ at sufficiently large distances r from the scatterer. For the *elastic* scattering (when the energy E of the scattered particles is the same as that of the incident particles) this may be done by solving the stationary Schrödinger equation (1.65). Let us rewrite it in the form

$$\left(E - \hat{H}_0\right)\psi = U(\mathbf{r})\psi, \qquad \text{with } \hat{H}_0 \equiv -\frac{\hbar^2}{2m}\nabla^2, \text{ and } E = \frac{\hbar^2 k^2}{2m}, \tag{3.63}$$

where the potential energy $U(\mathbf{r})$ describes the scatterer's effect. Looking for the solution of Eq. (62) in the natural form

$$\psi = \psi_{\rm i} + \psi_{\rm s}, \tag{3.64}$$

where $\psi_{\rm i}$ is the incident wave (60) and $\psi_{\rm s}$ has the sense of the scattered wave, and taking into account that the former wave satisfies the free-space Schrödinger equation

$$\hat{H}_0\psi_{\rm i} = E\psi_{\rm i}, \tag{3.65}$$

we may reduce Eq. (63) to either of the following equivalent forms:

$$\left(E - \hat{H}_0\right)\psi_{\rm s} = U(\mathbf{r})(\psi_i + \psi_{\rm s}), \qquad \left(\nabla^2 + k^2\right)\psi_{\rm s} = \frac{2m}{\hbar^2}U(\mathbf{r})\psi. \tag{3.66}$$

For applications, an integral version of this equation is frequently more convenient. To derive it, we may look at the second of Eqs. (66) as a linear inhomogeneous differential equation for the function $\psi_{\rm s}$, thinking of its right-hand side as a known "source". The solution of such an equation obeys the linear superposition principle, i.e. we may represent it as the sum of the waves outcoming from all elementary volumes d^3r' of the scatterer. Mathematically, this sum may be expressed as either

$$\psi_{\rm s}(\mathbf{r}) = \frac{2m}{\hbar^2}\int U(\mathbf{r}')\psi(\mathbf{r}')G(\mathbf{r},\mathbf{r}')d^3r', \tag{3.67a}$$

or, equivalently, as[30]

$$\psi(\mathbf{r}) = \psi_i(\mathbf{r}) + \frac{2m}{\hbar^2}\int U(\mathbf{r}')\psi(\mathbf{r}')G(\mathbf{r},\mathbf{r}')d^3r', \tag{3.67b}$$

where $G(\mathbf{r}, \mathbf{r}')$ is the *spatial Green's function*, defined as such an elementary, spherically symmetric response of the 3D Helmholtz equation to a point source, i.e. the outward-propagating solution of the following equation[31]

$$\left(\nabla^2 + k^2\right)G = \delta(\mathbf{r} - \mathbf{r}'). \tag{3.68}$$

But we already know such a solution of this equation – see Eq. (7) and its discussion:

$$G(\mathbf{r},\mathbf{r}') = \frac{f_+}{R}e^{ikR}, \qquad \text{where } \mathbf{R} \equiv \mathbf{r} - \mathbf{r}', \tag{3.69}$$

so we need just to calculate the coefficient f_+ for Eq. (68). This can be done in several ways, for example by noticing that at $R << k^{-1}$, the second term on the left-hand side of Eq. (68) is negligible, so it is reduced to the well-known Poisson equation with a delta-functional right-hand side, which describes, for example, the electrostatic potential induced by a point electric charge. Either recalling the Coulomb law or applying the Gauss theorem,[32] we readily get the asymptote

$$G \to -\frac{1}{4\pi R}, \qquad \text{at } kR << 1, \tag{3.70}$$

which is compatible with Eq. (69) only if $f_+ = -1/4\pi$, i.e. if

$$G(\mathbf{r},\mathbf{r}') = -\frac{1}{4\pi R}e^{ikR}. \tag{3.71}$$

Plugging this result into Eq. (67a), we get the following formal solution of Eq. (66):

Scattering problem: formal solution

$$\boxed{\psi_s(\mathbf{r}) = -\frac{m}{2\pi\hbar^2}\int U(\mathbf{r}')\frac{\psi(\mathbf{r}')}{R}e^{ikR}d^3r'.} \tag{3.72}$$

Note that if the function $U(\mathbf{r})$ is smooth, the singularity in the denominator is integrable (i.e. not dangerous); indeed, the contribution of a sphere with some radius $\mathcal{R} \to 0$, with the center at point $\mathbf{r}'$, into this integral scales as

$$\int_{R<\mathcal{R}} \frac{d^3R}{R} \equiv 4\pi\int_0^{\mathcal{R}} \frac{R^2dR}{R} \equiv 4\pi\int_0^{\mathcal{R}} RdR = 2\pi\mathcal{R}^2 \to 0. \tag{3.73}$$

So far, our result (72) is exact, but its apparent simplicity is deceiving because the wavefunction ψ on its right-hand side generally includes not only the incident wave ψ_I but also the scattered wave ψ_s

[30] This formula is sometimes called the *Lipmann-Schwinger equation,* though more frequently this term is reserved for either its operator form or the resulting equation for the spatial Fourier components of ψ and ψ_i.

[31] Please notice both the similarity and difference between this Green's function and the propagator discussed in Sec. 2.1. In both cases, we use the linear superposition principle to solve wave equations, but while Eq. (67) gives the solution of the *inhomogeneous* equation (66), Eq. (2.44) does that for a *homogeneous* Schrödinger equation. In the latter case, the elementary wave sources are the elementary parts of the initial wavefunction, rather than of the equation's right-hand side as in our current problem.

[32] See, e.g., EM Sec. 1.2.

– see Eq. (64). The most straightforward, and most common simplification of this problem, called the *Born approximation*,[33] is possible if the scattering potential $U(\mathbf{r})$ is in some sense small. (We will derive the quantitative condition of this smallness in a minute.) Since at $U(\mathbf{r}) = 0$, the scattering wave ψ_s has to disappear, at small but non-zero $U(\mathbf{r})$, $|\psi_s|$ has to be much smaller than $|\psi_i|$. In this case, on the right-hand side of Eq. (73), we may ignore ψ_s in comparison with ψ_i, getting

$$\psi_s(\mathbf{r}) = -\frac{m}{2\pi\hbar^2}|\psi_i|\int U(\mathbf{r}')\frac{\exp\{i\mathbf{k}_i\cdot\mathbf{r}'\}}{R}e^{ikR}d^3r'. \qquad (3.74)$$

Born approximation

Actually, Eq. (74) gives us even *more* than we wanted: it evaluates the scattered wave at *any* point, including those within of the scattering object, while to spell out Eq. (62), we only need to find the wave *far* from the scatterer, at $r \to \infty$. However, before going to that limit, we can use Eq. (74) to find a quantitative criterion of the Born approximation's validity. For that, let us estimate the magnitude of the right-hand side of this equation for a scatterer of a linear size $\sim a$, and the potential magnitude's scale U_0. The results are different in the following two limits:

(i) If $ka << 1$, then inside the scatterer (i.e., at distances $\Delta r' \sim a$), both $\exp\{i\mathbf{k}\cdot\mathbf{r}'\}$ and the second exponent under the integral in Eq. (74) change little, and a crude but fair estimate of the solution's magnitude is

$$|\psi_s| \sim \frac{m}{2\pi\hbar^2}|\psi_i|U_0 a^2. \qquad (3.75)$$

(ii) In the opposite limit $ka >> 1$, the function under the integral is nearly periodic in one of the spatial directions (that of the incident wave's propagation), so the net integral accumulates only on distances of the order of the de Broglie wavelength, $\sim k^{-1}$, and the integral is correspondingly smaller:

$$|\psi_s| \sim \frac{m}{2\pi\hbar^2}|\psi_i|U_0\frac{a^2}{ka}. \qquad (3.76)$$

These relations allow us to spell out the Born approximation's condition, $|\psi_s| << |\psi_I|$, as

$$U_0 << \frac{\hbar^2}{ma^2}\max[ka, 1]. \qquad (3.77)$$

In the fraction on the right-hand side of this relation, we may readily recognize the scale of the kinetic (quantum-confinement) energy E_a of the particle inside a potential well of a size of the order of a, so the Born approximation is valid essentially if the potential energy of particle's interaction with the scatterer is smaller than E_a. Note, however, that the estimate (76) is not valid in some special situations when the effects of scattering *accumulate* in some direction. This is frequently the case for small angles θ of scattering by extended objects, when $ka >> 1$, but $ka\theta \lesssim 1$.

[33] Named after M. Born, who was the first to apply this approximation in quantum mechanics. However, the basic idea of this approach had been developed much earlier (in 1881) by Lord Rayleigh in the context of electromagnetic wave scattering – see, e.g., EM Sec. 8.3. Note also that the contents of that section repeat some aspects of our current discussion – perhaps regrettably but unavoidably so, because the Born approximation is a centerpiece of the theory of scattering/diffraction for both the electromagnetic waves and the de Broglie waves. Hence I felt I had to cover it in this course for the benefit of the readers who skipped the EM part of my series.

Now let us proceed to large distances $r >> r' \sim a$, and simplify Eq. (74) using an approximation similar to the dipole expansions in electrodynamics.[34] Namely, in the denominator's R, we may ignore r' in comparison with the much larger r, but the exponents require more care, because even if $r' \sim a << r$, the product $kr' \sim ka$ may still be of the order of 1. As Fig. 9a shows, in the first approximation in r', we may take

$$R \equiv |\mathbf{r} - \mathbf{r}'| \approx r - \mathbf{n}_r \cdot \mathbf{r}', \tag{3.78}$$

and since the directions of the vectors $\mathbf{k}$ and $\mathbf{r}$ coincide, i.e. $\mathbf{k} = k\mathbf{n}_r$, we get

$$kR \approx kr - \mathbf{k} \cdot \mathbf{r}', \quad \text{i.e. } e^{ikR} \approx e^{ikr} e^{-i\mathbf{k}\cdot\mathbf{r}'}. \tag{3.79}$$

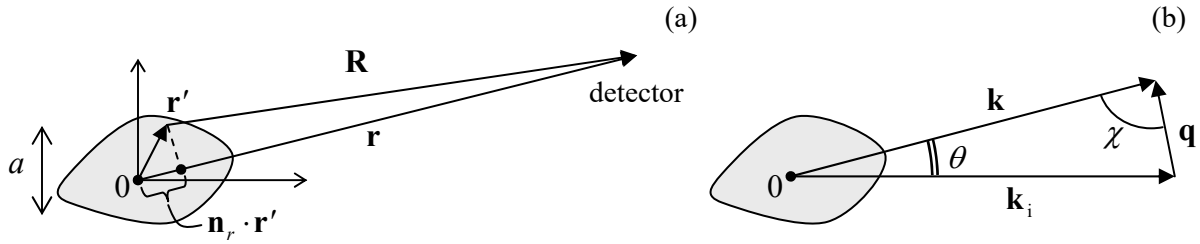

Fig. 3.9. (a) The long-range expansion of R, and (b) the definitions of $\mathbf{q}$, χ, and θ.

With this replacement, Eq. (74) yields

$$\psi_s(\mathbf{r}) = -\frac{m}{2\pi\hbar^2}\frac{|\psi_i|}{r} e^{ikr} \int U(\mathbf{r}') \exp\{-i(\mathbf{k} - \mathbf{k}_i)\cdot\mathbf{r}'\} d^3r'. \tag{3.80}$$

This relation is a particular case of a more general formula[35]

Scattering function: definition

$$\psi_s = |\psi_i| \frac{f(\mathbf{k}, \mathbf{k}_i)}{r} e^{ikr}, \tag{3.81}$$

where $f(\mathbf{k}, \mathbf{k}_i)$ is called the *scattering function*.[36] The physical sense of this function becomes clear from the calculation of the corresponding probability current density $\mathbf{j}_s$. For that, generally, we need to use Eq. (1.47) with the gradient operator having all spherical-coordinate components.[37] However, at $kr >> 1$, the main contribution to $\nabla\psi_s$, proportional to $k >> 1/r$, is provided by differentiating the factor e^{ikr}, which changes in the common direction of vectors $\mathbf{r}$ and $\mathbf{k}$, so

$$\nabla\psi_s \approx \mathbf{n}_r \frac{\partial}{\partial r}\psi_s \approx \mathbf{k}\psi_s, \qquad \text{at } kr >> 1, \tag{3.82}$$

and Eq. (1.47) yields

[34] See, e.g., EM Sec. 8.2.

[35] It is easy to prove that this form is an asymptotic form of *any* solution ψ_s of the scattering problem (even that beyond the Born approximation) at sufficiently large distances $r >> a, k^{-1}$.

[36] Note that the function f has the dimension of length, and does not account for the incident wave. This is why sometimes a dimensionless function, $S = 1 + 2ikf$, is used instead. This function S is called the *scattering matrix*, because it may be considered a natural generalization of the 1D matrix S defined by Eq. (2.124), to higher dimensionality.

[37] See, e.g., MA Eq. (10.8).

$$\mathbf{j}_s(\theta) \approx \frac{\hbar}{m}|\psi_i|^2 \frac{|f(\mathbf{k},\mathbf{k}_i)|^2}{r^2}\mathbf{k}\,. \tag{3.83}$$

Plugging this expression and also Eq. (61) into Eq. (62), for the differential cross-section we get simply

$$\frac{d\sigma}{d\Omega} = |f(\mathbf{k},\mathbf{k}_i)|^2, \tag{3.84}$$

while the total cross-section is

$$\sigma = \oint |f(\mathbf{k},\mathbf{k}_i)|^2 d\Omega, \tag{3.85}$$

so the scattering function $f(\mathbf{k}, \mathbf{k}_i)$ gives us everything we need – and in fact more because the function also contains information about the phase of the scattered wave.

Comparing Eqs. (80) and (81), we see that in the Born approximation, the scattering function is given by the so-called *Born integral*

$$f(\mathbf{k},\mathbf{k}_i) = -\frac{m}{2\pi\hbar^2}\int U(\mathbf{r}) e^{-i\mathbf{q}\cdot\mathbf{r}} d^3r, \tag{3.86}$$

Born integral

where, just for the notation simplicity, $\mathbf{r}'$ was replaced with $\mathbf{r}$, and $\mathbf{q}$ is the following *scattering vector*:

$$\mathbf{q} \equiv \mathbf{k} - \mathbf{k}_i, \tag{3.87}$$

with the length $q = 2k\sin(\theta/2)$, where θ is the *scattering angle* between the vectors $\mathbf{k}$ and $\mathbf{k}_i$ – see Fig. 9b. For the differential cross-section, Eqs. (84) and (86) yield[38]

$$\frac{d\sigma}{d\Omega} = \left(\frac{m}{2\pi\hbar^2}\right)^2 \left|\int U(\mathbf{r}) e^{-i\mathbf{q}\cdot\mathbf{r}} d^3r\right|^2. \tag{3.88}$$

$d\sigma/d\Omega$: Born approximation

This is the basic result of this section; it may be further simplified for spherically symmetric scatterers, with

$$U(\mathbf{r}) = U(r). \tag{3.89}$$

In this case, it is convenient to represent the exponent in the Born integral as $\exp\{-iqr\cos\chi\}$, where χ is the angle between the vectors $\mathbf{k}$ (i.e. the direction $\mathbf{n}_r$ toward the detector) and $\mathbf{q}$ (rather than the incident wave vector $\mathbf{k}_i$!) – see Fig. 9b. Now, for a fixed $\mathbf{q}$, we can take this vector's direction for the polar axis of a spherical coordinate system, and reduce Eq. (86) to a 1D integral:

$$\begin{aligned} f(\mathbf{k},\mathbf{k}_i) &= -\frac{m}{2\pi\hbar^2}\int_0^\infty r^2 dr U(r) \int_0^{2\pi} d\varphi \int_0^{\pi} \sin\chi d\chi \exp\{-iqr'\cos\chi\} \\ &\equiv -\frac{m}{2\pi\hbar^2}\int_0^\infty r^2 dr U(r)\; 2\pi \frac{2\sin qr}{qr} \equiv -\frac{2m}{\hbar^2 q}\int_0^\infty U(r)\sin(qr)\, r dr. \end{aligned} \tag{3.90}$$

[38] Note that according to Eq. (88), in the Born approximation, the scattering intensity does not depend on the sign of the potential U, and also that scattering in a certain direction is completely determined by a specific Fourier component of the function $U(\mathbf{r})$, namely by its harmonic with the wave vector equal to the scattering vector $\mathbf{q}$.

As a simple example, let us use the Born approximation to analyze scattering on the following spherically symmetric potential:

$$U(\mathbf{r}) = U_0 \exp\left\{-\frac{r^2}{2a^2}\right\}. \tag{3.91}$$

In this particular case, it is better to avoid the temptation to exploit the spherical symmetry by using Eq. (90), and instead, use the general Eq. (88) because it may be represented as a product of three similar Cartesian factors:

$$f(\mathbf{k},\mathbf{k}_i) = -\frac{mU_0}{2\pi\hbar^2} I_x I_y I_z, \qquad \text{with } I_x \equiv \int_{-\infty}^{+\infty} \exp\left\{-\left(\frac{x^2}{2a^2} + iq_x x\right)\right\} dx, \tag{3.92}$$

and similar integrals for I_y and I_z. From Chapter 2, we already know that the Gaussian integrals like I_x may be readily worked out by complementing the exponent to the full square, in our current case giving

$$\begin{aligned} I_x &= (2\pi)^{1/2} a \exp\left\{-\frac{q_x^2 a^2}{2}\right\}, \text{ etc.; so:} \\ \frac{d\sigma}{d\Omega} &= \left(\frac{mU_0}{2\pi\hbar^2} I_x I_y I_z\right)^2 = 2\pi a^2 \left(\frac{mU_0 a^2}{\hbar^2}\right)^2 e^{-q^2 a^2}. \end{aligned} \tag{3.93}$$

Now, the total cross-section σ is an integral of $d\sigma/d\Omega$ over all directions of the vector $\mathbf{k}$. Since in our case the scattering intensity does not depend on the azimuthal angle φ, the only nontrivial integration is over the scattering angle θ (see Fig. 9b again):

$$\begin{aligned} \sigma &\equiv \oint \frac{d\sigma}{d\Omega} d\Omega = 2\pi \int_0^{\pi} \frac{d\sigma}{d\Omega} \sin\theta d\theta = 4\pi^2 a^2 \left(\frac{mU_0 a^2}{\hbar^2}\right)^2 \int_0^{\pi} \exp\left\{-\left(2k\sin\frac{\theta}{2}\right)^2 a^2\right\} \sin\theta d\theta \\ &\equiv 4\pi^2 a^2 \left(\frac{mU_0 a^2}{\hbar^2}\right)^2 \int_{\theta=0}^{\theta=\pi} \exp\left\{-2k^2 a^2 (1-\cos\theta)\right\} d(1-\cos\theta) = \frac{2\pi^2}{k^2}\left(\frac{mU_0 a^2}{\hbar^2}\right)^2 \left(1 - e^{-4k^2 a^2}\right). \end{aligned} \tag{3.94}$$

Let us analyze these results. In the low-energy limit, $ka << 1$ (and hence $qa << 1$ for any scattering angle), the scattered wave is virtually isotropic: $d\sigma/d\Omega \approx$ const – a very typical feature of a scalar-wave scattering[39] by small objects, in any approximation. Note that according to Eq. (77), the Born expression for σ, following from Eq. (94) in this limit,

$$\sigma = 8\pi^2 a^2 \left(\frac{mU_0 a^2}{\hbar^2}\right)^2, \tag{3.95}$$

is only valid if σ is much smaller than the scale a^2 of the physical cross-section of the scatterer. In the opposite, high-energy limit $ka >> 1$, the scattering is dominated by small angles $\theta \approx q/k \sim 1/ka \sim \lambda/a$:

[39] Note that this is only true for scalar (e.g., the de Broglie) waves but not the vector ones, in particular, the electromagnetic waves where the intensity of the dipole radiation, and hence the scattering by small objects vanishes in the direction of the incident field's polarization – see, e.g., EM Eqs. (8.26) and (8.139).

$$\frac{d\sigma}{d\Omega} \approx 2\pi a^2 \left(\frac{mU_0 a^2}{\hbar^2} \right)^2 \exp\left\{ -k^2 a^2 \theta^2 \right\}. \tag{3.96}$$

This is, again, very typical for diffraction. Note, however, that due to the smooth character of the Gaussian potential (91), the diffraction pattern (98) exhibits no oscillations of $d\sigma/d\Omega$ as a function of the diffraction angle θ.

Such oscillations naturally appear for scatterers with sharp borders. Indeed, let us consider a uniform spherical scatterer described by the potential

$$U(\mathbf{r}) = \begin{cases} U_0, & \text{for } r < R, \\ 0, & \text{otherwise.} \end{cases} \tag{3.97}$$

In this case, integration by parts of Eq. (90) readily yields

$$f(\mathbf{k}, \mathbf{k}_i) = \frac{2mU_0}{\hbar^2 q^3} (qR \cos qR - \sin qR), \qquad \text{so } \frac{d\sigma}{d\Omega} = \left(\frac{2mU_0}{\hbar^2 q^3} \right)^2 (qR \cos qR - \sin qR)^2. \tag{3.98}$$

According to this result, the scattered wave's intensity drops very fast with q, so one needs a semi-log plot (such as that used in Fig. 10) to reveal small diffraction fringes,[40] with the n^{th} destructive interference (zero-intensity) point tending to $qR = \pi(n + ½)$ at $n \to \infty$. Since, as Fig. 9b shows, q may only change from 0 to $2k$, these intensity minima are only observable at sufficiently large values of the parameter kR when they correspond to real values of the scattering angle θ. (At $kR >> 1$, approximately kR/π of these minima, i.e. "dark rings" of low scattering probability, are observable.) On the contrary, at $kR << 1$ all allowed values of qR are much smaller than 1, so in this limit, the differential cross-section does not depend on qR, i.e. the scattering by the sphere (as by *any* object in this limit) is isotropic.

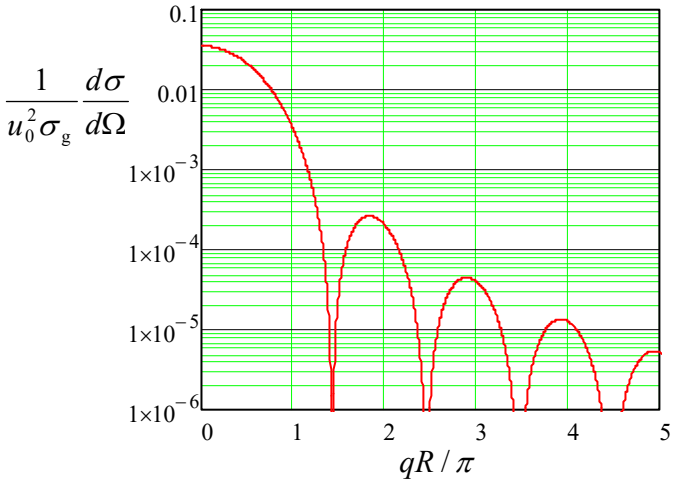

Fig. 3.10. The differential cross-section of the Born scattering of a particle by a "hard" (sharp-border) sphere (97), normalized to its geometric cross-section $\sigma_g \equiv \pi R^2$ and the square of the potential's magnitude parameter $u_0 \equiv U_0/(\hbar^2/2mR^2)$, as a function of the normalized magnitude of the scattering vector $\mathbf{q}$.

This example shows that in quantum mechanics, the notions of particle scattering and diffraction are essentially inseparable.

[40] Their physics is very similar to that of the Fraunhofer diffraction on a 1D scatterer – see, e.g., EM Sec. 8.4.

The Born approximation, while being very simple and used more than any other scattering theory, is not without shortcomings. For example, it is not too difficult (and hence is left for the reader's exercise) to prove the so-called *optical theorem*, valid for an arbitrary scatterer:

Optical theorem

$$\operatorname{Im} f(\mathbf{k}_i, \mathbf{k}_i) = \frac{k}{4\pi}\sigma . \tag{3.99}$$

However, Eq. (86) shows that in the Born approximation, the function f is purely real at $q = 0$ (i.e. for $\mathbf{k} = \mathbf{k}_i$), and hence cannot satisfy the optical theorem. Even more evidently, it cannot describe such a simple effect as a dark shadow ($\psi \approx 0$) cast by a virtually opaque object (say, with $U >> E$). There are several ways to improve the Born approximation, while still keeping its general idea of an approximate treatment of U.

(i) Instead of the main assumption $\psi_s \propto U_0$, we may use a complete perturbation series:

$$\psi_s = \psi_1 + \psi_2 + ... \tag{3.100}$$

with $\psi_n \propto U_0^n$, and find successive approximations ψ_n one by one. In the 1st approximation, we return to the Born formula, but already the 2nd approximation yields

$$\operatorname{Im} f_2(\mathbf{k}_i, \mathbf{k}_i) = \frac{k}{4\pi}\sigma_1 , \tag{3.101}$$

where σ_1 is the total cross-section calculated in the 1st approximation, so the optical theorem (99) is "almost satisfied".[41]

(ii) As was mentioned above, the Born approximation does not work very well for the objects stretched along the direction (say, x) of the initial wave vector $\mathbf{k}_i$. This deficiency may be corrected by the so-called *eikonal*[42] *approximation*, which replaces the plane-wave representation (60) of the incident wave with a WKB-like exponent, though still in the 1st approximation in $U \to 0$:

$$\begin{aligned} \exp\{i\mathbf{k}_i \cdot \mathbf{r}\} \equiv \exp\{ikx\} \to \exp\left\{i\int_0^x k(\mathbf{r}')dx'\right\} \equiv \exp\left\{i\int_0^x \frac{\{2m[E - U(\mathbf{r}')]\}^{1/2}}{\hbar}dx'\right\} \\ \approx \exp\left\{i\left[kx - \frac{m}{\hbar^2 k}\int_0^x U(\mathbf{r}')dx'\right]\right\}. \end{aligned} \tag{3.102}$$

The results of this approach satisfy the optical theorem (99) already in the 1st approximation.

Another way toward quantitative results in the theory of scattering, beyond the Born approximation, may be pursued for spherically symmetric potentials (89); I will discuss it in Sec. 8, after a general discussion of particle motion in such potentials in Sec. 7.

3.4. Energy bands in higher dimensions

In Sec. 2.7, we have discussed the 1D band theory for potential profiles $U(x)$ that obey the periodicity condition (2.192). For what follows, let us notice that the condition may be rewritten as

[41] An even simpler way to satisfy the theorem (even in the Born approximation) is to change the definition of the function $f(\mathbf{k}, \mathbf{k}_i)$ so that for forward scattering ($\mathbf{k} = \mathbf{k}_i$), it includes the incident de Broglie wave as well.

[42] From the Greek word εικον, meaning "image". In our current context, this term is purely historic.

$$U(x+X)=U(x), \tag{3.103}$$

where $X = \tau a$, with τ being an arbitrary integer. One may say that the set of points X forms a periodic *1D lattice* in the direct (**r**-) space. We have also seen that each Bloch state (i.e., each eigenstate of the Schrödinger equation for such periodic potential) is characterized by the quasimomentum $\hbar q$, and its energy does not change if q is changed by a multiple of $2\pi/a$. Hence if we form, in the reciprocal (**q**-) space, a 1D lattice of points $Q = lb$, with $b \equiv 2\pi/a$ and integer l, any two points from these two mutually reciprocal lattices satisfy the following rule:

$$\exp\{iQX\} = \exp\left\{ il\frac{2\pi}{a}\tau a \right\} \equiv e^{2\pi i l\tau} = 1, \tag{3.104}$$

because the product of any two integers l and τ is also an integer.

In this form, the results of Sec. 2.7 may be readily generalized to d-dimensional periodic potentials whose translational symmetry obeys the following natural generalization of Eq. (103):

$$U(\mathbf{r}+\mathbf{R})=U(\mathbf{r}), \tag{3.105}$$

where the points **R**, which may be numbered by d integers τ_j, form the so-called *Bravais lattice*:[43]

$$\mathbf{R}=\sum_{j=1}^{d}\tau_j\mathbf{a}_j, \tag{3.106}$$

Bravais lattice

with d *primitive vectors* $\mathbf{a}_j$. The simplest example of a 3D Bravais lattice is given by the *simple cubic lattice* (Fig. 11a), which may be described by a system of mutually perpendicular primitive vectors $\mathbf{a}_j$ of equal length. However, not in any lattice these vectors are perpendicular; for example, Figs. 11b and 11c show possible sets of the primitive vectors describing, respectively, the *face-centered cubic* (fcc) lattice and the *body-centered cubic* (bcc) lattice. In 3D, the science of crystallography based on group theory distinguishes, by their symmetry properties, 14 different Bravais lattices, which may be grouped into 7 distinct *lattice systems*.[44]

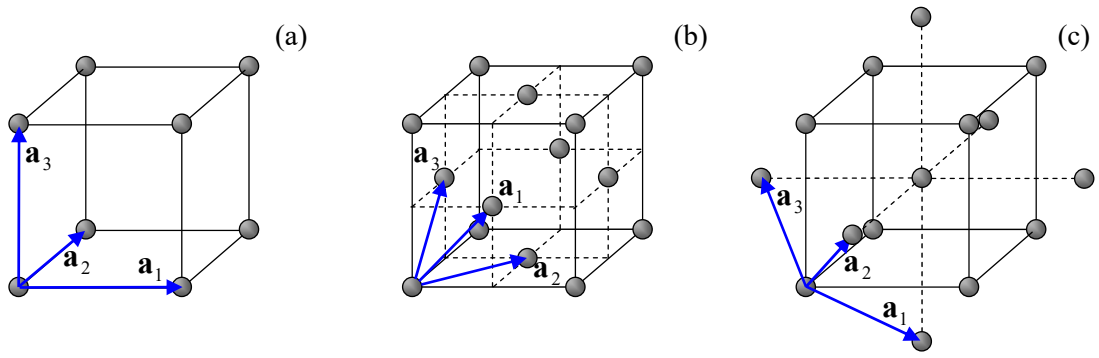

Fig. 3.11. The simplest (and most common) 3D Bravais lattices: (a) simple cubic, (b) face-centered cubic (fcc), and (c) body-centered cubic (bcc), and possible choices of their primitive vector sets (blue arrows).

[43] Named after A. Bravais, the crystallographer who introduced this notion in 1850.

[44] An exceptionally clear and well-illustrated introduction to the Bravais lattices is given in Chapters 4 and 7 of the famous textbook by N. Ashcroft and N. Mermin, *Solid State Physics*, Saunders College, 1976.

Note, however, not all highly symmetric sets of single points form Bravais lattices. As probably the most striking example, the nodes of the very simple 2D *honeycomb lattice* (Fig. 12a)[45] cannot be described by a Bravais lattice – while those of the 2D *hexagonal lattice* shown in Fig. 12b, can. The most prominent 3D case of such a lattice is the diamond structure (Fig. 12c), which describes, in particular, silicon crystals.[46] In cases like these, the band theory is much facilitated by the fact that the Bravais lattices using some point groups called *unit cells* (or "bases", or "cells with basis", or "motifs") may describe these systems.[47] For example, Fig. 12a shows a possible choice of the primitive vectors for the honeycomb lattice, with the unit cell formed by any two adjacent points of the original lattice (say, within the dashed ovals on that panel). Similarly, the diamond lattice may be described as an fcc Bravais lattice with a two-point unit cell – see Fig. 12c.

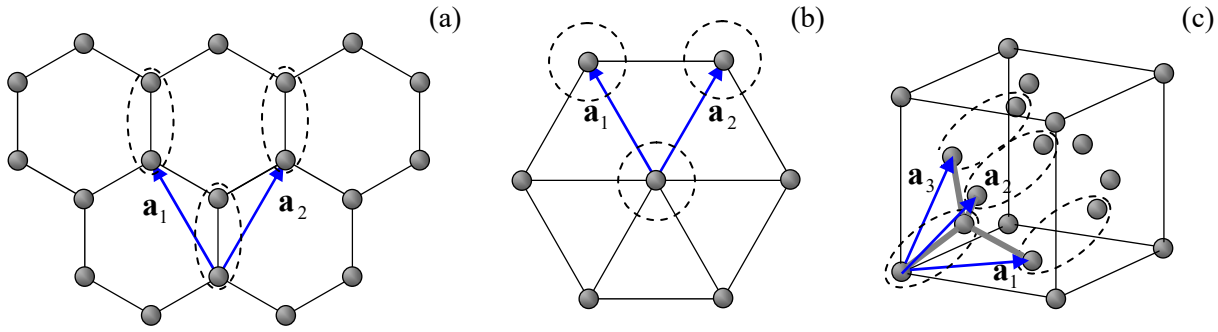

Fig. 3.12. Two important periodic structures that require two-point unit cells for their Bravais lattice representation: (a) 2D honeycomb lattice and (c) 3D diamond lattice, and their primitive vectors. For contrast, panel (b) shows the 2D hexagonal lattice that forms a Bravais lattice with a single-point unit cell.

Now we are ready for the following generalization of the 1D Bloch theorem, given by Eqs. (2.193) and (2.210), to higher dimensions: any eigenfunction of the Schrödinger equation describing a particle's motion in the spatially-unlimited periodic potential (105) may be represented either as

3D Bloch theorem

$$\psi(\mathbf{r}+\mathbf{R}) = \psi(\mathbf{r}) e^{i\mathbf{q}\cdot\mathbf{R}}, \tag{3.107}$$

or as

$$\psi(\mathbf{r}) = u(\mathbf{r}) e^{i\mathbf{q}\cdot\mathbf{r}}, \quad \text{with } u(\mathbf{r}+\mathbf{R}) = u(\mathbf{r}), \tag{3.108}$$

where the quasimomentum $\hbar\mathbf{q}$ is again a constant of motion, but now it is a vector. The key notion of the band theory in d dimensions is the *reciprocal lattice* in the wave vector (**q**-) space, formed as

Reciprocal lattice in **q**-space

$$\mathbf{Q} = \sum_{j=1}^{d} l_j \mathbf{b}_j, \tag{3.109}$$

[45] This structure describes, for example, the now-famous *graphene* – isolated monolayer sheets of carbon atoms arranged in a honeycomb lattice with an interatomic distance of 0.142 nm.

[46] This diamond structure may be best understood as an overlap of two fcc lattices of side a, mutually shifted by the vector $\{1, 1, 1\}\times a/4$, so the distances between each point of the combined lattice and its 4 nearest neighbors (see the solid gray lines in Fig. 12c) are all equal.

[47] A harder case is presented by so-called *quasicrystals* (whose idea may be traced down to medieval Islamic tilings, but was discovered in natural crystals, by D. Shechtman *et al.*, only in 1984), which obey a high (say, the 5-fold) rotational symmetry, but cannot be described by a Bravais lattice with *any* finite unit cell. For a popular review of quasicrystals, see, for example, P. Stephens and A. Goldman, *Sci. Amer.* **264**, #4, 24 (1991).

with integer l_j, and vectors $\mathbf{b}_j$ selected in such a way that the following natural generalization of Eq. (104) is valid for any two points of the direct and reciprocal lattices:

$$e^{i\mathbf{Q}\cdot\mathbf{R}} = 1. \tag{3.110}$$

One way to describe the physical sense of the lattice $\mathbf{Q}$ is to say that according to Eqs. (80) and/or (86), it gives the set of the vectors $\mathbf{q} \equiv \mathbf{k} - \mathbf{k}_i$ for that the interference of the waves scattered by all Bravais lattice points is constructive, and hence strongly enhanced.[48] Another way to look at the reciprocal lattice follows from the first formulation of the Bloch theorem, given by Eq. (107): if we add to the quasimomentum $\mathbf{q}$ of a particle any vector $\mathbf{Q}$ of the reciprocal lattice, the wavefunction does not change. This means, in particular, that all information about the system's eigenfunctions is contained inside just one elementary cell of the reciprocal space $\mathbf{q}$. Its most frequent choice, called the *1st Brillouin zone*, is the set of all points $\mathbf{q}$ that are closer to the origin than to any other point of the lattice $\mathbf{Q}$. (Evidently, the 1st Brillouin zone in one dimension, discussed in Sec. 2.7, falls under this definition – see, e.g., Figs. 2.26 and 2.28.)

It is easy to see that the primitive vectors $\mathbf{b}_j$ of the reciprocal lattice may be constructed as

Reciprocal lattice: primitive vectors

$$\mathbf{b}_1 = 2\pi\frac{\mathbf{a}_2\times\mathbf{a}_3}{\mathbf{a}_1\cdot(\mathbf{a}_2\times\mathbf{a}_3)}, \quad \mathbf{b}_2 = 2\pi\frac{\mathbf{a}_3\times\mathbf{a}_1}{\mathbf{a}_1\cdot(\mathbf{a}_2\times\mathbf{a}_3)}, \quad \mathbf{b}_3 = 2\pi\frac{\mathbf{a}_1\times\mathbf{a}_2}{\mathbf{a}_1\cdot(\mathbf{a}_2\times\mathbf{a}_3)}. \tag{3.111}$$

Indeed, from the "operand rotation rule" of the vector algebra[49] it is evident that $\mathbf{a}_j\cdot\mathbf{b}_{j'} = 2\pi\delta_{jj'}$. Hence, with the account of Eq. (109), the exponent on the left-hand side of Eq. (110) is reduced to

$$e^{i\mathbf{Q}\cdot\mathbf{R}} = \exp\{2\pi i(l_1\tau_1 + l_2\tau_2 + l_3\tau_3)\}. \tag{3.112}$$

Since all l_j and all τ_j are integers, the expression in the parentheses is also an integer, so the exponent indeed equals 1, thus satisfying the definition of the reciprocal lattice given by Eq. (110).

As the simplest example, let us return to the simple cubic lattice of a period a (Fig. 11a), oriented in space so that

$$\mathbf{a}_1 = a\mathbf{n}_x, \quad \mathbf{a}_2 = a\mathbf{n}_y, \quad \mathbf{a}_3 = a\mathbf{n}_z. \tag{3.113}$$

According to Eq. (111), its reciprocal lattice is also simple cubic:

$$\mathbf{Q} = \frac{2\pi}{a}(l_x\mathbf{n}_x + l_y\mathbf{n}_y + l_z\mathbf{n}_z), \tag{3.114}$$

so the 1st Brillouin zone is a cube with the side $b = 2\pi/a$.

Almost equally simple calculations show that the reciprocal lattice of fcc is bcc, and vice versa. Figure 13 shows the resulting 1st Brillouin zone of the fcc lattice.

The notion of the reciprocal lattice makes the multi-dimensional band theory not much more complex than that in 1D, especially for numerical calculations, at least for the single-point Bravais

[48] This is why the notion of the **Q**-lattice is also the main starting point of X-ray diffraction studies of crystals. Indeed, it allows rewriting the well-known Bragg condition for diffraction peaks in an extremely simple form: $\mathbf{k} = \mathbf{k}_i + \mathbf{Q}$, where $\mathbf{k}_i$ and $\mathbf{k}$ are the wave vectors of the, respectively, incident and diffracted waves – see, e.g., EM Sec. 8.4 (where it was more convenient for me to use the notation $\mathbf{k}_0$ for $\mathbf{k}_i$).

[49] See, e.g., MA Eq. (7.6).

lattices. Indeed, repeating all the steps that have led us to Eq. (2.218), but now with a d-dimensional Fourier expansion of the functions $U(\mathbf{r})$ and $u(\mathbf{r})$, we readily get its generalization:

$$\sum_{\mathbf{l}'\neq\mathbf{l}} U_{\mathbf{l}'-\mathbf{l}} u_{\mathbf{l}'} = (E - E_{\mathbf{l}}) u_{\mathbf{l}}, \tag{3.115}$$

where $\mathbf{l}$ is now a d-dimensional vector of integer indices l_j. The summation in Eq. (115) should be carried over all essential components of this vector (i.e. over all relevant nodes of the reciprocal lattice), so writing a corresponding computer code requires a bit more care than in 1D. However, this is just a homogeneous system of linear equations for coefficients $u_{\mathbf{l}}$, and numerous routines of finding its eigenvalues E are readily available from both public sources and commercial software packages.

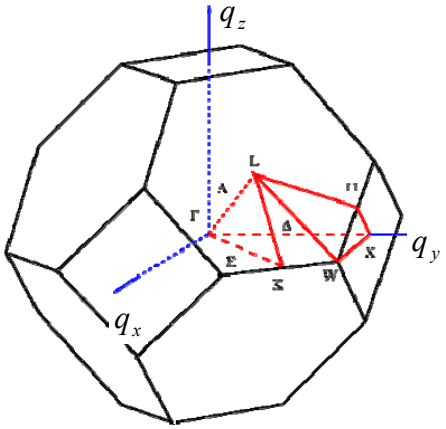

Fig. 3.13. The 1st Brillouin zone of the fcc lattice, and the traditional notation of its main directions. Adapted from http://en.wikipedia.org/wiki/Band_structure, as a public domain material.

What is indeed more complex than in 1D is the representation (and hence comprehension :-) of the calculated results and experimental data. Typically, the representation is limited to plotting the Bloch state eigenenergy as a function of the vector q's components along certain special directions in the reciprocal space of quasimomentum (see, e.g., the red lines in Fig. 13), typically on a single panel. Fig. 14 shows perhaps the most famous (and certainly the most practically important) of such plots, the band structure of electrons in crystalline silicon. The dashed horizontal lines mark the so-called *indirect gap* of width ~1.12 eV between the lower "valence" (nominally occupied) and the next "conduction" (nominally unoccupied) energy bands.

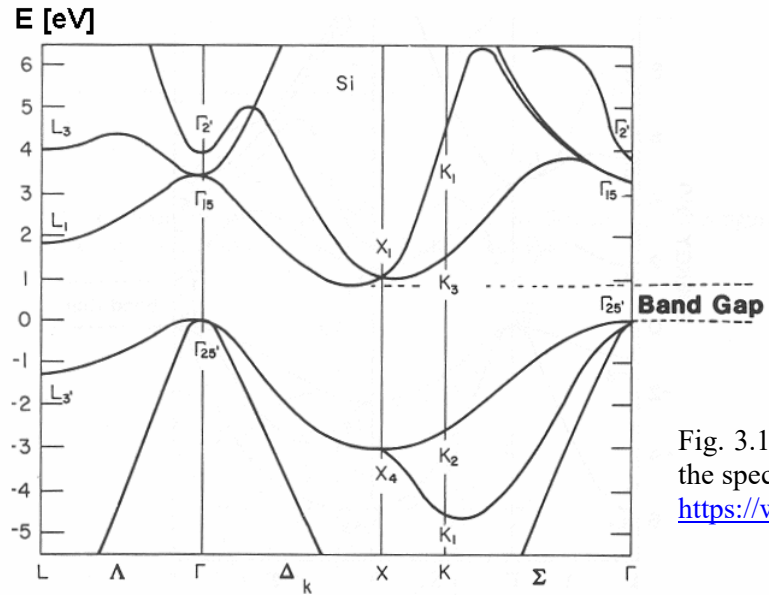

Fig. 3.14. The band structure of silicon, plotted along the special directions shown in Fig. 13. (Adapted from https://www.tf.uni-kiel.de/matwis/amat/semi_en/.)

In order to understand the reason for such complexity, let us see how would we start to calculate such a picture in the weak-potential approximation, for the simplest case of a 2D square lattice – which is a subset of the cubic lattice (106), with $\tau_3 = 0$. Its 1st Brillouin zone is of course also a square, of the area $(2\pi/a)^2$ – see the dashed lines in Fig. 15. Let us draw the lines of the constant energy of a free particle ($U = 0$) in this zone. Repeating the arguments of Sec. 2.7 (see especially Fig. 2.28 and its discussion), we may conclude that Eq. (2.216) should be now generalized as follows,

$$E = \frac{\hbar^2 k^2}{2m} = \frac{\hbar^2}{2m}\left[\left(q_x - \frac{2\pi l_x}{a}\right)^2 + \left(q_y - \frac{2\pi l_y}{a}\right)^2\right], \tag{3.116}$$

with all possible integers l_x and l_y. Considering this result only within the 1st Brillouin zone, we see that as the particle's energy E grows, the lines of equal energy, for the lowest energy band, evolve as shown in Fig. 15. Just like in 1D, the weak-potential effects are only important at the Brillouin zone boundaries and may be crudely represented as the appearance of narrow energy gaps. However, one can see that the band structure in the **q**-space is complex enough even without these effects – and becomes even more involved at higher E.

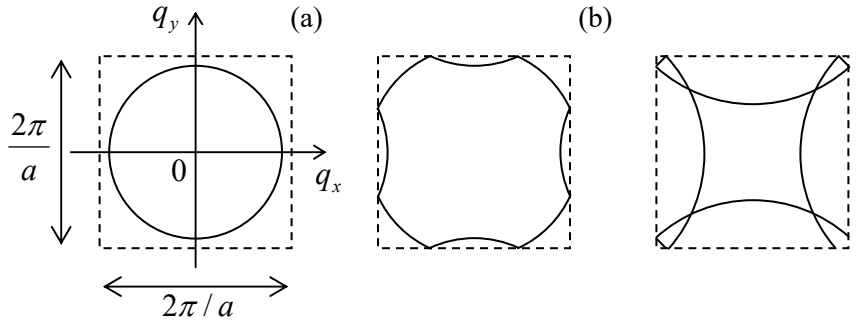

Fig. 3.15. The lines of constant energy E of a free particle, within the 1st Brillouin zone of a square Bravais lattice, for: (a) $E/E_1 \approx 0.95$, (b) $E/E_1 \approx 1.05$; and (c) $E/E_1 \approx 2.05$, where $E_1 \equiv \pi^2\hbar^2/2ma^2$.

The tight-binding approximation is usually easier to follow. For example, for the same square 2D lattice, we may repeat the arguments that have led us to Eq. (2.203), to write [50]

$$i\hbar\dot{a}_{0,0} = -\delta_n\left(a_{-1,0} + a_{+1,0} + a_{0,+1} + a_{0,-1}\right), \tag{3.117}$$

where the indices correspond to the deviations of the integers τ_x and τ_y from an arbitrarily selected minimum of the potential energy – and hence of the wavefunction's "hump" that is quasi-localized at this minimum. Now, looking for the stationary solution of these equations, that would obey the Bloch theorem (107), instead of Eq. (2.206) we get

$$E = E_n + \varepsilon_n = E_n - \delta_n\left(e^{iq_x a} + e^{-iq_x a} + e^{iq_y a} + e^{-iq_y a}\right) \equiv E_n - 2\delta_n\left(\cos q_x a + \cos q_y a\right). \tag{3.118}$$

Figure 16 shows this result, within the 1st Brillouin zone, in two forms: as color-coded lines of equal energy, and as a 3D plot. It is evident that the plots of this function along different lines on the **q**-plane, for example along one of the axes (say, q_x) and along a diagonal of the 1st Brillouin zone (say, with $q_x = q_y$) give different curves $E(q)$, qualitatively similar to those of silicon (Fig. 14).

[50] Actually, using the same values of δ_n in both directions (x and y) implies some sort of symmetry of the quasi-localized states. For example, the s-states of axially-symmetric potentials (see the next section) always have such symmetry.

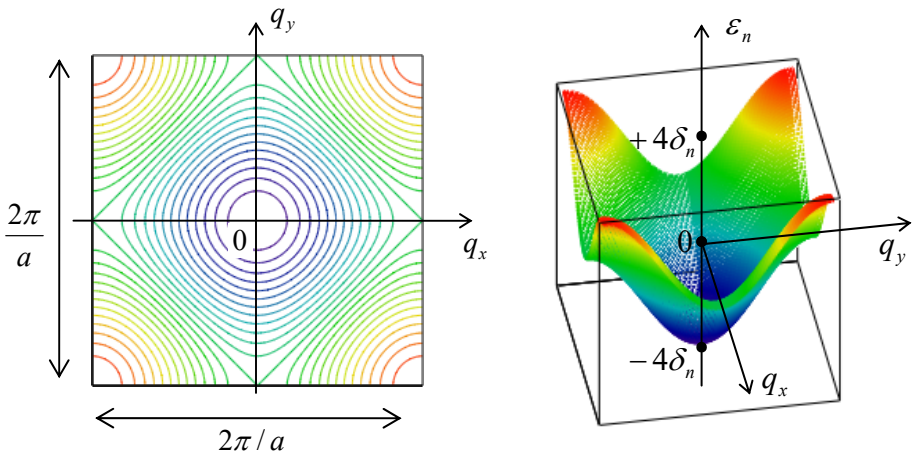

Fig. 3.16. The allowed band energy $\varepsilon_n \equiv E - E_n$ for a square 2D lattice, in the tight-binding approximation.

However, the latter structure is further complicated by the fact that the unit cell of its Bravais lattice contains two atoms – see Fig. 12c and its discussion. In this case, even the tight-binding picture becomes more complex. Indeed, even if the atoms at different positions of the unit cell are similar (as they are, for example, in both graphene and silicon), and hence the potential wells near those points and the corresponding local wavefunctions $u(\mathbf{r})$ are similar as well, the Bloch theorem (which only pertains to Bravais lattices!) does not forbid them from having different complex probability amplitudes $a(t)$ whose time evolution should be described by a specific differential equation.

As the simplest example, to describe the honeycomb lattice shown in Fig. 12a, we have to prescribe different probability amplitudes to the "top" and "bottom" points of its unit cell – say, α and β, correspondingly. Since each of these points is surrounded (and hence weakly interacts) with three neighbors of the opposite type, instead of Eq. (117) we have to write two equations:

$$i\hbar\dot{\alpha} = -\delta_n \sum_{j=1}^{3} \beta_j, \qquad i\hbar\dot{\beta} = -\delta_n \sum_{j'=1}^{3} \alpha_{j'}, \tag{3.119}$$

where each summation is over three nearest-neighbor points. (In these two sums, I am using different summation indices just to emphasize that these directions are different for the "top" and "bottom" points of the unit cell – see Fig. 12a.) Now using the Bloch theorem (107) in the form similar to Eq. (2.205), we get two coupled systems of linear algebraic equations:

$$(E - E_n)\alpha = -\delta_n \beta \sum_{j=1}^{3} e^{i\mathbf{q}\cdot\mathbf{r}_j}, \qquad (E - E_n)\beta = -\delta_n \alpha \sum_{j'=1}^{3} e^{i\mathbf{q}\cdot\mathbf{r}'_{j'}}, \tag{3.120}$$

where $\mathbf{r}_j$ and $\mathbf{r}'_{j'}$ are the nearest-neighbor positions, as seen from the top and bottom points, respectively. Writing the condition of consistency of this system of homogeneous linear equations, we get two equal and opposite values for energy correction for each value of $\mathbf{q}$:

$$E_{\pm} = E_n \pm \delta_n \Sigma^{1/2}, \qquad \text{where } \Sigma \equiv \sum_{j,j'=1}^{3} e^{i\mathbf{q}\cdot\left(\mathbf{r}_j + \mathbf{r}'_{j'}\right)}. \tag{3.121}$$

According to Eq. (120), these two energy bands correspond to the phase shifts (on the top of the regular Bloch shift $\mathbf{q}\cdot\Delta\mathbf{r}$) of either 0 or π between the adjacent quasi-localized wavefunctions $u(\mathbf{r})$.

The most interesting corollary of such energy symmetry, augmented by the honeycomb lattice's symmetry, is that for certain values $\mathbf{q}_D$ of the vector $\mathbf{q}$ (that turn out to be in each of six corners of the honeycomb-shaped 1st Brillouin zone), the double sum Σ vanishes, i.e. the two band surfaces $E_\pm(\mathbf{q})$ touch each other. As a result, in the vicinities of these so-called *Dirac points*,[51] the dispersion relation is linear:

$$E_\pm\Big|_{\mathbf{q}\approx\mathbf{q}_D} \approx E_n \pm \hbar v_n \left|\tilde{\mathbf{q}}\right|, \quad \text{where } \tilde{\mathbf{q}} \equiv \mathbf{q} - \mathbf{q}_D, \tag{3.122}$$

with $v_n \propto \delta_n$ being a constant with the dimension of velocity – for graphene, close to 10^6 m/s. Such a linear dispersion relation ensures several interesting transport properties of graphene, in particular of the quantum Hall effect in it – as was already mentioned in Sec. 2. For their more detailed discussion, I have to refer the reader to special literature.[52]

3.5. Axially symmetric systems

I cannot conclude this chapter (and hence our review of wave mechanics) without addressing the exact solutions of the stationary Schrödinger equation[53] possible in the cases of highly symmetric functions $U(\mathbf{r})$. Such solutions are very important, in particular, for atomic and nuclear physics, and will be used in the later chapters of this course.

In some rare cases, such symmetries may be exploited by the separation of variables in Cartesian coordinates. The most famous (and rather important) example is the d-dimensional isotropic harmonic oscillator – a particle moving inside the potential well

$$U = \frac{m\omega_0^2}{2}\sum_{j=1}^{d} r_j^2 \ . \tag{3.123}$$

Separating the variables exactly as we did in Sec. 1.7 for the rectangular hard-wall box (1.77), for each degree of freedom we get the Schrödinger equation (2.261) of a 1D oscillator, whose eigenfunctions are

[51] This term is based on a (rather indirect) analogy with the Dirac theory of relativistic quantum mechanics, to be discussed in Chapter 9 below.

[52] See, e.g., the reviews by A. Castro Neto *et al*., *Rev. Mod. Phys*. **81**, 109 (2009) and by X. Lu *et al*., *Appl. Phys. Rev*. **4**, 021306 (2017). Note that the transport properties of graphene are determined by coupling of $2p_z$-states of its carbon atom electrons (see Secs. 6 and 7 below), whose wavefunctions are proportional to $\exp\{\pm i\varphi\}$ rather than are axially symmetric as implied by Eqs. (120). However, due to the lattice symmetry, this fact does not affect the above dispersion relation $E(\mathbf{q})$.

[53] This is my best chance to mention, in passing, that the eigenfunctions $\psi_n(\mathbf{r})$ of any such problem do not feature the instabilities typical for the *deterministic chaos* effects of classical mechanics – see, e.g., CM Chapter 9. (This is why the term *quantum mechanics of classically chaotic systems* is preferable to the occasionally used term "quantum chaos".) It is curious that at the initial stages of the time evolution of the wavefunctions of such systems, their certain correlation functions still grow exponentially, reminding the *Lyapunov exponents* λ of their classical chaotic dynamics. This growth stops at the so-called *Ehrenfest times* $t_E \sim \lambda^{-1}\ln(S/\hbar)$, where S is the action scale of the problem – see, e.g., I. Aleiner and A. Larkin, *Phys. Rev. E* **55**, R1243 (1997). In a stationary quantum state, the most essential trace of the classical chaos in a system is the unusual statistics of its eigenvalues, in particular of the energy spectra. We will have a chance for a brief look at such statistics in Chapter 5, but unfortunately, I will not have time/space to discuss this field in much detail. Perhaps the best available book for further reading is the monograph by M. Gutzwiller, *Chaos in Classical and Quantum Mechanics*, Springer, 1991.

given by Eq. (2.284), and the energy spectrum is described by Eq. (2.162). As a result, the total energy spectrum may be indexed by a vector $\mathbf{n} = \{n_1, n_2, \ldots, n_d\}$ of d independent integer quantum numbers n_j:

$$E_{\mathbf{n}} = \hbar\omega_0\left(\sum_{j=1}^{d} n_j + \frac{d}{2}\right), \tag{3.124}$$

each ranging from 0 to ∞. Note that every energy level of this system, with the only exception of its ground state,

$$\psi_g = \prod_{j=1}^{d}\psi_0(r_j) = \frac{1}{\pi^{d/4}x_0^{d/2}}\exp\left\{-\frac{1}{2x_0^2}\sum_{j=1}^{d} r_j^2\right\}, \tag{3.125}$$

is *degenerate*: several different wavefunctions, each with its own different set of the quantum numbers n_j, but the same value of their sum, have the same energy.

However, the harmonic oscillator problem is an exception: for other axially and spherically symmetric problems, the solution is made much easier by using the appropriate curvilinear coordinates. Let us start with the simplest axially symmetric problem: the so-called *planar rotor* (or "rotator"), i.e. a particle of mass $\mathscr{m}$,[54] constrained to move along a plane circle of radius R (Fig. 17).[55]

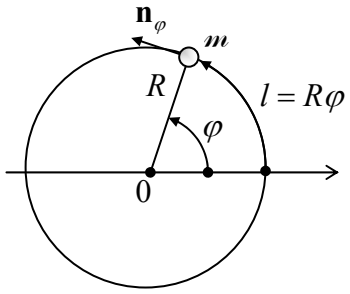

Fig. 3.17. A planar rigid rotor.

The classical state of such planar rotor may be described by just *one* coordinate, say, the angular displacement φ (or equivalently, the arc displacement $l \equiv R\varphi$) from some reference direction, with the energy (and the Hamiltonian function) $H = p^2/2\mathscr{m}$, where $\mathbf{p} \equiv \mathscr{m}\mathbf{v} = \mathscr{m}\mathbf{n}_\varphi(dl/dt)$, $\mathbf{n}_\varphi$ being the unit vector in the azimuthal direction – see Fig. 17. This function is similar to that of a free 1D particle (with the replacement $x \to l \equiv R\varphi$), and hence the rotor's quantum properties may be described by a similar Hamiltonian operator:

$$\hat{H} = \frac{\hat{p}^2}{2\mathscr{m}}, \qquad \text{with } \hat{\mathbf{p}} = -i\hbar\mathbf{n}_\varphi\frac{\partial}{\partial l} \equiv -i\frac{\hbar}{R}\mathbf{n}_\varphi\frac{\partial}{\partial\varphi}, \tag{3.126}$$

whose eigenfunctions have a similar structure:

$$\psi = Ce^{ikl} \equiv Ce^{ikR\varphi}. \tag{3.127}$$

[54] From this point on (until the chapter's end), I will use this exotic font for the particle's mass, to avoid any chance of its confusion with the impending "magnetic" quantum number m, traditionally used in axially-symmetric problems.

[55] This is a reasonable model for the confinement of light atoms, notably hydrogen, in some organic compounds, but I am addressing this system mostly as the basis for the forthcoming, more complex problems.

The "only" new feature is that in the rotor, all observables should be 2π-periodic functions of the angle φ. Hence, as we have already discussed in the context of the magnetic flux quantization (see Fig. 4 and its discussion), as the particle makes one turn around the central point 0, its wavefunction's phase $kR\varphi$ may only change by $2\pi m$, with an arbitrary integer m (ranging from $-\infty$ to $+\infty$):

$$\psi_m(\varphi + 2\pi) = \psi_m(\varphi) e^{2\pi i m}. \tag{3.128}$$

With the eigenfunctions (127), this periodicity condition immediately gives $2\pi kR = 2\pi m$. Thus, the wave number k can take only quantized values $k_m = m/R$, so the eigenfunctions should be indexed by this *magnetic* quantum number m:

$$\psi_m = C_m \exp\left\{ im \frac{l}{R} \right\} \equiv C_m \exp\{ im\varphi \}, \tag{3.129}$$

Planar rotor: eigenfunctions

and the energy spectrum is discrete[56]:

$$E_m = \frac{p_m^2}{2m} = \frac{\hbar^2 k_m^2}{2m} = \frac{\hbar^2 m^2}{2mR^2}. \tag{3.130}$$

Planar rotor: eigenenergies

This simple model allows exact analysis of an external magnetic field's effect on a confined motion of an electrically charged particle. Indeed, in the simplest case when this field is axially symmetric (or just uniform) and directed normally to the rotor's plane, it does not violate the axial symmetry of the system. According to Eq. (26), in this case, we have to generalize Eq. (126) as

$$\hat{H} = \frac{1}{2m}\left(-i\hbar \mathbf{n}_\varphi \frac{\partial}{\partial l} - q\mathbf{A} \right)^2 \equiv \frac{1}{2m}\left(-i\frac{\hbar}{R} \mathbf{n}_\varphi \frac{\partial}{\partial \varphi} - q\mathbf{A} \right)^2. \tag{3.131}$$

Here, in contrast to the Cartesian gauge choice (44), which was so instrumental for the solution of the Landau level problem, it is beneficial to take the vector potential in the axially symmetric form $\mathbf{A} = A(\rho)\mathbf{n}_\varphi$, where $\boldsymbol{\rho} \equiv \{x, y\}$ is the 2D radius vector, with the magnitude $\rho = (x^2 + y^2)^{1/2}$. Using the well-known expression for the curl operator in the cylindrical coordinates,[57] we can readily check that the requirement $\nabla \times \mathbf{A} = \mathcal{B}\mathbf{n}_z$, with $\mathcal{B}$ = const, is satisfied by the following function (which was already mentioned in Sec. 2):

$$\mathbf{A} = \mathbf{n}_\varphi \frac{\mathcal{B}\rho}{2}. \tag{3.132}$$

For the planar rotor, $\rho = R$ = const, so the stationary Schrödinger equation becomes

$$\frac{1}{2m}\left(-i\frac{\hbar}{R}\frac{\partial}{\partial \varphi} - q\frac{\mathcal{B}R}{2} \right)^2 \psi_m = E_n \psi_m. \tag{3.133}$$

A little bit surprisingly, this equation is still satisfied with the eigenfunctions (127)! Moreover, since the periodicity condition (128) is also unaffected by the applied magnetic field, we return to the periodic eigenfunctions (129), independent of $\mathcal{B}$. However, the field does affect the system's eigenenergies:

[56] Note that E_m does not include the radial confinement energy. (See Sec. 2.1 and the solution of Problem 2.1.)
[57] See, e.g., MA Eq. (10.5).

Planar rotor: magnetic field's effect

$$E_m = \frac{1}{\psi_m}\frac{1}{2m}\left(-i\frac{\hbar}{R}\frac{\partial}{\partial\varphi} - q\frac{\mathcal{B}R}{2}\right)^2\psi_m = \frac{1}{2m}\left(\frac{\hbar m}{R} - q\frac{\mathcal{B}R}{2}\right)^2 \equiv \frac{\hbar^2}{2mR^2}\left(m - \frac{\Phi}{\Phi_0'}\right)^2, \qquad (3.134)$$

where $\Phi \equiv \pi R^2\mathcal{B}$ is the magnetic flux through the area limited by the particle's trajectory, and $\Phi_0' \equiv 2\pi\hbar/q$ is the "normal" magnetic flux quantum we have already met in the AB effect's context – see Eq. (34) and its discussion. The field also changes the circular electric current of the particle for each m:

$$I_m = q\frac{\hbar}{2imR}\left[\psi_m^*\left(\frac{\partial}{\partial\varphi} - \frac{iqR\mathcal{B}}{2\hbar}\right)\psi_m - \text{c.c.}\right] = q\frac{\hbar}{mR}|C_m|^2\left(m - \frac{\Phi}{\Phi_0'}\right). \qquad (3.135)$$

Normalizing the wavefunction (129) to have $W_m = 1$, we get $|C_m|^2 = 1/2\pi R$, so Eq. (135) becomes

$$I_m = \left(m - \frac{\Phi}{\Phi_0'}\right)I_0, \qquad \text{with } I_0 \equiv \frac{\hbar q}{2\pi m R^2}. \qquad (3.136)$$

The functions $E_m(\Phi)$ and $I_m(\Phi)$ are shown in Fig. 18. Note that since $\Phi_0' \propto 1/q$, for any sign of the particle's charge q, $dI_m/d\Phi < 0$. It is easy to verify that this means that the current is *diamagnetic* for any sign of q:[58] the field-induced current flows in such a direction that its own magnetic field tries to compensate for the external magnetic flux applied to the loop. This result may be interpreted as a different manifestation of the AB effect.[59] In contrast to the interference experiment that was discussed in Sec. 1, in the situation shown in Fig. 17 the particle is not absorbed by the detector but travels around the ring continuously. As a result, its wavefunction is "rigid": due to the periodicity condition (128), the quantum number m is discrete, and the applied magnetic field cannot change the wavefunction gradually. In this sense, the system is similar to a superconducting loop – see Fig. 4 and its discussion. The difference between these systems is two-fold:

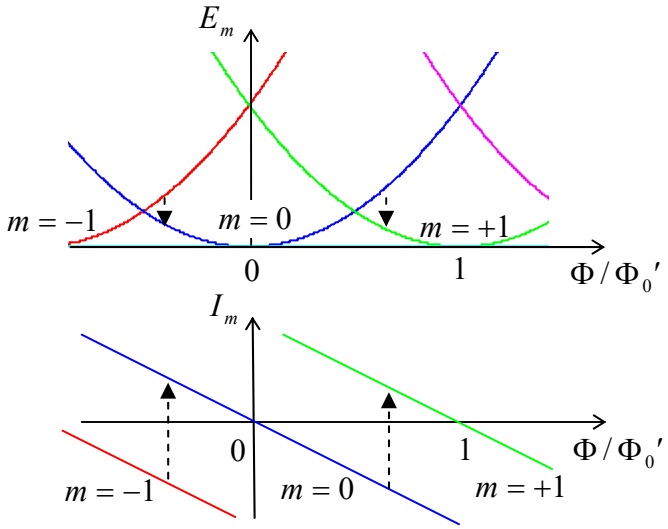

Fig. 3.18. The magnetic field's effect on a charged planar rotor. Dashed arrows show possible inelastic transitions between metastable and ground states, due to weak interaction with the environment, as the external magnetic field is slowly increased.

[58] This effect, whose qualitative features remain the same for all 2D or 3D localized states (see Chapter 6 below), is frequently referred to as *orbital diamagnetism*. In magnetic materials consisting of particles with uncompensated spins, this effect competes with an opposite effect, *spin paramagnetism* – see, e.g., EM Sec. 5.5.

[59] It is straightforward to check that the final forms of Eqs. (134)-(136) remain valid even if the magnetic field is localized well inside the rotor's circumference so its lines do not touch the particle's trajectory.

(i) For a single charged particle, in macroscopic systems with practicable values of q, R, and m, the scale I_0 of the induced current is very small. For example, for $m = m_e$, $q = -e$, and $R = 1$ μm, Eq. (136) yields $I_0 \approx 3$ pA.[60] With the ring's inductance $\mathscr{L}$ of the order of $\mu_0 R$,[61] the contribution $\Phi_I = \mathscr{L} I \sim \mu_0 R I_0 \sim 10^{-24}$ Wb of such a small current to the net magnetic flux Φ is negligible in comparison with $\Phi_0' \sim 10^{-15}$ Wb, so the wavefunction quantization does not lead to the constancy of the total magnetic flux.

(ii) As soon as the magnetic field raises the eigenstate energy E_m above that of another eigenstate $E_{m'}$, the former state becomes metastable, and a weak interaction of the system with its environment (which is neglected in our simple model, but will be discussed in Chapter 7) may induce a quantum transition of the system to the lower-energy state, thus reducing the diamagnetic current's magnitude – see the dashed lines in Fig. 18. The flux quantization in superconductors is much more robust to such perturbations.[62]

Now let us return, once again, to the key Eq. (129), and see what it gives for one more important observable, the particle's angular momentum

$$\mathbf{L} \equiv \mathbf{r} \times \mathbf{p}\,, \tag{3.137}$$

In this particular geometry, the vector $\mathbf{L}$ has just one component, normal to the rotor plane:

$$L_z = Rp\,. \tag{3.138}$$

In classical mechanics, the rotor's L_z should be conserved (due to the absence of an external torque), but it may take arbitrary values. In quantum mechanics, the situation changes: with $p = \hbar k$, our result $k_m = m/R$ for the m^{th} eigenstate may be rewritten as

$$\boxed{(L_z)_m = R\hbar k_m = \hbar m\,.} \tag{3.139}$$

Angular momentum quantization

Thus, the angular momentum is quantized: it may be only a multiple of the Planck constant $\hbar$ – confirming the N. Bohr's guess – see Eq. (1.8). As we will see in Chapter 5, this result is very general (though it may be modified by spin effects), and the wavefunctions (129) may be interpreted as eigenfunctions of the angular momentum operator.

Let us see whether this quantization persists in more general but still axial-symmetric systems. To implement the planar rotor in our 3D world, we needed to provide rigid confinement of the particle both in the motion plane and along the 2D radius ρ. Let us consider a more general situation when only the former confinement is strict, i.e. the case when a 2D particle moves in an arbitrary axially symmetric potential

$$U(\boldsymbol{\rho}) = U(\rho)\,. \tag{3.140}$$

[60] Such weak persistent, macroscopic diamagnetic currents in non-superconducting systems have been experimentally observed by measuring the weak magnetic field induced by the currents, in systems of a large number (~10^7) of similar conducting rings – see L. Lévy *et al.*, *Phys. Rev. Lett.* **64**, 2074 (1990). Due to the dephasing effects of electron scattering by phonons and other electrons (unaccounted for in our simple theory), the effect's observation required submicron rings and millikelvin temperatures.

[61] See, e.g., EM Sec. 5.3.

[62] Interrupting a superconducting ring with a weak link (Josephson junction), i.e. forming a SQUID, we may get a switching behavior similar to that shown with dashed arrows in Fig. 18 – see, e.g., EM Sec. 6.5.

Using the well-known expression for the 2D Laplace operator in polar coordinates,[63] we may represent the 2D stationary Schrödinger equation in the form

$$-\frac{\hbar^2}{2m}\left[\frac{1}{\rho}\frac{\partial}{\partial\rho}\left(\rho\frac{\partial}{\partial\rho}\right)+\frac{1}{\rho^2}\frac{\partial^2}{\partial\varphi^2}\right]\psi+U(\rho)\psi=E\psi\,. \tag{3.141}$$

Separating the radial and angular variables as[64]

$$\psi=\mathcal{R}(\rho)\mathcal{F}(\varphi)\,, \tag{3.142}$$

we get, after the division of all terms by ψ and their multiplication by ρ^2, the following equation:

$$-\frac{\hbar^2}{2m}\left[\frac{\rho}{\mathcal{R}}\frac{d}{d\rho}\left(\rho\frac{d\mathcal{R}}{d\rho}\right)+\frac{1}{\mathcal{F}}\frac{d^2\mathcal{F}}{d\varphi^2}\right]+\rho^2U(\rho)=\rho^2E\,. \tag{3.143}$$

The fraction $(d^2\mathcal{F}/d\varphi^2)/\mathcal{F}$ should be a constant (because all other terms of the equation may be functions only of ρ), so for the function $\mathcal{F}(\varphi)$ we get an ordinary differential equation,

$$\frac{d^2\mathcal{F}}{d\varphi^2}+\nu^2\mathcal{F}=0\,, \tag{3.144}$$

where ν^2 is the variable separation constant. The fundamental solutions of Eq. (144) are evidently $\mathcal{F}\propto\exp\{\pm i\nu\varphi\}$. Now requiring, as we did for the planar rotor, the 2π periodicity of any observable, i.e.

$$\mathcal{F}(\varphi+2\pi)=\mathcal{F}(\varphi)e^{2\pi i m}\,, \tag{3.145}$$

where m is an integer, we see that the constant ν has to be equal to m. Thus we get, for the angular factor, the same result as for the full wavefunction of the planar rotor – cf. Eq. (129):

$$\mathcal{F}_m=C_m e^{im\varphi}\,,\qquad \text{with } m=0,\pm1,\pm2,... \tag{3.146}$$

Plugging the resulting relation $(d^2\mathcal{F}/d\varphi^2)/\mathcal{F}=-m^2$ back into Eq. (143), we may rewrite it as

$$-\frac{\hbar^2}{2m}\left[\frac{1}{\rho\mathcal{R}}\frac{d}{d\rho}\left(\rho\frac{d\mathcal{R}}{d\rho}\right)-\frac{m^2}{\rho^2}\right]+U(\rho)=E\,. \tag{3.147}$$

The physical interpretation of this equation is that the full energy is a sum,

$$E=E_\rho+E_\varphi\,, \tag{3.148}$$

of the radial-motion part

$$E_\rho=-\frac{\hbar^2}{2m}\frac{1}{\rho}\frac{d}{d\rho}\left(\rho\frac{d\mathcal{R}}{d\rho}\right)+U(\rho)\,. \tag{3.149}$$

and the angular-motion part

[63] See, e.g., MA Eq. (10.3) with $\partial/\partial z = 0$.

[64] At this stage, I do not want to mark the particular solution (eigenfunction) ψ and corresponding eigenenergy E with any single index, because based on our experience in Sec. 1.7, we already may expect that in a 2D problem, the role of this index will be played by *two* integers – two quantum numbers.

$$E_\varphi = \frac{\hbar^2 m^2}{2\mathscr{m}\rho^2}. \tag{3.150}$$

Now let us recall that a similar separation exists in classical mechanics, because the total energy of either 2D or 3D particle moving in a central field may be represented as [65]

$$E = \frac{\mathscr{m}}{2}v^2 + U(\rho) = \frac{\mathscr{m}}{2}\left(\dot\rho^2 + \rho^2\dot\varphi^2\right) + U(\rho) \equiv E_\rho + E_\varphi, \tag{3.151}$$

$$\text{with } E_\rho \equiv \frac{p_\rho^2}{2\mathscr{m}} + U(\rho), \qquad \text{and } E_\varphi \equiv \frac{\mathscr{m}}{2}\rho^2\dot\varphi^2 \equiv \frac{p_\varphi^2}{2\mathscr{m}} \equiv \frac{L_z^2}{2\mathscr{m}\rho^2}. \tag{3.152}$$

The comparison of the latter relation with Eqs. (139) and (150) gives us grounds to expect that the quantization rule $L_z = m\hbar$ may be valid not only for this 2D problem but in 3D cases as well. In Sec. 5.6 below, we will see that this is indeed the case.

Returning to Eq. (147), with our 1D wave mechanics experience we may expect that at any fixed m, this ordinary, linear, second-order differential equation should have (for a motion confined to a certain final region of its argument ρ) a discrete energy spectrum described by another integer quantum number – say, n. This means that the eigenfunctions (142) and corresponding eigenenergies (148) and $\mathscr{R}(\rho)$ should be indexed by two quantum numbers, m and n. So, the variable separation is not as "clean" as it was for the rectangular potential well. Normalizing the angular function $\mathscr{f}$ to the full circle, $\Delta\varphi = 2\pi$, we may rewrite Eq. (142) as

$$\psi_{m,n} = \mathscr{R}_{m,n}(\rho)\mathscr{f}_m(\varphi) = \frac{1}{(2\pi)^{1/2}}\mathscr{R}_{m,n}(\rho)e^{im\varphi}. \tag{3.153}$$

A good (and important) example of an analytically solvable problem of this type is a 2D particle whose motion is rigidly confined to a disk of radius R, but otherwise free:

$$U(\rho) = \begin{cases} 0, & \text{for } 0 \le \rho < R, \\ +\infty, & \text{for } R < \rho. \end{cases} \tag{3.154}$$

In this case, the solutions $\mathscr{R}_{m,n}(\rho)$ of Eq. (147) are proportional to the first Bessel functions $J_m(k_n\rho)$, ща epy ашкые лштв[66] with the spectrum of possible values k_n following from the boundary condition $\mathscr{R}_{m,n}(R) = 0$. Let me leave a detailed analysis of this problem for the reader's exercise.

3.6. Spherically symmetric systems: Brute force approach

Now let us proceed to the mathematically more involved, but practically even more important case of the 3D motion in a spherically symmetric potential

$$U(\mathbf{r}) = U(r). \tag{3.155}$$

[65] See, e.g., CM Sec. 3.5.

[66] A summary of the main properties of these functions, including the most important plots and a useful table of values, may be found in EM Sec. 2.7.

Let us start, again, with solving the eigenproblem for a rotor – now a *spherical rotor*, i.e. a particle confined to move on the spherical surface of radius R. The classical rotor's position on the surface is completely described by two coordinates – say, the polar angle θ and the azimuthal angle φ. Its kinetic energy is limited to the angular motion, so for the quantum-mechanical description, in the Laplace operator expressed in spherical coordinates[67] we may keep only those parts, with fixed $r = R$. Because of this, the stationary Schrödinger equation becomes

$$-\frac{\hbar^2}{2mR^2}\left[\frac{1}{\sin\theta}\frac{\partial}{\partial\theta}\left(\sin\theta\frac{\partial}{\partial\theta}\right)+\frac{1}{\sin^2\theta}\frac{\partial^2}{\partial\varphi^2}\right]\psi = E\psi\,. \tag{3.156}$$

(Again, we will attach indices to ψ and E in a minute.) With the natural variable separation,

$$\psi = \Theta(\theta)\mathcal{F}(\varphi)\,, \tag{3.157}$$

Eq. (156), with all terms multiplied by $\sin^2\theta/\Theta\mathcal{F}$, yields

$$-\frac{\hbar^2}{2mR^2}\left[\frac{\sin\theta}{\Theta}\frac{d}{d\theta}\left(\sin\theta\frac{d\Theta}{d\theta}\right)+\frac{1}{\mathcal{F}}\frac{d^2\mathcal{F}}{d^2\varphi}\right] = E\sin^2\theta\,. \tag{3.158}$$

Just as in Eq. (143), the fraction $(d^2\mathcal{F}/dx^2)/\mathcal{F}$ may be a function of φ only and hence has to be constant, giving Eq. (144) for it. So, with the same periodicity condition (145), the azimuthal functions are expressed by (146) again; in the normalized form,

$$\mathcal{F}_m(\varphi) = \frac{1}{(2\pi)^{1/2}}e^{im\varphi}\,. \tag{3.159}$$

With this, the fraction $(d^2\mathcal{F}/d\varphi^2)/\mathcal{F}$ in Eq. (158) equals $(-m^2)$, and after the multiplication of all terms of that equation by $\Theta/\sin^2\theta$, it is reduced to the following ordinary linear differential equation for the polar eigenfunctions $\Theta(\theta)$:

$$-\frac{1}{\sin\theta}\frac{d}{d\theta}\left(\sin\theta\frac{d\Theta}{d\theta}\right)+\frac{m^2}{\sin^2\theta}\Theta = \varepsilon\Theta, \qquad \text{with } \varepsilon \equiv E\Big/\frac{\hbar^2}{2mR^2}\,. \tag{3.160}$$

It is common to recast it into an equation for a new function $P(\xi) \equiv \Theta(\theta)$, with $\xi \equiv \cos\theta$:

$$\frac{d}{d\xi}\left[\left(1-\xi^2\right)\frac{dP}{d\xi}\right]+\left[l(l+1)-\frac{m^2}{1-\xi^2}\right]P = 0\,, \tag{3.161}$$

where a new notation for the normalized energy is introduced: $l(l+1) \equiv \varepsilon$. The motivation for such notation is that, according to the mathematical analysis of Eq. (161) with integer m,[68] it has physically suitable solutions, with P being an either odd or even function of ξ, only if l (called the *orbital quantum number*) is an integer: $l = 0, 1, 2,\ldots$, and only it is not smaller than $|m|$, i.e. if

$$-l \le m \le +l\,. \tag{3.162}$$

[67] See, e.g., MA Eq. (10.9).

[68] This analysis was first carried out by A.-M. Legendre (1752-1833). Just as a historic note: besides many original mathematical achievements, Dr. Legendre had authored a famous textbook, *Éléments de Géométrie,* which dominated teaching geometry through the 19th century.

This fact immediately gives the following spectrum of the spherical rotor's angular[69] energy E – and, as we will see later, that of any spherically symmetric system:

$$E_l = \frac{\hbar^2 l(l+1)}{2mR^2}, \tag{3.163}$$

Angular energy spectrum

so the only effect of the magnetic quantum number m here is imposing the restriction (162) on the non-negative orbital quantum number l. This means, in particular, that each energy level (163) corresponds to $(2l + 1)$ different values of m, i.e. is $(2l + 1)$–degenerate.

To understand the nature of this degeneracy, we need to explore the corresponding eigenfunctions of Eq. (161). They are naturally numbered by two integers, m and l, and are called the a*ssociated Legendre functions* P_l^m. (Note that here m is an upper index, not a power!) For the particular, simplest case $m = 0$, these functions are the so-called *Legendre polynomials* $P_l(\xi) \equiv P_l^0(\xi)$, which may be defined as the solutions of the following *Legendre equation*, resulting from Eq. (161) at $m = 0$:

$$\frac{d}{d\xi}\left[\left(1-\xi^2\right)\frac{d}{d\xi}P\right] + l(l+1)P = 0, \tag{3.164}$$

Legendre equation

and may be calculated explicitly from the following *Rodrigues formula*:[70]

$$P_l(\xi) = \frac{1}{2^l l!}\frac{d^l}{d\xi^l}(\xi^2-1)^l, \quad l = 0, 1, 2, \ldots. \tag{3.165}$$

Legendre polynomials

Using this formula, it is easy to spell out a few lowest Legendre polynomials:

$$P_0(\xi) = 1, \quad P_1(\xi) = \xi, \quad P_2(\xi) = \frac{1}{2}\left(3\xi^2 - 1\right), \quad P_3(\xi) = \frac{1}{2}\left(5\xi^3 - 3\xi\right), \ldots, \tag{3.166}$$

though such explicit expressions become bulkier and bulkier as l is increased. As these expressions (and Fig. 19) show, as the argument ξ is increased, all these functions end up at the same point, $P_l(+1) = +1$, while starting at either at the same point or at the opposite point: $P_l(-1) = (-1)^l$.

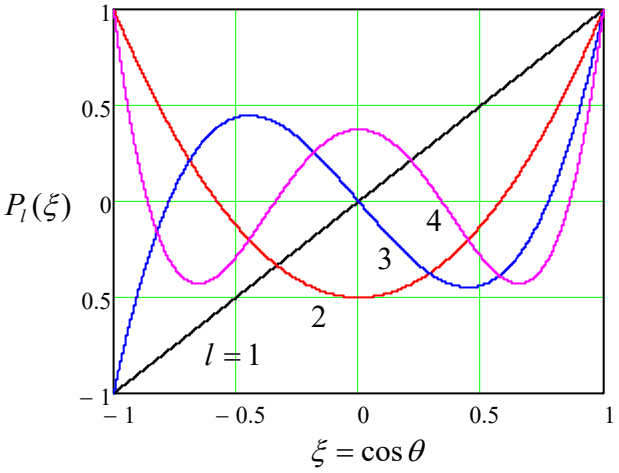

Fig. 3.19. A few lowest Legendre polynomials.

[69] This qualification is important because this E does not include the energy of radial confinement – see Sec. 2.1.

[70] This wonderful formula may be readily proved by plugging it into Eq. (164), but was not so easy to discover! This was done (independently) by B. O. Rodrigues in 1816, J. Ivory in 1824, and C. Jacobi in 1827.

On the way between these two endpoints, the l^{th} polynomial crosses the horizontal axis exactly l times, i.e. Eq. (164) has exactly l roots. (In this behavior, we may readily recognize the "standing wave" pattern typical for all 1D eigenproblems – cf. Figs. 1.8 and 2.35, as well as the discussion of the Sturm oscillation theorem at the end of Sec. 2.9.) It is also easy to use the Rodrigues formula (165) and the integration by parts to show that on the segment $-1 \le \xi \le +1$, th polynomials form a full orthogonal set of functions, with the following normalization rule:

$$\int_{-1}^{+1} P_l(\xi) P_{l'}(\xi) d\xi = \frac{2}{2l+1} \delta_{ll'}. \tag{3.167}$$

For $m > 0$, the associated Legendre functions (now *not* necessarily polynomials!), may be expressed via the Legendre polynomials (165) using the following formula:[71]

Associated Legendre functions

$$P_l^m(\xi) = (-1)^m (1-\xi^2)^{m/2} \frac{d^m}{d\xi^m} P_l(\xi), \tag{3.168}$$

while the functions with a negative magnetic quantum number may be found as

$$P_l^{-m}(\xi) = (-1)^m \frac{(l-m)!}{(l+m)!} P_l^m(\xi), \qquad \text{for } m > 0. \tag{3.169}$$

On the segment $-1 \le \xi \le +1$, the associated Legendre functions with a fixed index m form a full orthogonal set, with the normalization relation

$$\int_{-1}^{+1} P_l^m(\xi) P_{l'}^m(\xi) d\xi = \frac{2}{2l+1} \frac{(l+m)!}{(l-m)!} \delta_{ll'}, \tag{3.170}$$

which is evidently a generalization of Eq. (167) to arbitrary m.

Since the difference between the angles θ and φ is, to a large extent, artificial (due to an arbitrary direction of the polar axis), physicists prefer to use not the functions $\Theta(\theta) \propto P_l^m(\cos\theta)$ and $\mathcal{T}_m(\varphi) \propto e^{im\varphi}$ separately, but normalized products of the type (157), which are called the s*pherical harmonics*:

Spherical harmonics

$$Y_l^m(\theta,\varphi) \equiv \left[\frac{(2l+1)}{4\pi} \frac{(l-m)!}{(l+m)!}\right]^{1/2} P_l^m(\cos\theta) e^{im\varphi}. \tag{3.171}$$

The specific front factor in Eq. (171) is chosen in a way to simplify the following two expressions: the relation of the spherical harmonics with opposite signs of the magnetic quantum number:

$$Y_l^{-m}(\theta,\varphi) = (-1)^m \left[Y_l^m(\theta,\varphi)\right]^*, \tag{3.172}$$

and the following normalization relation:

$$\oint_{4\pi} Y_l^m(\theta,\varphi) \left[Y_{l'}^{m'}(\theta,\varphi)\right]^* d\Omega = \delta_{ll'} \delta_{mm'}, \tag{3.173}$$

[71] Note that some texts use different choices for the front factor (called the *Condon-Shortley phase*) in the functions P_l^m, which do not affect the final results for the spherical harmonics Y_l^m.

with the integration over the whole solid angle. The last formula shows that on a spherical surface, the spherical harmonics form an orthonormal set of functions. This set is also full, so any function defined on the surface may be uniquely represented as a linear combination of Y_l^m.

Despite the somewhat intimidating character of the formulas given above, they yield quite simple expressions for the lowest spherical harmonics, which are most important for applications:

$$l = 0: \quad Y_0^0 = (1/4\pi)^{1/2}, \tag{3.174}$$

$$l = 1: \quad \begin{cases} Y_1^{-1} = (3/8\pi)^{1/2} \sin\theta\, e^{-i\varphi}, \\ Y_1^0 = (3/4\pi)^{1/2} \cos\theta, \\ Y_1^1 = -(3/8\pi)^{1/2} \sin\theta\, e^{i\varphi}, \end{cases} \tag{3.175}$$

$$l = 2: \quad \begin{cases} Y_2^{-2} = (15/32\pi)^{1/2} \sin^2\theta\, e^{-2i\varphi}, \\ Y_2^{-1} = (15/8\pi)^{1/2} \sin\theta\cos\theta\, e^{-i\varphi}, \\ Y_2^0 = (3/16\pi)^{1/2} (3\cos^2\theta - 1), \\ Y_2^1 = -(15/8\pi)^{1/2} \sin\theta\cos\theta\, e^{i\varphi}, \\ Y_2^2 = (15/32\pi)^{1/2} \sin^2\theta\, e^{2i\varphi}. \end{cases} \tag{3.176}$$

It is important to understand the general structure and symmetry of these functions, and in such matters, pictures are invaluable. Since the spherical harmonics with $m \neq 0$ are complex, the most popular way of their graphical representation is to normalize their real and imaginary parts as

$$Y_{lm} \equiv \sqrt{2}(-1)^m \times \begin{cases} \mathrm{Im}\left(Y_l^{|m|}\right) \propto \sin m\varphi, & \text{for } m < 0, \\ \mathrm{Re}\left(Y_l^{|m|}\right) \propto \cos m\varphi, & \text{for } m > 0, \end{cases} \tag{3.177}$$

(for $m = 0$, $Y_{l0} \equiv Y_l^0$), and then plot the magnitude of these real functions[72] in the spherical coordinates as the distance from the origin, while using two colors to show their sign – see Fig. 20.

Let us start from the simplest case $l = 0$. According to Eq. (162), for this lowest orbital quantum number, there may be only one magnetic quantum number: $m = 0$, and according to Eq. (174), the spherical harmonic corresponding to that state is just a constant. Thus the wavefunction of this so-called *s state*[73] is uniformly distributed over the sphere. Since this function has no gradient in any angular direction, it is only natural that the angular kinetic energy (163) of a particle in this state equals zero.

According to the same Eq. (162), for $l = 1$, there are 3 different *p states*, with $m = -1$, $m = 0$, and $m = +1$ – see Eq. (175). As the second row of Fig. 20 shows, these states are essentially identical in structure and are just differently oriented in space, thus readily explaining the 3-fold degeneracy of the kinetic energy (163).

[72] Such real functions Y_{lm}, which also form a full orthonormal set, and are frequently called the *real* (or "tesseral") *spherical harmonics*, are more convenient than the complex harmonics Y_l^m for several applications, especially when the variables of interest are real by definition.

[73] The letter names for the states with various values of l stem from the history of optical spectroscopy – for example, the letter "*s*" (used for states with $l = 0$) originally denoted the "sharp" optical line series, etc. The sequence of the letters is as follows: *s, p, d, f, g*, and then continuing in alphabetical order.

Such a simple explanation, however, is not valid for the 5 different *d states* ($l = 2$), shown in the third row of Fig. 20, as well as the states with higher l: despite their equal energies, they differ not only by their spatial orientation but their structure as well. All states with $m = 0$ have a nonzero gradient only in the θ direction. On the contrary, the states with the ultimate values of m ($\pm l$), change only monotonically (as $\sin^l\theta$) in the polar direction, while oscillating in the azimuthal direction. The states with intermediate values of m provide a gradual transition between these two extremes, oscillating in both directions, stronger and stronger in the azimuthal direction as $|m|$ is increased. Still, the magnetic quantum number, surprisingly, does not affect the angular energy for any l.

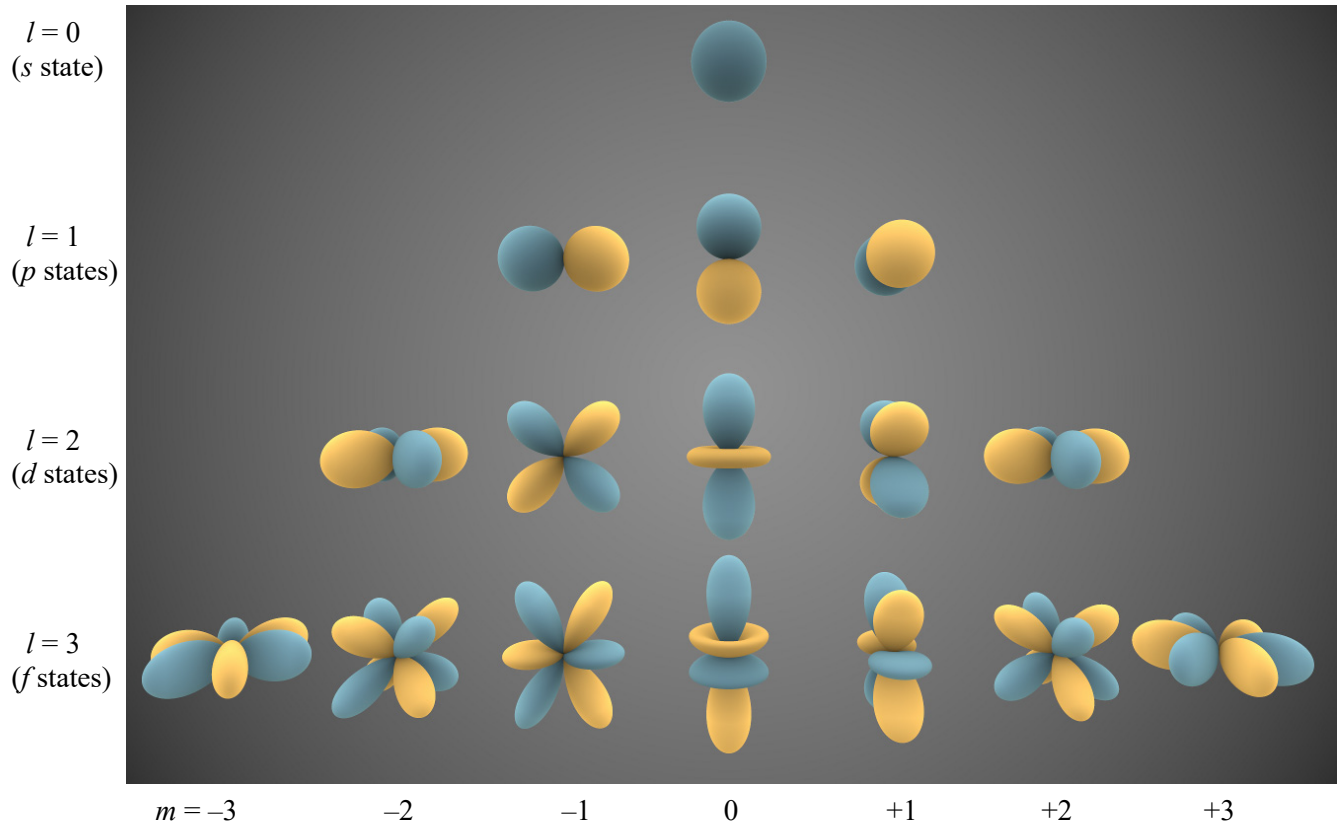

Fig. 3.20. Plots of several lowest real spherical harmonics Y_{lm}. (Adapted from https://en.wikipedia.org/wiki/Spherical_harmonics under the CC BY-SA 3.0 license.)

Another counter-intuitive feature of the spherical harmonics follows from the comparison of Eq. (163) with the second of Eqs. (152), which, in classical mechanics, is valid for the total angular momentum as well. They coincide only if we interpret

$$L^2 \equiv \hbar^2 l(l+1), \tag{3.178}$$

as the value of the total $L^2 \equiv |\mathbf{L}^2|$, including the θ and φ components of the vector $\mathbf{L}$, in the state with eigenfunction Y_l^m. On the other hand, the structure (159) of the azimuthal component $\mathcal{F}(\varphi)$ of the wavefunction is exactly the same as in 2D axially symmetric problems, implying that Eq. (139) still gives correct values $L_z = m\hbar$ for the z-component of the angular momentum. This fact invites a question: why for any state with $l > 0$, $(L_z)^2 = m^2\hbar^2 \le l^2\hbar^2$ is always less than $L^2 = l(l+1)\hbar^2$? In other words, what prevents the angular momentum vector to be fully aligned with the z-axis?

Besides the difficulty of answering this question using the above formulas, this analysis (though mathematically complete), is as intellectually unsatisfactory as the harmonic oscillator analysis in Sec. 2.9. In particular, it does not explain the meaning of the extremely simple relations for the eigenvalues of the energy and the angular momentum, coexisting with rather complicated eigenfunctions.

We will obtain natural answers to all these questions and concerns in Sec. 5.6 below, and now let us proceed to the extension of our wave-mechanical analysis to the 3D motion in an *arbitrary* spherically symmetric potential (155). In this case, we have to use the full form of the Laplace operator in spherical coordinates.[74] The variable separation procedure is an evident generalization of what we have done above, with the particular solutions of the type

$$\psi = \mathcal{R}(r)\Theta(\theta)\mathcal{F}(\varphi), \tag{3.179}$$

whose substitution into the stationary Schrödinger equation yields

$$-\frac{\hbar^2}{2mr^2}\left[\frac{1}{\mathcal{R}}\frac{d}{dr}\left(r^2\frac{d\mathcal{R}}{dr}\right)+\frac{1}{\Theta}\frac{1}{\sin\theta}\frac{d}{d\theta}\left(\sin\theta\frac{d\Theta}{d\theta}\right)+\frac{1}{\sin^2\theta}\frac{1}{\mathcal{F}}\frac{d^2\mathcal{F}}{d\varphi^2}\right]+U(r)=E. \tag{3.180}$$

It is evident that the angular part of the left-hand side (the two last terms in the square brackets) separates from the radial part, and that for the former part, we get Eq. (156) again, with the only change, $R \to r$. This change does not affect the fact that the eigenfunctions of that equation are still the spherical harmonics (171), which obey Eq. (164). As a result, Eq. (180) gives the following equation for the radial function $\mathcal{R}(r)$:

$$-\frac{\hbar^2}{2mr^2}\left[\frac{1}{\mathcal{R}}\frac{d}{dr}\left(r^2\frac{d\mathcal{R}}{dr}\right)-l(l+1)\right]+U(r)=E. \tag{3.181a}$$

Note that no information about the magnetic quantum number m has crept into this radial equation (besides setting the limitation (162) for the possible values of l) so it includes only the orbital quantum number l. The equation may be also rewritten in a form similar to Eq. (148):

$$E = E_r + E_{\theta,\varphi}, \quad \text{with } E_r = -\frac{\hbar^2}{2mr^2}\frac{1}{\mathcal{R}}\frac{d}{dr}\left(r^2\frac{d\mathcal{R}}{dr}\right)+U(r) \text{ and } E_{\theta,\varphi}=\frac{\hbar^2 l(l+1)}{2mr^2}, \tag{3.181b}$$

expressing the same separability of the particle's energy in the central field into the radial and angular components as in classical mechanics – cf. Eqs. (151)-(152), and also Eq. (163). In particular, since the expectation value of the latter component cannot be negative at $l \geq 0$, this means that the ground state of any spherically symmetric system is an *s*-state, with $l = 0$ and hence $m = 0$.

Let us explore the radial equation for the simple case of a 3D particle free to move inside the sphere of radius R – say, confined there by the potential[75]

$$U = \begin{cases} 0, & \text{for } 0 \leq r < R, \\ +\infty, & \text{for } R < r. \end{cases} \tag{3.182}$$

In this case, Eq. (181a) is reduced to

[74] Again, see MA Eq. (10.9).

[75] This problem, besides giving a simple example of the quantization in spherically symmetric systems, is also an important precursor for the discussion of scattering by spherically symmetric potentials in Sec. 8.

$$-\frac{\hbar^2}{2mr^2}\left[\frac{1}{\mathcal{R}}\frac{d}{dr}\left(r^2\frac{d\mathcal{R}}{dr}\right)-l(l+1)\right]=E. \tag{3.183}$$

Multiplying both parts of this equality by $r^2\mathcal{R}$, and introducing the dimensionless argument $\xi \equiv kr$, where k^2 is defined by the usual relation $\hbar^2k^2/2m = E$, we obtain the canonical form of this equation,

$$\xi^2\frac{d^2\mathcal{R}}{d\xi^2}+2\xi\frac{d\mathcal{R}}{d\xi}+\left[\xi^2-l(l+1)\right]\mathcal{R}=0, \tag{3.184}$$

which is satisfied with the so-called *spherical Bessel functions* of the first and second kind, $j_l(\xi)$ and $y_l(\xi)$.[76] These functions are directly related to the Bessel functions of semi-integer order,[77]

$$j_l(\xi)=\left(\frac{\pi}{2\xi}\right)^{1/2}J_{l+\frac{1}{2}}(\xi), \qquad y_l(\xi)=\left(\frac{\pi}{2\xi}\right)^{1/2}Y_{l+\frac{1}{2}}(\xi), \tag{3.185}$$

but are actually much simpler than even the "usual" Bessel functions, such as $J_n(\xi)$ and $Y_n(\xi)$ of an integer order n, because the former ones may be directly expressed via elementary functions:

$$\begin{aligned} &j_0(\xi)=\frac{\sin\xi}{\xi}, && j_1(\xi)=\frac{\sin\xi}{\xi^2}-\frac{\cos\xi}{\xi}, && j_2(\xi)=\left(\frac{3}{\xi^3}-\frac{1}{\xi}\right)\sin\xi-\frac{3}{\xi^2}\cos\xi,...,\\ &y_0(\xi)=-\frac{\cos\xi}{\xi}, && y_1(\xi)=-\frac{\cos\xi}{\xi^2}-\frac{\sin\xi}{\xi}, && y_2(\xi)=-\left(\frac{3}{\xi^3}-\frac{1}{\xi}\right)\cos\xi-\frac{3}{\xi^2}\sin\xi,... \end{aligned} \tag{3.186}$$

A few lowest-order spherical Bessel functions are plotted in Fig. 21.

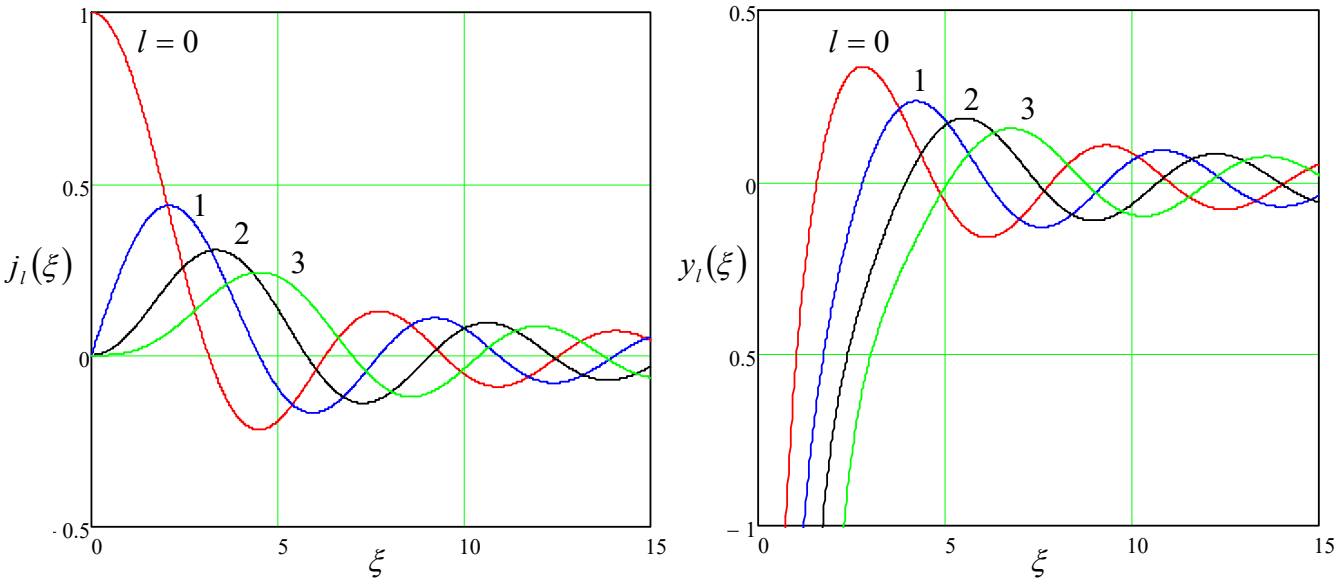

Fig. 3.21. Several lowest-order spherical Bessel functions.

[76] Alternatively, $y_l(\xi)$ are called "spherical Weber functions" or "spherical Neumann functions".

[77] Note that the Bessel functions $J_\nu(\xi)$ and $Y_\nu(\xi)$ of *any* order ν obey the universal recurrence relations and asymptotic formulas (discussed, e.g., in EM Sec. 2.7), so many properties of the functions $j_l(\xi)$ and $y_l(\xi)$ may be readily derived from these relations and Eqs. (185).

As these formulas and plots show, the functions $y_l(\xi)$ are diverging at $\xi \to 0$, and thus cannot be used in the solution of our current problem (182), so we have to take

$$\mathcal{R}_l(r) = \text{const} \times j_l(kr). \tag{3.187}$$

Still, even for these functions, with the sole exception of the simplest function $j_0(\xi)$, the characteristic equation $j_l(kR) = 0$, resulting from the boundary condition $\mathcal{R}(R) = 0$, can be solved only numerically. However, the roots $\xi_{l,n}$ of the equation $j_l(\xi) = 0$, where the integer n (= 1, 2, 3,…) is the root's number, are tabulated in virtually any math handbook, and we may express the eigenvalues we are interested in,

$$k_{l,n} = \frac{\xi_{l,n}}{R}, \qquad E_{l,n} = \frac{\hbar^2 k_{l,n}^2}{2m} \equiv \frac{\hbar^2 \xi_{l,n}^2}{2mR^2}, \tag{3.188}$$

via these tabulated numbers. The table on the right lists several smallest roots, and the corresponding eigenenergies (normalized to their natural unit $E_0 \equiv \hbar^2/2mR^2$), in the order of their growth. It shows a very interesting effect: going up the energy spectrum, the first energies grow due to unit increments of the orbital quantum number l and the corresponding increases of the first roots of the functions $j_l(\xi)$, at the same (lowest) radial quantum number $n = 1$. Then, suddenly, the second root of $j_0(\xi)$, accompanied by a jump to $n = 2$, cuts into this orderly sequence, just to be followed by the first root of $j_3(\xi)$, returning to the initial sequence with $n = 1$. With the further growth of energy, the sequences of l and n become even more entangled.

l	n	$\xi_{l,n}$	$E_{l,n}/E_0 = (\xi_{l,n})^2$
0	1	$\pi \approx 3.1415$	$\pi^2 \approx 9.87$
1	1	4.493	20.19
2	1	5.763	33.21
0	2	$2\pi \approx 6.283$	$4\pi^2 \approx 39.48$
3	1	6.988	48.83

To complete the discussion of our current problem (182), note again that the energy levels listed in the table above are $(2l+1)$-degenerate because each of them corresponds to $(2l + 1)$ different eigenfunctions, each with a specific value of the magnetic quantum number m:

$$\psi_{n,l,m} = C_{l,n} j_l\left(\frac{\xi_{l,n} r}{R}\right) Y_l^m(\theta,\varphi), \qquad \text{with } -l \le m \le +l. \tag{3.189}$$

3.7 Atoms

Now we are ready to discuss atoms, starting from the simplest, exactly solvable *Bohr atom problem*, i.e. that of a single particle's motion in the so-called *attractive Coulomb potential*[78]

$$U(r) = -\frac{C}{r}, \quad \text{with } C > 0. \tag{3.190}$$

Attractive Coulomb potential

The natural scales of E and r in this problem are commonly defined by the requirement of equality of the kinetic and potential energy magnitude scales (dropping all numerical coefficients):

[78] Historically, the solution of this problem in 1928, which reproduced the main results (1.12)-(1.13) of the "old" quantum theory developed by N. Bohr in 1912, but without its phenomenological assumptions, was the decisive step toward the general acceptance of Schrödinger's wave mechanics.

$$E_0 \equiv \frac{\hbar^2}{mr_0^2} \equiv \frac{C}{r_0}, \tag{3.191}$$

similar to its particular case (1.13b). Solving this system of two equations, we get[79]

$$E_0 \equiv \frac{\hbar^2}{mr_0^2} \equiv m\left(\frac{C}{\hbar}\right)^2, \qquad \text{and} \quad r_0 \equiv \frac{\hbar^2}{mC}. \tag{3.192}$$

In the normalized units $\varepsilon \equiv E/E_0$ and $\xi \equiv r/r_0$, Eq. (181) for our case (190) looks relatively simple,

$$\frac{d^2\mathcal{R}}{d\xi^2} + \frac{2}{\xi}\frac{d\mathcal{R}}{d\xi} - l(l+1)\mathcal{R} + 2\left(\varepsilon + \frac{1}{\xi}\right)\mathcal{R} = 0, \tag{3.193}$$

but unfortunately, its eigenfunctions may be called elementary only in the most generous meaning of the word. With the normalization

$$\int_0^\infty \mathcal{R}_{n,l}\mathcal{R}_{n',l} r^2 dr = \delta_{nn'}, \tag{3.194}$$

these (mutually orthogonal) functions may be represented as

Bohr atom: radial functions

$$\mathcal{R}_{n,l}(r) = -\left\{\left(\frac{2}{nr_0}\right)^3 \frac{(n-l-1)!}{2n[(n+l)!]^3}\right\}^{1/2} \exp\left\{-\frac{r}{nr_0}\right\}\left(\frac{2r}{nr_0}\right)^l L_{n-l-1}^{2l+1}\left(\frac{2r}{nr_0}\right). \tag{3.195}$$

Here $L_p^q(\xi)$ are the so-called *associated Laguerre* polynomials, which may be calculated as

Associated Laguerre polynomials

$$L_p^q(\xi) = (-1)^q \frac{d^q}{d\xi^q} L_{p+q}(\xi). \tag{3.196}$$

from the *simple Laguerre polynomials* $L_p(\xi) \equiv L_p^0(\xi)$.[80] In turn, the easiest way to obtain $L_p(\xi)$ is to use the following *Rodrigues formula*:[81]

Rodrigues formula for Laguerre polynomials

$$L_p(\xi) = e^\xi \frac{d^p}{d\xi^p}\left(\xi^p e^{-\xi}\right). \tag{3.197}$$

Note that in contrast with the associated Legendre *functions* P_l^m, participating in the spherical harmonics, all L_p^q are just *polynomials*, and those with small indices p and q are indeed quite simple:

[79] For the most important case of the hydrogen atom, with $C = e^2/4\pi\varepsilon_0$, these scales are reduced, respectively, to the Bohr radius r_B (1.10) and the Hartree energy E_H (1.13a). Note also that according to Eq. (192), for the so-called *hydrogen-like atom* (actually, a positive ion) with $C = Z(e^2/4\pi\varepsilon_0)$, these two key parameters are rescaled as $r_0 = r_B/Z$ and $E_0 = Z^2E_H$.

[80] In Eqs. (196)-(197), p and q are non-negative integers, with no relation whatsoever to the particle's momentum or electric charge. Sorry for this notation, but it is absolutely common, and can hardly result in any confusion.

[81] Named after the same B. O. Rodrigues, and belonging to the same class as his other famous result, Eq. (165) for the Legendre polynomials.

$$\begin{aligned} &L_0^0(\xi)=1, \qquad L_1^0(\xi)=-\xi+1, \qquad L_2^0(\xi)=\xi^2-4\xi+2, \\ &L_0^1(\xi)=1, \qquad L_1^1(\xi)=-2\xi+4, \qquad L_2^1(\xi)=3\xi^2-18\xi+18, \\ &L_0^2(\xi)=2, \qquad L_1^2(\xi)=-6\xi+18, \qquad L_2^2(\xi)=12\xi^2-96\xi+144, \text{ etc.} \end{aligned} \tag{3.198}$$

Returning to Eq. (195), we see that the natural quantization of the radial equation (193) has brought us a new integer quantum number n. To understand its range, we should notice that according to Eq. (197), the highest power of terms in the polynomial L_{p+q} is $(p + q)$, and hence, according to Eq. (196), that of L_p^q is p, so the highest power in the polynomial participating in Eq. (195) is $(n - l - 1)$. Since the power cannot be negative to avoid the unphysical divergence of wavefunctions at $r \to 0$, the radial quantum number n has to obey the restriction $n \geq l + 1$. Since l, as we already know, may take the values $l = 0, 1, 2,\ldots$, we may conclude n may only take the following values:

$$n = 1, 2, 3,... \tag{3.199}$$

What makes this relation very important is the following, most surprising result: the eigenenergies corresponding to the wavefunctions (179), which are indexed with *three* quantum numbers:

$$\psi_{n,l.m} = \mathcal{R}_{n,l}(r)Y_l^m(\theta,\varphi), \tag{3.200}$$

depend only on *one* of them, n:

$$\varepsilon = \varepsilon_n = -\frac{1}{2n^2}, \qquad \text{i.e. } E_n = -\frac{E_0}{2n^2} = -\frac{1}{2n^2}m\left(\frac{C}{\hbar}\right)^2. \tag{3.201}$$

i.e. agree with Bohr's formula (1.12). Because of this reason, n is usually called the *principal quantum number*, and the above relation between it and the "more subordinate" orbital quantum number l is rewritten as

$$l \leq n-1. \tag{3.202}$$

Together with the inequality (162), this gives us the following, very important hierarchy of the three quantum numbers involved in the Bohr atom problem:

Bohr atom: quantum numbers

$$\boxed{1 \leq n \leq \infty \quad \Rightarrow \quad 0 \leq l \leq n-1 \quad \Rightarrow \quad -l \leq m \leq +l.} \tag{3.203}$$

Taking into account the $(2l + 1)$-degeneracy related to m, and using the well-known formula for the arithmetic progression,[82] we see that the n^{th} energy level (201) has the following *orbital degeneracy*:

$$g = \sum_{l=0}^{n-1}(2l+1) \equiv 2\sum_{l=0}^{n-1} l + \sum_{l=0}^{n-1} 1 = 2\frac{n(n-1)}{2} + n \equiv n^2. \tag{3.204}$$

Due to its importance for atoms, let us spell out the hierarchy (203) of a few lowest-energy states, using the traditional state notation in that the value of n is followed by the letter that denotes the value of l:

$$n = 1: \quad l = 0 \quad (\text{one } 1s \text{ state}) \quad m = 0. \tag{3.205}$$

$$\begin{aligned} n = 2: \quad & l = 0 \quad (\text{one } 2s \text{ state}) \quad m = 0, \\ & l = 1 \quad (\text{three } 2p \text{ states}) \quad m = 0, \pm 1. \end{aligned} \tag{3.206}$$

[82] See, e.g., MA Eq. (2.5a).

$$\begin{aligned} n=3:\quad & l=0 \quad (\text{one } 3s \text{ state}) && m=0, \\ & l=1 \quad (\text{three } 3p \text{ states}) && m=0,\pm 1, \\ & l=2 \quad (\text{five } 3d \text{ states}) && m=0,\pm 1,\pm 2. \end{aligned} \tag{3.207}$$

Figure 22 shows plots of the radial functions (195) of the listed states. The most important of them is of course the ground ($1s$) state with $n = 1$ and hence $E = -E_0/2$. According to Eqs. (195) and (198), its radial function is just a simple decaying exponent

Ground state: radial function

$$\mathcal{R}_{1,0}(r) = \frac{2}{r_0^{3/2}} e^{-r/r_0}, \tag{3.208}$$

while its angular distribution is uniform – see Eq. (174). The gap between the ground state energy $E_g = -E_0/2$ and the energy $E = -E_0/8$ of the lowest excited states (with $n = 2$) in a hydrogen atom (in which $E_0 = E_H \approx 27.2$ eV) is as large as ~ 10 eV, so their thermal excitation requires temperatures as high as ~10^5 K, and the overwhelming part of all hydrogen atoms in the visible Universe are in their ground state. Since atomic hydrogen makes up about 75% of the "normal" matter,[83] we are very fortunate that such simple formulas as Eqs. (174) and (208) describe the atomic states prevalent in Mother Nature!

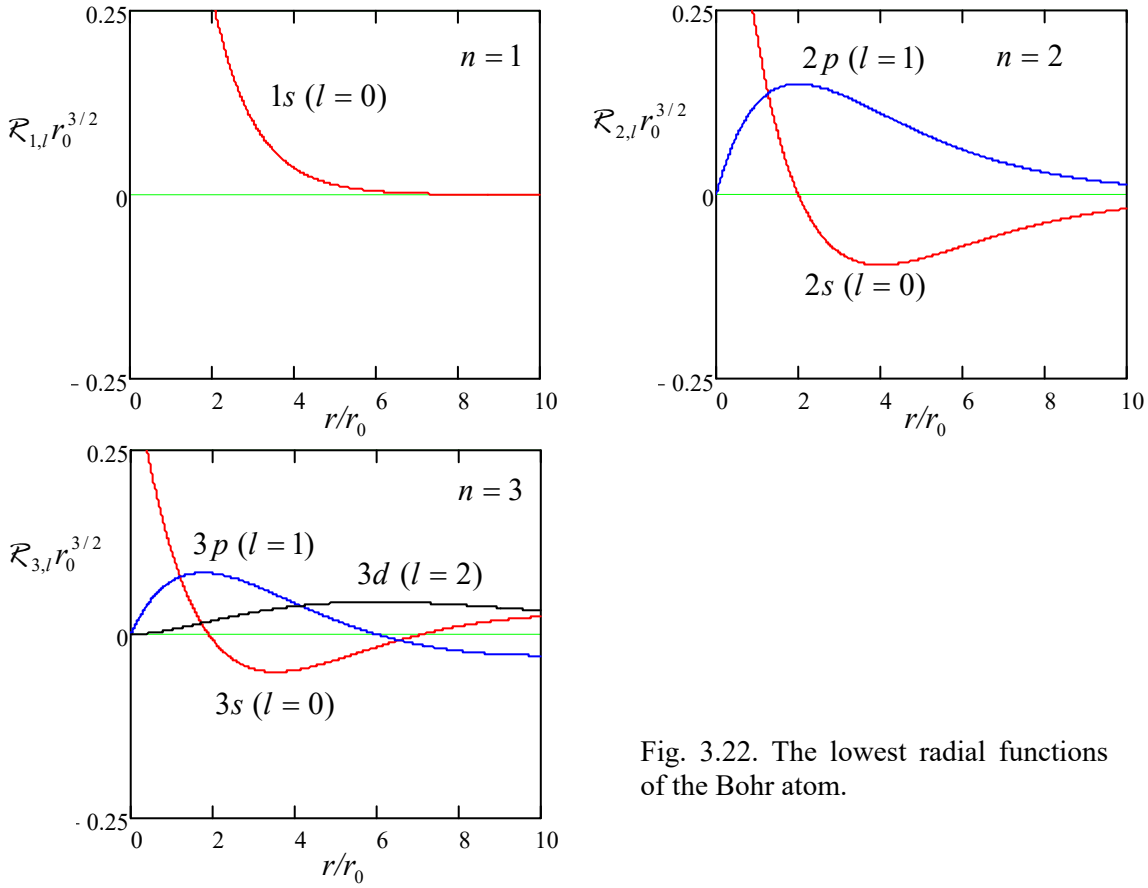

Fig. 3.22. The lowest radial functions of the Bohr atom.

According to Eqs. (195) and (198), the radial functions of the lowest excited states, $2s$ (with $n = 2$ and $l = 0$), and $2p$ (with $n = 2$ and $l = 1$) are also not too complicated:

[83] Excluding the so-far hypothetical *dark matter* and *dark energy*.

$$\mathcal{R}_{2,0}(r) = \frac{1}{(2r_0)^{3/2}}\left(2 - \frac{r}{r_0}\right)e^{-r/2r_0}, \qquad \mathcal{R}_{2,1}(r) = \frac{1}{(2r_0)^{3/2}}\frac{r}{3^{1/2}r_0}e^{-r/2r_0}, \tag{3.209}$$

with the former of these states (2*s*) having a uniform angular distribution, and the three latter (2*p*) states, with different $m = 0, \pm 1$, having simple angular distributions, which differ only by their spatial orientation – see Eq. (175) and the second row of Fig. 20. The most important trend here, clearly visible from the comparison of the two top panels of Fig. 22 as well, is a larger radius of the decay exponent in the radial functions ($2r_0$ for $n = 2$ instead of r_0 for $n = 1$), and hence a larger radial extension of the states. This trend is confirmed by the following general formula:[84]

$$\langle r \rangle_{n,l} = \frac{r_0}{2}\left[3n^2 - l(l+1)\right]. \tag{3.210}$$

The second important trend is that at a fixed n, the orbital quantum number l determines how fast the wavefunction changes with r near the origin, and how much it oscillates in the radial direction at larger values of r. For example, the 2*s* eigenfunction $\mathcal{R}_{2,0}(r)$ is different from zero at $r = 0$, and "makes one wiggle" (has one root) in the radial direction, while the eigenfunctions 2*p* equal zero at $r = 0$ but do not cross the horizontal axis after that. Instead, those wavefunctions oscillate as the functions of an angle – see the second row of Fig. 20. The same trend is clearly visible for $n = 3$ (see the bottom panel of Fig. 22), and continues for the higher values of n.

The states with $l = l_{\max} \equiv n - 1$ may be viewed as crude analogs of the circular motion of a particle in a plane whose orientation defines the quantum number m. On the other hand, the best classical image of the *s*-state ($l = 0$) is a purely radial, spherically symmetric motion of the particle to and from the attracting center. (The latter image is especially imperfect because the motion needs to happen simultaneously in all radial directions.) The classical language becomes reasonable only for the highly degenerate *Rydberg states*, with $n >> 1$, whose linear superpositions may be used to compose wave packets closely following the classical (circular or elliptic) trajectories of the particle – just as was discussed in Sec. 2.2 for the free 1D motion.

Besides Eq. (210), mathematics gives us several other simple relations for the radial functions $\mathcal{R}_{n,l}$ (and, since the spherical harmonics are normalized to 1, for the eigenfunctions as the whole), including those that we will use later in the course:[85]

$$\left\langle \frac{1}{r} \right\rangle_{n,l} = \frac{1}{n^2 r_0}, \quad \left\langle \frac{1}{r^2} \right\rangle_{n,l} = \frac{1}{n^3\left(l+\tfrac{1}{2}\right)r_0^2}, \qquad \left\langle \frac{1}{r^3} \right\rangle_{n,l} = \frac{1}{n^3 l\left(l+\tfrac{1}{2}\right)(l+1)r_0^3}. \tag{3.211}$$

In particular, the first of these formulas means that for *any* eigenfunction $\psi_{n,l,m}$, with all its complicated radial and angular dependencies, there is a simple relation between the potential and full energies:

$$\langle U \rangle_{n,l} = -C\left\langle \frac{1}{r} \right\rangle_{n,l} = -\frac{C}{n^2 r_0} = -\frac{E_0}{n^2} = 2E_n, \tag{3.212}$$

so the average kinetic energy of the particle, $\langle T \rangle_{n,l} = E_n - \langle U \rangle_{n,l}$, is equal to $E_n - 2E_n = |E_n| > 0$.

[84] Note that even at the largest value of l, equal to $(n-1)$, the second term $l(l+1)$ in the square brackets of Eq. (210) is equal to $(n^2 - n)$, and hence cannot over-compensate the first term $3n^2$.

[85] The first of these relations may be proved using the Hellmann-Feynman theorem (see Sec. 1.8); this proof will be offered for the reader's exercise after a more general form of this theorem has been proved in Chapter 6.

As in the several previous cases we have met, simple results (201), (210)-(212) are in sharp contrast with the rather complicated expressions for the corresponding eigenfunctions. Historically, this contrast gave an additional motivation for the development of more general approaches to quantum mechanics, that would replace or at least complement the brute-force (wave-mechanics) analysis. A discussion of such an approach will be the main topic of the next chapter.

Rather strikingly, the above classification of the quantum numbers, with a few steals from the later chapters of this course, allows a semi-quantitative explanation of the whole system of chemical elements. The "only" two additions we need are the following facts:

(i) due to their unavoidable interaction with relatively low-temperature environments, atoms tend to relax into their lowest-energy state, and

(ii) due to the Pauli principle (valid for electrons as the Fermi particles), each *orbital eigenstate* discussed above may house two electrons with opposite spins.

Of course, atomic electrons do interact, so their quantitative description requires quantum mechanics of multiparticle systems, which is rather complex. (Its main concepts will be discussed in Chapter 8.) However, the lion's share of this interaction is reduced to simple electrostatic *screening*, i.e. a partial compensation of the electric charge of the atomic nucleus, as felt by a particular electron, by other electrons of the atom. This screening changes quantitative results (such as the energy scale E_0) much; however, the quantum number hierarchy and hence the state classification, are not affected.

The system of atoms is most often represented as the famous *periodic table of chemical elements*,[86] whose simple version is shown in Fig. 23. (The table in Fig. 24 presents a sequential list of the elements with their electron configurations, following the convention already used in Eqs. (205)-(207), with the additional upper index showing the number of electrons with the indicated values of quantum numbers n and l.) The number in each table's cell, and in the first column of the list, is the so-called *atomic number* Z, which physically is the number of protons in the particular atomic nucleus, and hence the number of electrons in an electrically neutral atom.

The simplest atom, with $Z = 1$, is hydrogen (chemical symbol H) – the only atom for which the theory discussed above is quantitatively correct.[87] According to Eq. (191), the ground state of its only electron corresponds to the quantum number values $n = 1$, $l = 0$, and $m = 0$ – see Eq. (205). In most versions of the periodic table, the cell of H is placed in the top left corner.

In the next atom, helium (symbol He, $Z = 2$), the same orbital quantum state (1s) houses two electrons. As will be discussed in detail in Chapter 8, electrons of the same atom are actually *indistinguishable*, so their quantum states are not independent and may be *entangled*. These factors are important for several properties of helium atoms (and heavier elements as well); however, a bit counter-intuitively, for atom classification purposes, they are not crucial, and we may think about the two electrons of a helium atom just having "opposite spins". Due to the twice higher electric charge of the nucleus of the helium atom, i.e. the twice higher value of the constant C in Eq. (190), resulting in a four-fold increase of the constant E_0 given by Eq. (192), the binding energy of each electron is crudely four times higher than that of the hydrogen atom – though the electron interaction decreases it by about 25%

[86] Also called the *Mendeleev table*, after D. I. Mendeleev who put forward the concept of the quasi-periodicity of chemical element properties as functions of Z phenomenologically in 1869. (The explanation of this periodicity had to wait for 60 more years until the advent of quantum mechanics in the late 1920s.)

[87] Besides very small *fine-structure* and *hyperfine-splitting* corrections – to be discussed, respectively, in Chapters 6 and 8.

– see Sec. 8.2 below. This is why taking one electron away (i.e. the *positive ionization* of a helium atom) requires relatively high energy, ~24.6 eV, which is not available in the usual chemical reactions. On the other hand, a neutral helium atom cannot bind one more electron (i.e. form a *negative ion*) either. As a result, helium, and all other elements with fully completed electron *shells* (the term meaning the sets of states with eigenenergies well separated from higher energy levels) is a chemically inert *noble gas*, thus starting the whole right-most column of the periodic table, allocated for such elements.

1 H	Property legend:																2 He
3 Li	4 Be	alkali metals				transition metals				metalloids		5 B	6 C	7 N	8 O	9 F	10 Ne
11 Na	12 Mg	alkali-earth metals				nonmetals				halogens		13 Al	14 Si	15 P	16 S	17 Cl	18 Ar
19 K	20 Ca	rare-earth metals	21 Sc	22 Ti	23 V	other metals	25 Mn	26 Fe	27 Co	noble gases	29 Cu	30 Zn	31 Ga	32 Ge	33 As	34 Se	35 Br	36 Kr
37 Rb	38 Sr		39 Y	40 Zr	41 Nb	42 Mo	43 Tc	44 Ru	45 Rh	46 Pd	47 Ag	48 Cd	49 In	50 Sn	51 Sb	52 Te	53 I	54 Xe
55 Cs	56 Ba	57-71	72 Hf	73 Ta	74 W	75 Re	76 Os	77 Ir	78 Pt	79 Au	80 Hg	81 Tl	82 Pb	83 Bi	84 Po	85 At	86 Rn	
87 Fr	88 Ra	89-102	104 Rf	105 Db	106 Sg	107 Bh	108 Hs	109 Mt	110 Ds	111 Rg	112 Cn	113 Nh	114 Fl	115 Mc	116 Lv	117 Ts	118 Og	

Lanthanides:	57 La	58 Ce	59 Pr	60 Nd	61 Pm	62 Sm	63 Eu	64 Gd	65 Tb	66 Dy	67 Ho	68 Er	69 Tm	70 Yb	71 Lu
Actinides:	89 Ac	89 Ac	90 Th	91 Pa	92 U	93 Np	94 Pu	95 Am	96 Cm	97 Bk	98 Cf	99 Es	100 Fm	101 Md	102 Lr

Fig. 3. 23. The periodic table of elements, showing their atomic numbers and chemical symbols, as well as the color-coded basic physical/chemical properties at the so-called *ambient* (meaning usual laboratory) conditions.

The situation changes rather dramatically as we move to the next element, lithium (Li), with $Z = 3$ electrons. Two of them are still accommodated by the inner shell with $n = 1$ (listed in Fig. 24 as the *helium shell* [He]), but the third one has to reside in the next shell with $n = 2$, $l = 0$, and $m = 0$, i.e. in the 2*s* state. According to Eq. (201), the binding energy of this electron is much lower, especially if we take into account that according to Eqs. (210)-(211), the 1*s* electrons of the [He] shell are much closer to the nucleus and almost completely compensate for two-thirds of its electric charge +3*e*. As a result, the 2*s*-state electron is approximately but reasonably described by Eq. (201) with $Z = 1$ and $n = 2$, giving its binding energy close to 3.4 eV (actually, ~5.39 eV), so a lithium atom can give out that electron rather easily – to either an atom/ion of another element to form a chemical compound or to the common conduction band of the solid-state lithium; as a result, at the ambient conditions, this is a typical *alkali metal*. The similarity of chemical properties of lithium and hydrogen, with the *chemical valence* of one,[88] places Li as the starting element of the second *period* (row), with the first period limited to only H and He – see Fig. 23.

[88] Chemical valence (or "valency") is a not very precise term describing the number of the atom's electrons involved in chemical bonding. For the same atom, especially with a large number of electrons in its outer shell, this number may depend on the chemical compound formed. (For example, the valence of iron is two in the *ferrous* oxide, FeO, and three in the *ferric* oxide, Fe_2O_3.)

Atomic number	Atomic symbol	Electron states
Period 1		
1	H	$1s^1$
2	He	$1s^2$
Period 2		[He] shell, plus:
3	Li	$2s^1$
4	Be	$2s^2$
5	B	$2s^2 2p^1$
6	C	$2s^2 2p^2$
7	N	$2s^2 2p^3$
8	O	$2s^2 2p^4$
9	F	$2s^2 2p^5$
10	Ne	$2s^2 2p^6$
Period 3		[Ne] shell, plus:
11	Na	$3s^1$
12	Mg	$3s^2$
13	Al	$3s^2 3p^1$
14	Si	$3s^2 3p^2$
15	P	$3s^2 3p^3$
16	S	$3s^2 3p^4$
17	Cl	$3s^2 3p^5$
18	Ar	$3s^2 3p^6$
Period 4		[Ar] shell, plus:
19	K	$4s^1$
20	Ca	$4s^2$
21	Sc	$3d^1 4s^2$
22	Ti	$3d^2 4s^2$
23	V	$3d^3 4s^2$
24	Cr	$3d^4 4s^2$
25	Mn	$3d^5 4s^2$
26	Fe	$3d^6 4s^2$
27	Co	$3d^7 4s^2$
28	Ni	$3d^8 4s^2$
29	Cu	$3d^9 4s^1$
30	Zn	$3d^{10} 4s^2$
31	Ga	$3d^{10} 4s^2 4p^1$
32	Ge	$3d^{10} 4s^2 4p^2$
33	As	$3d^{10} 4s^2 4p^3$
34	Se	$3d^{10} 4s^2 4p^4$
35	Br	$3d^{10} 4s^2 4p^5$
36	Kr	$3d^{10} 4s^2 4p^6$

Atomic number	Atomic symbol	Electron states
Period 5		[Kr] shell, plus:
37	Rb	$5s^1$
38	Sr	$5s^2$
39	Y	$4d^1 5s^2$
40	Zr	$4d^2 5s^2$
41	Nb	$4d^4 5s^1$
42	Mo	$4d^5 5s^1$
43	Tc	$4d^6 5s^1$
44	Ru	$4d^7 5s^1$
45	Rh	$4d^8 5s^1$
46	Pd	$4d^{10}$
47	Ag	$4d^{10} 5s^1$
48	Cd	$4d^{10} 5s^2$
49	In	$4d^{10} 5s^2 5p^1$
50	Sn	$4d^{10} 5s^2 5p^2$
51	Sb	$4d^{10} 5s^2 5p^3$
52	Te	$4d^{10} 5s^2 5p^4$
53	I	$4d^{10} 5s^2 5p^5$
54	Xe	$4d^{10} 5s^2 5p^6$
Period 6		[Xe] shell, plus:
55	Cs	$6s^1$
56	Ba	$6s^2$
57	La	$5d^1 6s^2$
58	Ce	$4f^1 5d^1 6s^2$
59	Pr	$4f^3 6s^2$
60	Nd	$4f^4 6s^2$
61	Pm	$4f^5 6s^2$
62	Sm	$4f^6 6s^2$
63	Eu	$4f^7 6s^2$
64	Gd	$4f^7 5d^1 6s^2$
65	Tb	$4f^9 6s^2$
66	Dy	$4f^{10} 6s^2$
67	Ho	$4f^{11} 6s^2$
68	Er	$4f^{12} 6s^2$
69	Tm	$4f^{13} 6s^2$
70	Yb	$4f^{14} 6s^2$
71	Lu	$4f^{14} 5d^1 6s^2$
72	Hf	$4f^{14} 5d^2 6s^2$
73	Ta	$4f^{14} 5d^3 6s^2$
74	W	$4f^{14} 5d^4 6s^2$
75	Re	$4f^{14} 5d^5 6s^2$
76	Os	$4f^{14} 5d^6 6s^2$

Atomic number	Atomic symbol	Electron states
77	Ir	$4f^{14} 5d^7 6s^2$
78	Pt	$4f^{14} 5d^9 6s^1$
79	Au	$4f^{14} 5d^{10} 6s^1$
80	Hg	$4f^{14} 5d^{10} 6s^2$
81	Tl	$4f^{14} 5d^{10} 6s^2 6p^1$
82	Pb	$4f^{14} 5d^{10} 6s^2 6p^2$
83	Bi	$4f^{14} 5d^{10} 6s^2 6p^3$
84	Po	$4f^{14} 5d^{10} 6s^2 6p^4$
85	At	$4f^{14} 5d^{10} 6s^2 6p^5$
86	Rn	$4f^{14} 5d^{10} 6s^2 6p^6$
Period 7		[Rn] shell, plus:
87	Fr	$7s^1$
88	Ra	$7s^2$
89	Ac	$6d^1 7s^2$
90	Th	$6d^2 7s^2$
91	Pa	$5f^2 6d^1 7s^2$
92	U	$5f^3 6d^1 7s^2$
93	Np	$5f^4 6d^1 7s^2$
94	Pu	$5f^6 7s^2$
95	Am	$5f^7 7s^2$
96	Cm	$5f^7 6d^1 7s^2$
97	Bk	$5f^9 7s^2$
98	Cf	$5f^{10} 7s^2$
99	Es	$5f^{11} 7s^2$
100	Fm	$5f^{12} 7s^2$
101	Md	$5f^{13} 7s^2$
102	No	$5f^{14} 7s^2$
103	Lr	$5f^{14} 6d^1 7s^2$
104	Rf	$5f^{14} 6d^2 7s^2$
105	Db	$5f^{14} 6d^3 7s^2$
106	Sg	$5f^{14} 6d^4 7s^2$
107	Bh	$5f^{14} 6d^5 7s^2$
108	Hs	$5f^{14} 6d^6 7s^2$
109	Mt	$5f^{14} 6d^7 7s^2$
110	Ds	$5f^{14} 6d^8 7s^2$
111	Rg	$5f^{14} 6d^9 7s^2$
112	Cn	$5f^{14} 6d^{10} 7s^2$
113	Nh	$5f^{14} 6d^{10} 7s^2 7p^1$
114	Fl	$5f^{14} 6d^{10} 7s^2 7p^2$
115	Mc	$5f^{14} 6d^{10} 7s^2 7p^3$
116	Lv	$5f^{14} 6d^{10} 7s^2 7p^4$
117	Ts	$5f^{14} 6d^{10} 7s^2 7p^5$
118	Og	$5f^{14} 6d^{10} 7s^2 7p^6$

Fig. 3.24. Atomic electron configurations. The upper index shows the number of electrons in the states with the indicated quantum numbers n (the first digit) and l (letter-coded as was discussed above).

In the next element, beryllium (symbol Be, $Z = 4$), the $2s$ state ($n = 2$, $l = 0$, $m = 0$) houses one more electron, with the "opposite spin". Due to the higher electric charge of the nucleus, $Q = +4e$, with only half of it compensated by $1s$ electrons of the [He] shell, the binding energy of the $2s$ electrons is somewhat higher than that in lithium, so the ionization energy increases to ~9.32 eV. As a result, beryllium is also chemically active with the valence of two, but not as active as lithium, and is also is metallic in its solid-state phase, but with a lower electric conductivity than lithium.

Moving in this way along the second row of the periodic table (from $Z = 3$ to $Z = 10$), we see a gradual filling of the rest of the total $2n^2 = 2\times2^2 = 8$ different electron states of the $n = 2$ shell (see Eq. (204), with the additional spin degeneracy factor of 2), including two $2s$ states with $m = 0$, and six $2p$ states with $m = 0, \pm1$, with a gradually growing ionization potential (up to ~21.6 eV in Ne with $Z = 10$), i.e. a growing reluctance to either conduct electricity or form *positive* ions. However, the last elements of the row, such as oxygen (O, with $Z = 8$) and especially fluorine (F, with $Z = 9$) can readily pick up extra electrons to fill up their $2p$ states, i.e. form *negative* ions. As a result, these elements are chemically active, with a double valence for oxygen and a single valence for fluorine. However, the final element of this row, neon, has its $n = 2$ shell completely full, and cannot form a stable negative ion. This is why it is a noble gas, like helium. Traditionally, in the periodic table, such elements are placed right under helium (Fig. 23), to emphasize the similarity of their chemical properties. But this necessitates making at least a 6-cell gap in the 1st row. (Actually, the gap is often made larger, to accommodate the next rows – keep reading.)

Period 3, i.e. the 3rd row of the table, starts exactly like period 2, with sodium (Na, with $Z = 11$), also a chemically active alkali metal whose atom features 2+8 = 10 electrons filling the shells with $n = 1$ and $n = 2$ (in Fig. 24, collectively called the neon shell [Ne]), plus one electron in the $3s$ state ($n = 3$, $l = 0$, $m = 0$), which may be again reasonably well described by the hydrogen atom theory – see, e.g., the red curve on the last panel of Fig. 22. Continuing along this row, we could naively expect that, according to Eq. (204), and with the account of double spin degeneracy, this period of the table should have $2n^2 = 2\times3^2 = 18$ elements, with a gradual, sequential filling of first, two $3s$ states, then six $3p$ states, and then ten $3d$ states. However, here we run into a big surprise: after argon (Ar, with $Z = 18$), a relatively inert element with an ionization energy of ~15.7 eV due to the fully filled $3s$ and $3p$ *subshells*, the next element, potassium (K, with $Z = 19$) is an alkali metal again!

The reason for that is the difference of the actual electron energies from those of the hydrogen atom, which is due mostly to electron-electron interactions, and gradually accumulates with the growth of Z. It may be semi-quantitatively understood from the results described in Sec. 6. In hydrogen-like atoms/ions, the electron state energies do not depend on the quantum number l (as well as m) – see Eq. (201). However, the orbital quantum number does affect the wavefunction of an electron. As Fig. 22 shows, the larger l the less the probability for an electron to be close to the nucleus, where its positive charge is less compensated by other electrons. As a result of this effect (and also the relativistic corrections to be discussed in Sec. 6.3), the electron's energy grows with l. Actually, this effect is visible already in period 2 of the table: it manifests itself in the filling order – the p states after the s states. However, for potassium (K, with $Z = 19$) and calcium (Ca, with $Z = 20$), the energies of the $3d$ states become so high that the energies of the two $4s$ states are lower, and the latter states are filled first. As described by Eq. (210), and also by the first of Eqs. (211), the effect of the principal number n on the distance from the nucleus is stronger than that of l, so the $4s$ wavefunctions of K and Ca are relatively far from the nucleus, and determine the chemical valence (equal to 1 and 2, correspondingly) of these elements. The next atoms, from Sc ($Z = 21$) to Zn ($Z = 30$), with the gradually filled "internal" $3d$ states,

are the so-called *transition metals* whose (comparable) ionization energies and chemical properties are determined by the 4*s* electrons.[89]

This fact is the origin of the difference between various forms of the "periodic" table. In its most popular option, shown in Fig. 23, K is used to start the next period 4, and then a new period is started each time and only when the first electron with the next principal quantum number (n) appears.[90] This topology of the table provides a very clear match of the chemical properties of the first element of each period (an alkali metal), as well as its last element (a noble gas). It also automatically means making gaps in all previous rows. Usually, this gap is made between the atoms with completely filled *s* states and with those with the first electron in a *p* state, because here the properties of the elements make a somewhat larger step. (For example, the step from Be to B makes the material an insulator, but the step from Mg to Al makes a smaller difference.) As a result, the elements of the same column have only *approximately* similar chemical valences and physical properties.

In order to accommodate the lower, longer rows, such representation is inconvenient, because the whole table would be too broad. This is why the so-called *rare earth* elements, including *lanthanides* (with Z from 57 to 70, of the 6th row, with a gradual filling of the 4*f* and 5*d* subshells) and *actinides* (Z from 89 to 103, of the 7th row, with a gradual filling of the 5*f* and 6*d* subshells), are usually represented as outlet rows – see Fig. 23. This is quite acceptable for basic chemistry because chemical properties of the elements within each such group are rather close.

To summarize my very short review of this extremely important topic,[91] the "periodic table of elements" is not periodic in the strict sense of the word. Nevertheless, it has had an enormous historic significance for chemistry, as well as atomic and solid-state physics, and is still very convenient for many purposes. For our course, the most important aspect of its discussion is the surprising possibility to describe, at least for classification purposes, such a complex multi-electron system as an atom as a system of quasi-independent electrons in certain quantum states indexed with the same quantum numbers n, l, and m as those of the hydrogen atom. This fact enables the use of various *perturbation theories*, which give a more quantitative description of atomic properties. Some of these techniques will be reviewed in Chapters 6 and 8.

3.8. Spherically symmetric scatterers

The machinery of the Legendre polynomials and the spherical Bessel functions, discussed in Sec. 6, may also be used for the analysis of particle scattering by spherically symmetric potentials (155) beyond the Born approximation (Sec. 3), provided that such a potential $U(r)$ is also localized, i.e. reduces sufficiently fast at $r \to \infty$.[92] Indeed, directing the z-axis along the propagation of the incident plane de Broglie wave ψ_i, and taking its origin in the center of the scatterer, we may expect the scattered wave ψ_s to be axially symmetric, so its expansion in the series over the spherical harmonics includes

[89] The sequence of shell and subshell formation with the atomic number's growth approximately follows the so-called *Madelung rule* (saying that the orbitals with the lowest sum $(n + l)$ are filled first), while the order of state filling inside each subshell closely follows the *Hund rules*, to be discussed in Sec. 8.3.

[90] Another popular option is to return to the first column as soon an atom has one electron in the *s* state (like it is in Cu, Ag, and Au, in addition to the alkali metals).

[91] For a bit more detailed (but still succinct) discussion of the valence and other chemical aspects of atomic structure, I can recommend Chapter 5 of the very clear text by L. Pauling, *General Chemistry*, Dover, 1988.

[92] The quantification of this condition is left for the reader's exercise.

only the terms with $m = 0$. Hence, the solution (64) of the stationary Schrödinger equation (63) in this case may be represented as[93]

$$\psi = \psi_{\rm i} + \psi_{\rm s} = a_{\rm i}\left[e^{ikz} + \sum_{l=0}^{\infty} \mathcal{R}_l(r) P_l(\cos\theta)\right], \tag{3.213}$$

where $k \equiv (2mE)^{1/2}/\hbar$ is defined by the energy E of the incident particle, while the radial functions $\mathcal{R}_l(r)$ have to satisfy Eq. (181), and be finite at $r \to 0$. At large distances $r >> R$, where R is the effective radius of the scatterer, the potential $U(r)$ is negligible, and Eq. (181) is reduced to Eq. (183). In contrast to its analysis in Sec. 6, we should look for its solution using a linear superposition of the spherical Bessel functions of both kinds:

$$\mathcal{R}_l(r) = A_l j_l(kr) + B_l y_l(kr), \qquad \text{at } r >> R, \tag{3.214}$$

because Eq. (183) is now invalid at $r \to 0$, so our former argument for dropping the functions $y_l(kr)$ is no more valid as well. In Eq. (214), A_l and B_l are some complex coefficients, determined by the scattering potential $U(r)$, i.e. by the solution of Eq. (181) at $r \sim R$.

As the explicit expressions (186) show, the spherical Bessel functions $j_l(\xi)$ and $y_l(\xi)$ represent *standing* de Broglie waves, with equal real amplitudes, so their simple linear combinations (called the *spherical Hankel functions of the first and second kind*),

$$h_l^{(1)}(\xi) \equiv j_l(\xi) + iy_l(\xi), \qquad \text{and } h_l^{(2)}(\xi) \equiv j_l(\xi) - iy_l(\xi), \tag{3.215}$$

represent *traveling* spherical waves propagating, respectively, from the origin (i.e. from the center of the scatterer), and toward the origin. In particular, at $\xi >> 1$, l, i.e. at large distances $r >> 1/k$, l/k,[94]

$$h_l^{(1)}(kr) \to \frac{(-i)^{l+1}}{kr} e^{ikr}, \qquad h_l^{(2)}(kr) \to \frac{i^{l+1}}{kr} e^{-ikr}. \tag{3.216}$$

But using the same physical argument as at the beginning of Sec. 1, we may argue that in the case of a localized scatterer, there should be no latter waves at $r >> R$; hence, we have to require the amplitude of the term proportional to $h_l^{(2)}$ to be zero. With the relations reciprocal to Eqs. (215),

$$j_l(\xi) = \frac{1}{2}\left[h_l^{(1)}(\xi) + h_l^{(2)}(\xi)\right], \qquad y_l(\xi) = \frac{1}{2i}\left[h_l^{(1)}(\xi) - h_l^{(2)}(\xi)\right], \tag{3.217}$$

which enable us to rewrite Eq. (214) as

$$\begin{aligned} \mathcal{R}_l(r) &= \frac{A_l}{2}\left[h_l^{(1)}(kr) + h_l^{(2)}(kr)\right] + \frac{B_l}{2i}\left[h_l^{(1)}(kr) - h_l^{(2)}(kr)\right] \\ &\equiv \left(\frac{A_l - iB_l}{2}\right) h_l^{(1)}(kr) + \left(\frac{A_l + iB_l}{2}\right) h_l^{(2)}(kr), \end{aligned} \tag{3.218}$$

this means that the combination $(A_l + iB_l)$ has to be equal zero, i.e. $B_l = iA_l$. Hence we have just one unknown coefficient (say, A_l) for each l,[95] and may rewrite Eq. (218) in an even simpler form:

[93] The particular terms in this sum are frequently called *partial waves*.

[94] For arbitrary l, this result may be confirmed using Eqs. (185) and the asymptotic formulas for the "usual" Bessel functions – see, e.g., EM Eqs. (2.135) and (2.152), valid for an arbitrary (not necessarily integer) index n.

$$\mathcal{R}_l(r) = A_l\left[j_l(kr) + iy_l(kr)\right] \equiv A_l h_l^{(1)}(kr), \qquad \text{at } r >> R, \tag{3.219}$$

and use Eqs. (213) and (216) to write the following expression for the scattered wave at large distances:

$$\psi_s \approx \frac{a_i}{kr} e^{ikr} \sum_{l=0}^{\infty} (-i)^{l+1} A_l P_l(\cos\theta), \qquad \text{for } r >> R, \frac{1}{k}, \frac{l}{k}. \tag{3.220}$$

Comparing this expression with the general Eq. (81), we see that for a spherically symmetric, localized scatterer,

$$f = \frac{1}{k} \sum_{l=0}^{\infty} (-i)^{l+1} A_l P_l(\cos\theta), \tag{3.221}$$

so the differential cross-section (84) is

$$\frac{d\sigma}{d\Omega} = \frac{1}{k^2} \left| \sum_{l=0}^{\infty} (-i)^{l+1} A_l P_l(\cos\theta) \right|^2 \equiv \frac{1}{k^2} \sum_{l,l'=0}^{\infty} i^{l'-l} A_l A_{l'}^* P_l(\cos\theta) P_{l'}(\cos\theta). \tag{3.222}$$

The last expression is more convenient for the calculation of the total cross-section (59):

$$\sigma = \oint_{4\pi} \frac{d\sigma}{d\Omega} d\Omega = 2\pi \int_{-1}^{+1} \frac{d\sigma}{d\Omega} d(\cos\theta) = \frac{2\pi}{k^2} \sum_{l,l'=0}^{\infty} i^{l'-l} A_l A_{l'}^* \int_{-1}^{+1} P_l(\xi) P_{l'}(\xi) d\xi, \tag{3.223}$$

where $\xi \equiv \cos\theta$, because this result may be much simplified by using Eq. (167):[96]

Spherically symmetric scatterer: σ

$$\boxed{\sigma = \sum_{l=0}^{\infty} \sigma_l, \quad \text{with } \sigma_l = \frac{4\pi}{k^2} \frac{|A_l|^2}{2l+1}.} \tag{3.224}$$

Hence the solution of the scattering problem is reduced to the calculation of the partial wave amplitudes A_l defined by Eq. (219) – and for the total cross-section, merely of their magnitudes. This task is much facilitated by using the following formula[97] for the expansion of the incident plane wave into a series over the Legendre polynomials,

$$e^{ikz} \equiv e^{ikr\cos\theta} = \sum_{l=0}^{\infty} i^l (2l+1) j_l(kr) P_l(\cos\theta). \tag{3.225}$$

As the simplest example, let us consider scattering by a completely impenetrable and "hard" (meaning sharp-boundary) sphere, which may be described by the following potential:

$$U(r) = \begin{cases} +\infty, & \text{for } r < R, \\ 0, & \text{for } R < r. \end{cases} \tag{3.226}$$

---

[95] Moreover, using the conservation of the orbital momentum, to be discussed in Sec. 5.6, it is possible to show that this *complex* coefficient may be further reduced to just one *real* parameter, usually recast as the *partial phase shift* δ_l between the l^{th} spherical harmonics of the incident and scattered waves. However, I will not use this notion, because practical calculations are more physically transparent (and not more complex) without it.

[96] Physically, this reduction of the double sum to a single one means that due to the orthogonality of the spherical harmonics, the total scattering probability flows due to each partial wave just add up.

[97] It may be proved by using the Rodrigues formula (165) and integration by parts – the task left for the reader's exercise.

In this case, the total wavefunction has to vanish at $r \le R$, and hence for the external problem ($r \ge R$), the sphere enforces the boundary condition $\psi \equiv \psi_0 + \psi_s = 0$ for all values of θ, at $r = R$. With Eqs. (213), (220), and (225), this condition becomes

$$a_i \sum_{l=0}^{\infty} \left[\mathcal{R}_l(R) + i^l (2l+1) j_l(kR) \right] P_l(\cos\theta) = 0 . \tag{3.227}$$

Due to the orthogonality of the Legendre polynomials, this condition may be satisfied for all angles θ only if all the coefficients before all $P_l(\cos\theta)$ vanish, i.e. if

$$\mathcal{R}_l(R) = -i^l (2l+1) j_l(kR). \tag{3.228}$$

On the other hand, for $r > R$, $U(r) = 0$, so Eq. (183) is valid, and its outward-wave solution (219) has to be valid even at $r \to R$, giving

$$\mathcal{R}_l(R) = A_l \left[j_l(kR) + i y_l(kR) \right]. \tag{3.229}$$

Requiring the two last expressions to give the same result, we get

$$A_l = -i^l (2l+1) \frac{j_l(kR)}{j_l(kR) + i y_l(kR)}, \tag{3.230}$$

so Eqs. (222) and (224) yield:

$$\frac{d\sigma}{d\Omega} = \frac{1}{k^2} \left| \sum_{l=0}^{\infty} (2l+1) \frac{j_l(kR)}{j_l(kR) + i y_l(kR)} P_l(\cos\theta) \right|^2, \qquad \sigma_l = \frac{4\pi(2l+1)}{k^2} \frac{j_l^2(kR)}{j_l^2(kR) + y_l^2(kR)} . \tag{3.231}$$

As Fig. 25a shows, the first of these results gives an angular structure of the scattered de Broglie wave, which is qualitatively similar to that given by the Born approximation – cf. Eq. (98) and Fig. 10.

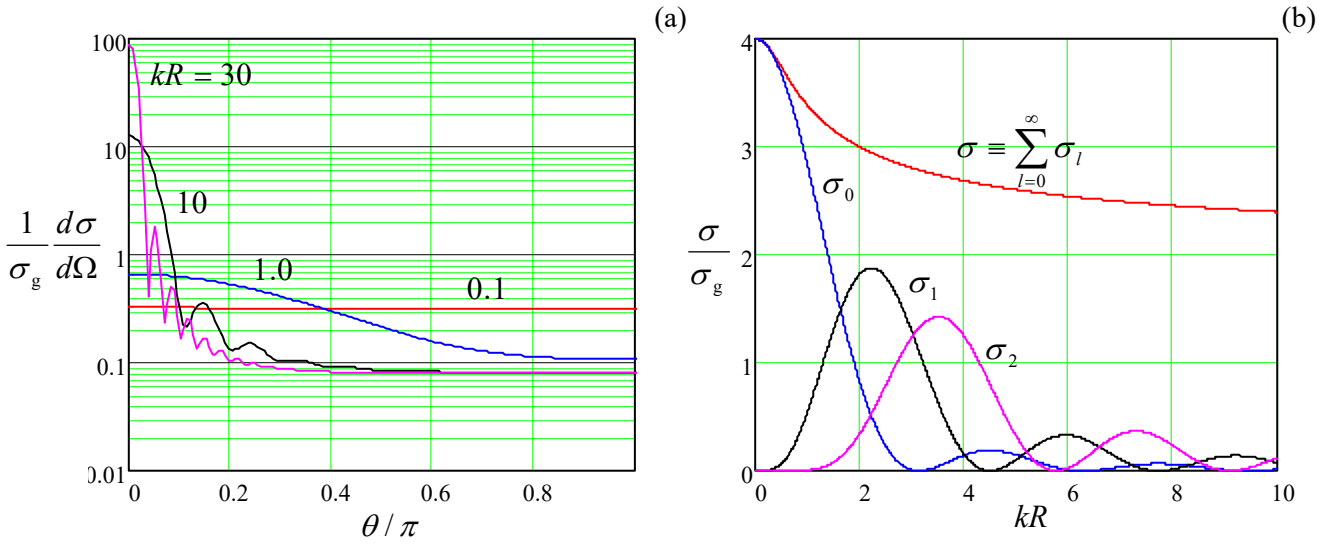

Fig. 3.25. Particle scattering by an impenetrable hard sphere: (a) the differential cross-section normalized to the geometric cross-section $\sigma_g \equiv \pi R^2$ of the sphere, as a function of the scattering angle θ, and (b) the (similarly normalized) total cross-section and its lowest spherical components, as functions of the dimensionless product $kR \propto E^{1/2}$.

Namely, at low particle's energies ($kR << 1$), the scattering is essentially isotropic, while in the opposite, high-energy limit $kR >> 1$, it is mostly confined to small angles $\theta \sim \pi/kR << 1$, and exhibits numerous local destructive-interference minima at angles $\theta_n \sim \pi n/kR$. However, in our current (exact!) theory, these minima are different from zero because the theory describes an effective bending of the de Broglie waves along the back side of the sphere, which smears the interference pattern.

This bending is also responsible for a rather counter-intuitive fact (sometimes called *wave extinction paradox*), described by the second of Eqs. (231) and clearly visible in Fig. 25b: even at $kR \to \infty$, the total cross-section σ of scattering tends to $2\sigma_g \equiv 2\pi R^2$, rather than to the geometric cross-section σ_g as in the purely-classical scattering theory. First discovered for optical waves, this effect is common for all large non-absorbing scatterers. The fact that at $kR << 1$, the cross-section is also larger than σ_g, approaching $4\sigma_g$ at $kR \to 0$, is much less surprising, because in this limit the de Broglie wavelength $\lambda = 2\pi/k$ is much larger than the sphere's radius R, so the sphere effect on the incident wave extends to the area of the order of $\lambda^2 >> \sigma_g \equiv \pi R^2$.

The above analysis may be readily generalized to the case of a step-like (*sharp* but finite) potential (97) – the problem left for the reader's exercise. On the other hand, for a finite and *smooth* scattering potential $U(r)$, by plugging Eq. (225) into Eq. (213) and the result into Eq. (66), and requiring the coefficients before each angular function $P_l(\cos\theta)$ to be balanced, we get the following inhomogeneous generalization of Eq. (181) for the radial functions defined by Eq. (213):

$$\left[E - U(r)\right]\mathcal{R}_l + \frac{\hbar^2}{2mr^2}\left[\frac{d}{dr}\left(r^2\frac{d}{dr}\right) - l(l+1)\right]\mathcal{R}_l(r) = U(r)i^l(2l+1)j_l(kr). \tag{3.232}$$

This differential equation has to be solved in the whole scatterer volume (i.e. for all $r \sim R$) with the boundary conditions for the functions $\mathcal{R}_l(r)$ to be finite at $r \to 0$, and to tend to the asymptotic form (219) at $r >> R$. The last requirement enables the evaluation of the coefficients A_l that are needed for spelling out Eqs. (222) and (224), for any particular potential $U(r)$. Unfortunately, due to the lack of time/space, for particular examples, I have to refer the interested reader to special literature.[98]

3.9. Exercise Problems

3.1. A particle of energy E is incident (in the figure on the right, within the plane of the drawing) on a sharp potential step:

$$U(\mathbf{r}) = \begin{cases} 0, & \text{for } x < 0, \\ U_0, & \text{for } 0 < x. \end{cases}$$

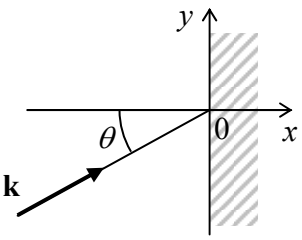

Calculate the particle reflection probability $\mathscr{R}$ as a function of the incidence angle θ, and discuss this function for various magnitudes and signs of U_0.

3.2. For a charged particle moving in a magnetic field $\mathscr{B}$, calculate the commutation relations between Cartesian components of the kinetic ("$m\mathbf{v}$-") momentum operator defined by Eq. (20). Can the result be represented in a vector form?

[98] See, e.g., J. Taylor, *Scattering Theory*, Dover, 2006.

3.3. In the classical mechanics version of the Landau-level problem discussed in Sec. 3.2 of the lecture notes, the geometric center of the particle's orbit is an integral of motion, determined by initial conditions. Calculate the commutation relation between the quantum-mechanical operators corresponding to the Cartesian coordinates of the center.

3.4.* Analyze how are the Landau levels (50) modified by an additional uniform electric field $\mathscr{E}$ directed along the plane of the particle's motion. Contemplate the physical meaning of your result and its implications for the quantum Hall effect in a gate-defined Hall bar. (The area $l \times w$ of such a bar is defined by metallic "gate" electrodes parallel to the 2D electron gas plane – see the figure on the right. The negative voltage V_g applied to the gates squeezes the 2D gas from the area under them into the complementary, Hall-bar part of the plane.)

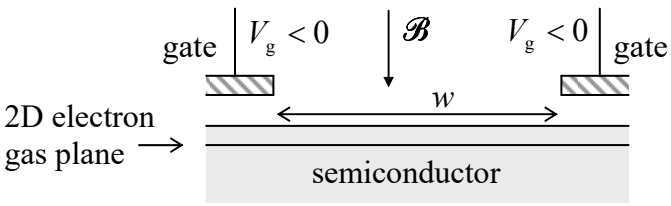

3.5. Analyze how are the Landau levels (50) modified if a 2D particle is confined in an additional 1D potential well $U(x) = m\omega_0^2 x^2/2$.

3.6. Find the stationary states of a spinless, charged 3D particle moving in "crossed" (mutually perpendicular) uniform electric and magnetic fields, with $\mathscr{E} << c\mathscr{B}$. For such states, calculate the expectation values of the particle's velocity in the direction perpendicular to both fields and compare the result with the solution of the corresponding classical problem.

Hint: You may like to generalize Landau's solution for 2D particles, discussed in Sec. 2, to the 3D case.

3.7. Use the Born approximation to calculate the angular dependence and the total cross-section of scattering of an incident plane wave propagating along the x-axis, by the following pair of similar point inhomogeneities:

$$U(\mathbf{r}) = \mathscr{W}\left[\delta\left(\mathbf{r} - \mathbf{n}_z \frac{a}{2}\right) + \delta\left(\mathbf{r} + \mathbf{n}_z \frac{a}{2}\right)\right].$$

Analyze the results in detail. Derive the condition of the Born approximation's validity for such delta-functional scatterers.

3.8. Use the Born approximation to analyze the scattering of particles of energy E by a very thin, straight, uniform rod of length l, oriented normally to the incident particle's velocity. In particular, calculate the differential and total cross-sections of scattering and analyze the results in the low-energy and high-energy limits.

3.9. Complete the analysis of the Born scattering by a uniform spherical potential (97), started in Sec. 3, by calculation of its total cross-section. Analyze the result in the limits $kR << 1$ and $kR >> 1$.

3.10. Use the Born approximation to calculate the differential cross-section of particle scattering by a very thin spherical shell, whose potential may be approximated as $U(\mathbf{r}) = \mathscr{W}\delta(r - R)$. Analyze the

results in the limits $kR << 1$ and $kR >> 1$, and compare them with those for a uniform sphere considered in Sec. 3.

3.11. Use the Born approximation to calculate the differential and total cross-sections of electron scattering by a screened Coulomb field of a point charge Ze, with the electrostatic potential[99]

$$\phi(\mathbf{r}) = \frac{Ze}{4\pi\varepsilon_0 r} e^{-\lambda r},$$

neglecting spin interaction effects, and analyze the result's dependence on the screening parameter λ. Compare the results with those given by the classical ("Rutherford") formula[100] for the unscreened Coulomb potential ($\lambda \to 0$), and formulate the condition of Born approximation's validity in this limit.

3.12. A quantum particle with electric charge Q is scattered by the field of a localized distributed charge with a spherically symmetric density $\rho(r)$ and zero total charge. Use the Born approximation to calculate the differential cross-section of the *forward scattering* (with the scattering angle $\theta = 0$), and evaluate it for the scattering of electrons by a hydrogen atom in its ground state.

3.13. Prove the optical theorem (99).

Hint: For the general solution (64) of the scattering problem, with ψ_i given by Eq. (6) and ψ_s in the form (81), calculate the full probability current I through a spherical surface of radius $r >> k^{-1}$, and then require that in accordance with the continuity relation (1.48), in this stationary situation, $I = 0$.

3.14. Reformulate the Born approximation for the 1D case. Use the result to find the scattering and transfer matrices of a "rectangular" (flat-top) scatterer

$$U(x) = \begin{cases} U_0, & \text{for } |x| < d/2, \\ 0, & \text{otherwise.} \end{cases}$$

Compare the results with those of the exact calculations carried out earlier in Chapter 2 and analyze how their relationship changes in the eikonal approximation.

3.15. In the tight-binding approximation, find the lowest stationary states of a particle placed into a system of three similar, isotropic, weakly coupled potential wells located in the vertices of an equilateral triangle.

3.16. The figure on the right shows a fragment of a periodic 2D lattice, with the red and blue points showing the positions of different local potentials.

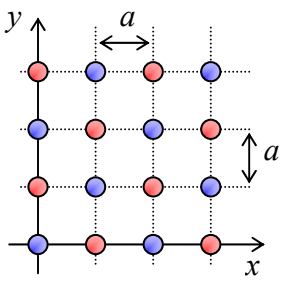

(i) Find the reciprocal lattice and the 1st Brillouin zone of the system.

(ii) Calculate the wave number k of the monochromatic de Broglie wave incident along the x-axis, at which the lattice creates the lowest-order diffraction peak within the $[x, y]$ plane, and the direction toward this peak.

(iii) Semi-quantitatively, describe the evolution of the intensity of the peak when all local potentials become similar.

[99] This *Yukawa potential* was first suggested in 1935 by H. Yukawa as a model for strong interactions.
[100] See, e.g., CM Sec. 3.5, in particular Eq. (3.73).

Hint: The *order of diffraction* on a multidimensional Bravais lattice is a somewhat ambiguous notion dependent on the lattice type, but the *lowest-order peak* is always that corresponding to the smallest non-zero magnitude of the vector **Q**.

3.17. For the 2D hexagonal lattice (Fig. 12b):

(i) find the reciprocal lattice **Q** and the 1st Brillouin zone;

(ii) use the tight-binding approximation to calculate the dispersion relation $E(\mathbf{q})$ for a 2D particle moving through a potential profile with such periodicity, with an energy close to the eigenenergy of similar isotropic states quasi-localized at the lattice points;

(iii) analyze and sketch/plot the resulting dispersion relation $E(\mathbf{q})$ inside the 1st Brillouin zone.

3.18. Complete the tight-binding-approximation calculation of the band structure of the honeycomb lattice, that was started at the end of Sec. 4. Analyze the results; in particular, prove that the Dirac points $\mathbf{q}_D$ are located in the corners of the 1st Brillouin zone, and express the velocity v_n participating in Eq. (122), in terms of the coupling energy δ_n. Show that the final results do not change if the quasi-localized wavefunctions are not isotropic but are proportional to $\exp\{im\varphi\}$ – as they are, with $m = 1$, for the $2p_z$ electrons of carbon atoms in graphene, which are responsible for its transport properties.

3.19. Examine the basic properties of the so-called *Wannier functions*[101] defined as

$$\phi_{\mathbf{R}}(\mathbf{r}) \equiv C \int_{\text{BZ}} \psi_{\mathbf{q}}(\mathbf{r}) e^{-i\mathbf{q}\cdot\mathbf{R}} d^3q ,$$

where $\psi_{\mathbf{q}}(\mathbf{r})$ is the Bloch wavefunction (108), **R** is any vector of the Bravais lattice, C is a normalization constant, and the integration over the quasimomentum **q** is extended over any (e.g., the first) Brillouin zone.

3.20. Evaluate the long-range interaction (the so-called *London dispersion force*) between two similar, electrically neutral atoms or molecules, modeling each of them as an isotropic 3D harmonic oscillator with the electric dipole moment $\mathbf{d} = q\mathbf{s}$, where **s** is the oscillator's displacement from its equilibrium position.

Hint: You may like to represent the total Hamiltonian of the system as a sum of Hamiltonians of independent 1D harmonic oscillators, and calculate their total ground-state energy as a function of the distance between the dipoles. [102]

3.21. Derive expressions for the stationary wavefunctions and the corresponding energies of a 2D particle of mass m, free to move inside a round disk of radius R. What is the degeneracy of each energy level? Calculate the five lowest energy levels with an accuracy better than 1%.

[101] Named after G. Wannier who introduced these functions in 1939.

[102] This explanation of the interaction between electrically-neutral atoms was put forward in 1930 by F. London, on the background of a prior (1928) work by C. Wang. Note that in some texts this interaction is (rather inappropriately) referred to as the "van der Waals force", though it is only one (long-range) component of the van der Waals model – see, e.g., SM Sec. 4.1.

3.22. Calculate the ground-state energy of a 2D particle of mass m, localized in a very shallow flat-bottom potential well

$$U(\rho)=\begin{cases}-U_0, & \text{for } \rho<R,\\ 0, & \text{for } \rho>R,\end{cases} \quad \text{with } 0<U_0<<\frac{\hbar^2}{mR^2}.$$

3.23. Estimate the energy E of the localized ground state of a 2D particle of mass m, in an axially symmetric potential well of a finite radius R, with an arbitrary but very small potential $U(\rho)$. (Quantify this condition.)

3.24. Spell out the spherical harmonics $Y_4^0(\theta,\varphi)$ and $Y_4^4(\theta,\varphi)$.

3.25. Calculate $\langle x\rangle$ and $\langle x^2\rangle$ in the ground states of the planar and spherical rotors of radius R. What can you say about $\langle p_x\rangle$ and $\langle p_x^2\rangle$?

3.26. A spherical rotor with $r=R=\text{const}$ and mass m is in a state with the following wavefunction: $\psi = C(⅓ + \sin^2\theta)$, where C is a constant. Calculate the energy of its angular motion.

3.27. According to the discussion at the beginning of Sec. 5, stationary wavefunctions of a 3D isotropic harmonic oscillator may be calculated as products of three similar 1D "Cartesian oscillators" – see, in particular Eq. (125), with $d = 3$. However, per the discussion in Sec. 6, the wavefunctions of the type (200), proportional to the spherical harmonics Y_l^m, also describe stationary states of this spherically symmetric system. Represent the wavefunctions (200) of:

(i) the ground state of the oscillator, and

(ii) each of its lowest excited states,

as linear combinations of products of the 1D oscillator's stationary wavefunctions. Also, calculate the degeneracy of the n^{th} energy level of the oscillator.

3.28. A particle of mass m is placed into a spherical, flat-bottom potential well

$$U(\mathbf{r})=\begin{cases}-U_0, & \text{for } r<R,\\ 0, & \text{for } R<r,\end{cases} \quad \text{with } U_0>0.$$

(i) Calculate the smallest U_0 at which the particle has a bound (localized) stationary state.

(ii) Calculate the energy of this state if U_0 is barely larger than that minimum value.

(iii) Does such a localized state exist in a very narrow and deep well that may be described as $U(\mathbf{r}) = -\mathcal{W}\delta(\mathbf{r})$ with a positive and finite $\mathcal{W}$?

3.29. A 3D particle of mass m is placed into a spherically symmetric potential well with $-\infty < U(r) \le U(\infty) = 0$. Relate its ground-state energy to that of a 1D particle of the same mass, moving in the following potential well:

$$U'(x)=\begin{cases}U(x), & \text{for } x\ge 0,\\ +\infty, & \text{for } x\le 0.\end{cases}$$

Use the found relation to:

(i) discuss the origin of the difference between the solutions of Task (i) of the previous problem and of Problem 2.21, and

(ii) calculate the energy spectrum of an electron moving over an impenetrable plane surface of a perfect conductor.

3.30. Calculate the smallest value of the parameter U_0, for that the following spherically symmetric potential well:

$$U(r) = -U_0 e^{-r/R}, \qquad \text{with } U_0, R > 0,$$

has a bound (localized) eigenstate for a particle of mass m.

Hint: You may like to introduce the following new variables: $f \equiv r\mathcal{R}$ and $\xi \equiv Ce^{-r/2R}$, with a proper constant C.

3.31.* A particle of mass m moves in the field of an attractive spherically symmetric potential $U(r) \le U(\infty) \equiv 0$. Find a condition necessary for it to have at least one bound state. Compare the result with those of Problems 28 and 30.

3.32. A particle of mass m, moving in a certain central potential $U(r)$, has a stationary state with the following wavefunction:

$$\psi = Cr^{\alpha} e^{-\beta r} \cos\theta,$$

where C, α, and $\beta > 0$ are constants. Calculate:

(i) the probabilities of all possible values of the quantum numbers m and l, and

(ii) the confining potential and the state's energy.

3.33. For an isotropic 3D harmonic oscillator, calculate:

(i) the energy spectrum resulting from the Bohr quantization of circular classical orbits, and

(ii) the energy spectrum of the s-states in the WKB approximation.

Compare the results with the exact energy spectrum of the oscillator, and comment.

3.34. For a particle of mass m, moving in the spherically symmetric potential $U(\mathbf{r}) = ar^4$:

(i) use the variational method to estimate the ground-state energy,

(ii) calculate the energy spectrum resulting from the Bohr quantization of circular orbits, and

(iii) calculate the energy spectrum of the s-states in the WKB approximation.

Compare the results and comment.

3.35. For a particle of mass m, moving in the attracting Coulomb potential $U(r) = -C/r$ (e.g., the electron in a hydrogen atom):

(i) estimate the ground state energy by using the trial wavefunction $\psi_{\text{trial}} = A/(r + a)^b$, where both $a > 0$ and $b > 1$ are fitting parameters, and

(ii) calculate the energy spectrum of the s-states in the WKB approximation.

Compare the results with the exact energy spectrum of the atom.

3.36. Calculate the energy spectrum of a particle moving in a monotonic but otherwise arbitrary spherically symmetric attractive potential $U(r) < 0$, in the approximation of very large orbital quantum numbers l. Formulate the quantitative condition(s) of validity of your theory. Check that for the Coulomb potential $U(r) = -C/r$, your result agrees with Eq. (201).

Hint: Try to solve Eq. (181) approximately by introducing the same new function $f(r) \equiv r\mathcal{R}(r)$ that was already used in Sec. 1 and in the solutions of a few earlier problems.

3.37. Prove Eq. (210) and the first two of Eqs. (211) for the ground state of a hydrogen-like atom/ion.

3.38. For the ground state of a particle in the Coulomb potential (190), calculate the probability to find it farther from the attracting center than the radius the same particle with the same energy would have on a classical circular orbit.

3.39. For the ground state and the lowest excited states of the hydrogen atom:

(i) calculate the spatial distribution of the electric current flowing around the nucleus,
(ii) evaluate its highest density, and
(iii) calculate and evaluate its magnetic field at the position of the nucleus.

3.40. An electron had been in the ground state of a hydrogen-like atom/ion with nuclear charge Ze when the charge suddenly changed to $(Z + 1)e$.[103] Calculate the probabilities for the electron of the changed system to be:

(i) in its ground state, and
(ii) in one of the lowest excited states.

3.41. Due to a very short pulse of an external force, the nucleus of a hydrogen-like atom/ion, initially at rest in its ground state, starts moving with velocity $\mathbf{v}$. Calculate the probability W_g that the atom remains in its ground state. Evaluate the energy to be given, by the pulse, to a hydrogen atom in order to reduce W_g to 50%.

3.42. Calculate $\langle x^2 \rangle$ and $\langle p_x^2 \rangle$ in the ground state of a hydrogen-like atom/ion. Compare the results with Heisenberg's uncertainty relation. What do these results tell about the electron's velocity in the system?

3.43. Use the Hellmann-Feynman theorem (see Problem 1.7) to prove:

(i) the first of Eqs. (211), and
(ii) the fact that for a spinless particle in an arbitrary spherically symmetric attractive potential $U(r)$, the ground state is always an s-state (with the orbital quantum number $l = 0$).

3.44. For the ground state of a hydrogen atom, calculate:

[103] Such a fast change happens, for example, at the beta-decay, when one of the nucleus' neurons spontaneously turns into a proton, emitting a high-energy electron and a neutrino, which leave the system very fast (instantly on the atomic time scale), and do not affect directly the atom transition's dynamics.

(i) the expectation value of $\mathscr{E}$, where $\boldsymbol{\mathscr{E}}$ is the electric field created by the atom as a whole, and

(ii) the expectation value of $\mathscr{E}^2$ at distances $r >> r_0$ from the nucleus.

Interpret the obtained relation between $\langle \mathscr{E} \rangle^2$ and $\langle \mathscr{E}^2 \rangle$ at distant observation points.

3.45. Find the condition at which a particle of mass m, moving in the field of a very thin spherical shell with $U(\mathbf{r}) = \mathscr{w}\delta(r - R)$ and $\mathscr{w} < 0$, has at least one localized ("bound") stationary state.

3.46. Calculate the lifetime of the lowest metastable state of a particle in the same spherical shell potential as in the previous problem, but now with $\mathscr{w} > 0$, for sufficiently large $\mathscr{w}$. (Quantify this condition.)

3.47. A particle of mass m and energy E is incident on a very thin spherical shell of radius R, whose localized states were the subject of two previous problems, with an arbitrary "weight" $\mathscr{w}$.

(i) Derive general expressions for the differential and total cross-sections of scattering.

(ii) Spell out the contribution σ_0 to the total cross-section σ, given by the spherically symmetric component of the scattered de Broglie wave.

(iii) Analyze the result for σ_0 in the limits of very small and very large magnitudes of $\mathscr{w}$, for both signs of this parameter. In particular, in the limit $\mathscr{w} \to +\infty$, relate the result to the metastable state's lifetime τ calculated in the previous problem.

3.48. Calculate the spherically symmetric contribution σ_0 to the total cross-section of particle scattering by a uniform sphere of radius R, described by the following potential:

$$U(r) = \begin{cases} U_0, & \text{for } r < R, \\ 0, & \text{otherwise,} \end{cases}$$

with an arbitrary constant U_0. Analyze the result in detail, and give an interpretation of its most remarkable features.

3.49. Use the finite difference method with the step $h = a/2$ to calculate as many energy levels as possible, for a particle confined to the interior of:

(i) a square with sides a, and

(ii) a cube with sides a,

with hard walls. For the square, repeat the calculations by using the finer step $h = a/3$. Compare the results for different values of h with each other and with the exact formulas.

Hint: It is advisable to either first solve (or review the solution of) the similar 1D Problem 1.18, or start from reading about the finite difference method.[104] Also: try to exploit the symmetry of the systems.

[104] See, e.g., CM Sec. 8.5 or EM Sec. 2.11.